Modeling Hand Movements in a Sequential Reach Task with Continuous Material

by

Justin Michael Haney

A dissertation submitted in partial fulfillment
of the requirements for the degree of
Doctor of Philosophy
(Industrial and Operations Engineering)
in the University of Michigan
2019

Doctoral Committee:

Assistant Professor Clive D'Souza, Chair
Associate Professor Melissa Gross
Assistant Research Scientist Monica L. H. Jones
Associate Professor Bernard Martin

Justin Michael Haney

haneyjm@umich.edu

ORCID iD: 0000-0002-8841-6670

DEDICATION

To my parents, Scott and Lisa Haney

ACKNOWLEDGMENTS

First, I would like to thank my advisor, Dr. Clive D'Souza, for all of his support and guidance during my time at the University of Michigan. His passion for ergonomics and research is truly inspiring and contagious. Thank you for your patience, the tremendous amount of time and feedback you provided me, helping me see the bigger picture of my work, and constantly pushing me to become a better researcher.

Thank you to my dissertation committee members, Dr. Melissa Gross, Dr. Monica Jones, and Dr. Bernard Martin for agreeing to support me through this entire process and providing me with their time and valuable feedback. I'd also like to thank Dr. Matt Reed for his time and expertise in the modeling aspect of my work. Everything I know about trajectory shape modeling, I owe to him.

I was fortunate to have financial support from the National Institute of Occupational Safety and Health Traineeship Program, Proctor & Gamble Inc. and the partners of the Human Motion Simulation Laboratory during my tenure as a graduate student. I would also like to thank Bradley Whitmore and Claudio Matos for their time, support, and knowledge pertaining to the direct application and relevance of this research.

I don't think I would've been able to run any experiments if it wasn't for the technical support of Chuck Woolley and Eyvind Claxton. Thank you for all your help in the workshop and laboratory which led to the construction of my experiment apparatus.

To Sol Ie Lim, I couldn't imagine a better office-mate and friend in which to share with the ups and downs of pursuing a PhD. Thank you for being a constant source of support inside and outside of the office, an excellent conference travel companion, and providing much needed comic-relief during difficult times. Your ability to maintain a positive attitude over the years was extremely comforting and for that I cannot thank you enough.

Lastly, I would like to give a special thanks to my family who have been a constant source of support throughout my graduate school journey. To my father and mother, thank you for your countless words of encouragement and teaching me that I can accomplish anything if I put my mind to it. To my siblings – Jason, Mitchell, and Paige – thank you for your support and helping me get through stressful times. To my grandparents, thank you for constantly keeping me in your prayers!

TABLE OF CONTENTS

LIST OF FIGURES

LIST OF TABLES

LIST OF APPENDICES

ABSTRACT

Manual precision tasks are a staple in many manufacturing and product assembly jobs. Sequential reach tasks in the assembly of products made with continuous material (e.g., textile threads and electrical wire), wherein operators manually route material to sequential target locations comprising multiple pulleys and idlers during routine operations, present unique physical and temporal demands on operators. Accurate predictions of human movement and task performance are important for evaluating and improving the ergonomics of such jobs. While the ergonomics literature is replete with models to predict speed-accuracy relationships during discrete reach movements in the Fitts' law paradigm, corresponding studies to quantify human performance in sequential reach tasks while manipulating continuous material are absent.

Thus, the goal of this research was to quantify the spatial and temporal properties of hand movements in sequential reach tasks that involve handling continuous material. Based on a series of human factors experiments, an original empirically-based model leveraging functional statistical analysis was developed to predict reach trajectory shapes, speed profiles, and task completion times when reaching to coplanar sequential targets with task parameters (e.g., target tolerances and location, reach direction and amplitude, and line of sight availability) as predictors. The analysis of measured trajectory shapes and speed provided unique theoretical insights into the speed-accuracy trade-off and the modulation of movement generation and speed control in sequential reach movements with continuous material. The resultant prediction model

is compatible with digital human modeling software and promises new simulation capabilities in the ergonomics analysis of industrial tasks that require manual precision handling of light-weight flexible material.

CHAPTER 1

Introduction

Manual precision tasks are a staple in many manufacturing and product assembly jobs. Tasks that are potentially harmful to operators, highly repetitive, or require high force exertions are increasingly selected for automation, whereas human operators are relegated to complex precision tasks that require intricate hand movements and fine motor control skills, i.e., dexterous tasks that are difficult to automate. Sequential reach tasks with continuous material are one example of a complex precision task, often performed by workers assembling products made with textiles, fabric, and electrical connections. This involves routing continuous material, such as threads, ribbons, and fine wire, to multiple sequential targets in a large system of pulleys and idlers during equipment set-up and maintenance operations. These tasks are characterized by reaches to different locations with different levels of precision, and time pressure to keep up with production demands. Workstation design can have a critical influence on the ability of the worker to complete such tasks in a safe, accurate and time-efficient manner. The ability to predict worker performance in terms of postural demands and task completion times, is essential to improving the design of a workstation. The dominant theme in prior research on reach kinematics has been on hand trajectories and movement times in discrete reach tasks. Examples include studies on movement times in rapid aiming tasks modeled using Fitts' law as a function of target precision and the amplitude of the movement (Fitts, 1954; Langolf, Chaffin, & Foulke,

1976) and to pick-and-place tasks (Annett, Golby, & Kay, 1958; Carlton, 1980). However, discrete reaches do not account for the unique task properties intrinsic to sequential reaching with continuous material. These task properties are introduced in the context of the real-world application and the theoretical underpinnings that motivate this research.

1.1 Applied Problem

The motivation for this research lies in the textile manufacturing wherein operators manually route continuous material (e.g. threads, films or webbing) through a system of pulleys in order to prepare machinery for operation. The routing task involves operators performing sequential reach movements to multiple coplanar target locations in a particular sequence around a workstation. A specific applied context for these tasks pertains to the manufacturing of baby care and feminine care products, where a human operator is required to set up and prepare machinery by routing thread through a large system of pulleys and idlers, i.e., reach targets (Figure 1.1). This task is performed routinely when loading new material stock at each assembly line, at startup, and during general maintenance tasks. Inefficiencies in the material routing process (i.e., excessive time, missed targets) can cause line stoppages. Thus, operators need to complete these tasks in an accurate and efficient manner.

From an operational standpoint, pulley design characteristics have the potential to impact process efficiency. For instance, the groove width and depth must be sufficient to support the material under tension and avoid the material from slipping out of position. Increasing arc length of contact will increase frictional force between the conveyor belt and pulley, which is important if traction is necessary. Equipment is often stacked vertically and located in confined spaces to limit its footprint and conserve floor space.

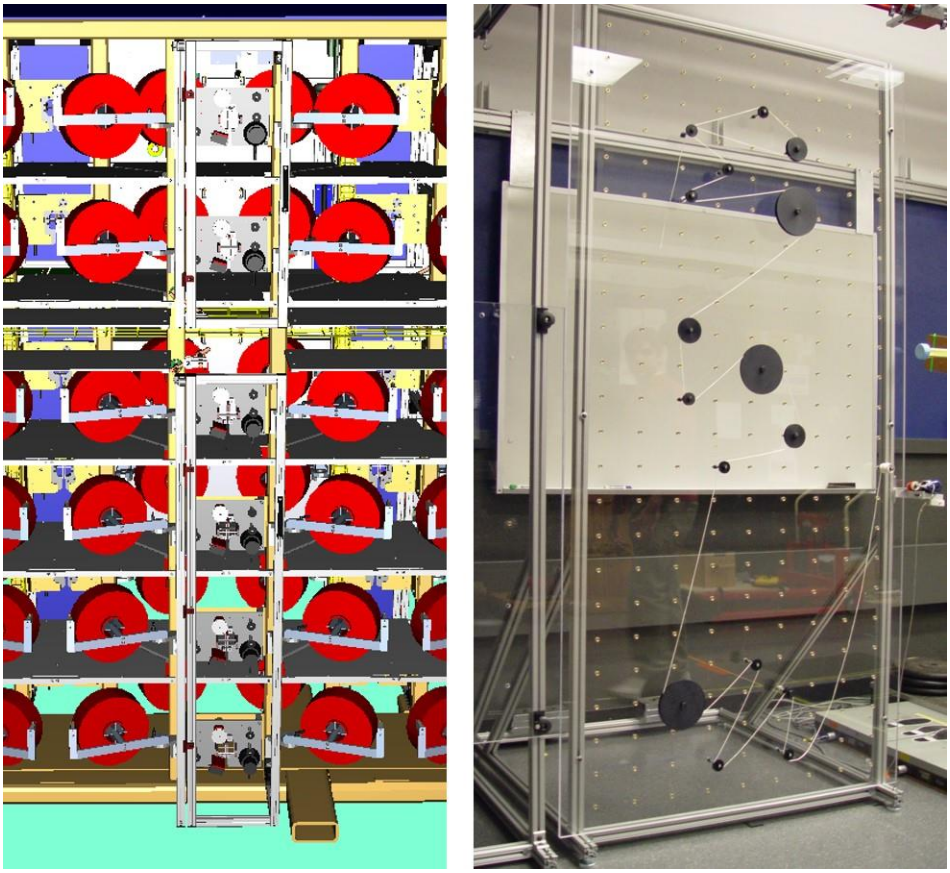

Figure 1.1. CAD representation of the actual equipment (Left) and a full-scale reconfigurable mock-up (Right) of the applied coplanar sequential reach task.

From a human factors perspective, understanding the effects of target tolerances (e.g., pulley diameters, groove widths, arc of contact) and layout (e.g., target locations, sequence) on task performance in routing (i.e., transport of material and threading of successive pulleys) is critical for production planning and for improving equipment design. The pulleys of different diameter and groove sizes for routing the material serve as reach targets. Targets situated in difficult, inaccessible locations or with low tolerance that contribute to high visual demands and high movement complexity for human operators can critically impact task performance. For instance, reaches to extreme locations (e.g., overhead, below knee, contralateral) and/or to targets with low tolerances (e.g., very narrow groove widths) require workers to adapt non-neutral,

extended work postures leading to higher error rates, increases in task completion times, and/or unsafe work postures due to potential loss of balance and fall risk if working on an elevated platform or step ladder. The ability to simulate operator performance in such tasks early in the equipment design process would allow engineers to optimize the workstation layout for safe and efficient task completion and accommodate the broadest range of worker anthropometry as possible.

Facilitating computer-aided ergonomic analyses and improving workstation design requires a quantitative understanding of the relationships between specific task parameters, worker characteristics, movement kinematics, and task performance. Digital human modeling (DHM) software, in particular, relies on algorithms characterizing these quantitative relationships, thereby providing engineers a cost-effective tool for improving workplace ergonomics and equipment design (Chaffin et al., 2001). Commercial DHM software, such as Siemens Jack and RAMSIS, allows for simulating human posture and movement in a variety of occupational tasks to assess biomechanical loads, visibility, reachability, and hand clearance issues across a simulated worker populations of diverse anthropometry. For example, automotive designers and ergonomists use DHM software to assess visibility of displays and reachability of driving controls from the driver's perspective (Chaffin et al., 2001).

Prior DHM research in occupational ergonomics has focused largely on simulating jobs where workers are at an increased risk of developing musculoskeletal disorders. One example includes research by Hoffman (2008) on the development of a 3D posture prediction model in tasks that require high hand-force.

Simulating tasks that impose low force demands but fine motor control, emblematic of sequential reach tasks with continuous material, remain relatively unexplored. This is partly due

to the lack of research on the influence of intrinsic task parameters such as the sequence of reach targets and their locations relative to the operator on hand movement kinematics and posture adaptations. A considerable amount of prior research on reach movement control has focused on rapid aiming movements. Most notable are models to predict movement times in rapid aiming tasks as a function of target tolerance and the amplitude of the movement in the Fitts' Law paradigm (Fitts, 1954; I. S. MacKenzie & Buxton, 1992; Meyer, Abrams, Kornblum, Wright, & Keith Smith, 1988; Murata & Iwase, 2001). These models are limited to simple discrete movements and lack the complexity of reaching to sequential targets with continuous material. Not surprisingly, commercial DHM software currently lacks the capability of simulating hand movements during sequential reach tasks with continuous material.

1.2 Theoretical Problem

For over a century, researchers have studied human motor control in rapid aiming reach movements, in which the arm, hand or finger is moved from one location to a specific target destination (Woodworth, 1899) Reach movements are a fundamental component to a number of activities performed in daily living, in sporting activities, and in occupational settings (e.g., manual assembly, surgery, driving).

Prior research in human motor control has focused on explaining how the central nervous system (CNS) plans and generates body segment kinematics that form a movement. For many actions performed over short durations and in known or predictable environments, humans form a set of pre-structured motor commands referred to as a motor program (Schmidt & Wrisberg, 2000). The motor program is based on a control system referred to as open-loop control where the movement execution is conducted without any feedback from the system. Target-directed movements that are deliberate and slow typically operate under closed-loop control. These

movements rely on sensory feedback (e.g. visual, tactile, auditory, and proprioceptive) for error detection to maintain the desired state. The effects of open-loop and closed-loop control are evident from performance measures such as movement time, movement speed (e.g., peak speed, time to peak speed), and reach trajectory path (e.g., maximum excursion, overshoot), measured particularly at the early vs. latter phase of the reach movement. Woodworth (1899) was the first to study discrete rapid-aiming movement tasks, and hypothesized that aiming movements are controlled by an initial impulse phase followed by a second current control phase (i.e., a "homing" phase that is under feedback-based control). Many others researchers have since investigated factors that influence motor planning, coordination, and performance in tasks that involve aimed movements (Crossman & Goodeve, 1983; Meyer et al., 1988; Schmidt, Zelaznik, Hawkins, Frank, & Quinn Jr, 1979; Todorov, 2004; Todorov & Jordan, 2002)

This research investigated movement performance in terms of trajectory shape and speed in sequential reach movements that involve transferring continuous material to consecutive coplanar target locations. Empirical research on modeling sequential reach tasks is generally lacking. Additionally, the underlying mechanisms that describe the control of reach movements while handling continuous material is unknown. The sequential properties and the transferring of continuous material introduce complexities to the task that potentially violate the assumptions for motor control models of discrete reach movements. Nonetheless, motor control mechanisms for sequential and discrete movements have some similarities. Moreover, the extensive research on reach movements in discrete aiming tasks and positioning movements in object transfer and placement tasks provide a start point for investigating sequential reaches with continuous material.

1.3 Research Background

1.3.1 Classification of Movement

Human movement behaviors are remarkably diverse, ranging from rhythmic patterns such as walking and running to complex movements such as athletic performance and fine object manipulations. Reach and positioning movements are made by humans when reaching for an artifact or manually moving an artifact to another location. Muratori et al. (2013) defined three characteristics of reach movements to help classify different types of reaches: (1) the size of the movement (gross or fine motor skills), (2) the beginning and end points (discrete or continuous), and (3) the stability of the environment in which the task is being performed (open or closed based on the temporal and spatial features of the environment where a task is performed such as reaching to coincide with a stationary vs. moving target). Fine motor skills use small muscles (e.g., of the hand for object manipulation, mouth for speech), whereas gross motor skills employ larger muscle groups of the torso and extremities and additionally may also use smaller muscles to complete a movement. Target-directed movements with continuous material could comprise of both gross movements (e.g., for transporting material by moving the arm and hand from one location to the target destination) and fine movements (e.g., when approaching the target location and manipulating the material with the hand and fingers around a pulley groove).

Discrete movements include singularly occurring events preceded and followed by a period without motion for a reasonable amount of time (Hogan & Sternad, 2007). These include target-directed movements, like reaching to grasp an object or placing an object in a specific location. In order for a reach movement to be discrete, the hand must reach and maintain zero speed for a distinct period of time. In contrast, continuous movements lack such recognizable endpoints. Rhythmic movements encompass movements that are continuous without interspersed

breaks or others that involve a contact event or rest (Hogan & Sternad, 2007), such as walking, swimming, or driving.

Differentiating between discrete vs. continuous movements is not always simple. For example, are continuous motions just a series of discrete motions, often referred to as serial or sequential movements, or are discrete motions just a unit of rhythmic motion? Repeated target-directed reach movements are classified as a series of discrete movements, such as in the Fitts' law paradigm where the hand is rapidly moved back and forth between two targets. During this task, there is a distinct period of time where the hand reaches zero speed between intervals. While some movements are unambiguously discrete and some are unambiguously rhythmic, there are also movements that could fall into both categories. For example, it is unclear if transferring continuous material to multiple targets in a sequence is a combination of discrete movements or one rhythmic movement.

1.3.2 Discrete Reach Movements

Repetitive target-directed reach movements can be characterized as a series of discrete movements, where the hand is rapidly moved back and forth between two locations or targets but has a distinct period of time where the hand attains zero terminal speed between movements. Paul Fitts (1954) was the first to model the control of hand movements in a simple discrete one handed reach task, where the hand moves back and forth between two target locations separated on a work surface. He demonstrated a fundamental principle in movement behavior, namely, a speed-accuracy tradeoff where the speed of the hand (i.e., end-effector) is inversely proportional to the accuracy of the movement. Fitts (1954) quantified this relationship in an equation to predict the movement time (*MT*) between two targets:

$$MT = a + b \log_2(2A/W), \qquad [1.1]$$

where *A* is the amplitude of the movement, *W* is the width of the target, and *a* and *b* are empirical constants specific to each task. Equation 1.1 models movement time to linearly increase with the index of difficulty ($\log_2(2A/W)$) of the task. This relationship was empirically derived from experiments on reciprocal tapping tasks with a stylus (Figure 1.2). Later, other studies demonstrated the ability of Fitts' law to predict movement times for a variety of experimental situations, such as pin transfer (Annett et al., 1958; Fitts, 1954) and washer transfer (Fitts, 1954) tasks, serial movements in response to a stimulus (Fitts & Peterson, 1964), and across a wide range of movement amplitudes (Langolf et al., 1976). Fitts' law is limited to tasks with an index of difficulty between 2 and 7 bits. Klapp (1975) showed that Fitts' law does not hold for movements with very small amplitude (≤ 11 mm) to targets of sizes between 2 mm and 64 mm. In these conditions, hand movements are predominantly ballistic and are under open-loop control (Klapp, 1975). In other words, successful task completion does not require visual feedback because there is little spatial accuracy and the movements are of short duration.

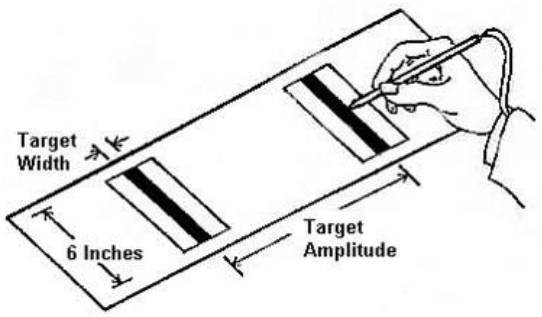

Figure 1.2. Typical experiment set-up for studying discrete, rapid-aiming movements using Fitts' law.

Subsequent researchers have extended Fitts' law to account for a variety of movements and task conditions. In the original reciprocal tapping task, the targets consisted of a 6-in long rectangular strip that varied in width and positioned flat on a table. Sheikh and Hoffmann (1994)

extended Fitts law to account for movements to targets that differ in shape (e.g., rectangle, square, diamond, or circle) by introducing a "shape" factor in the model. Prior studies have shown that movement direction affects trajectory shape and movement time (Bertucco, Cesari, & Latash, 2013; Murata & Iwase, 2001). For instance, Murata and Iwase (2001) investigated movement times in a three-dimensional pointing task where participants started with their index finger in contact with the center of a board that was oriented in the frontal plane and directed a reach movement toward a two-dimensional circular target. They compared movement times across the amplitude of the movement, diameter of the target, and location of the target relative to the center, defined by the target azimuth. The reach direction, in terms of the target azimuth, had an influence on movement times. Extending the conventional Fitts' model to incorporate a directional parameter, in terms of the target azimuth, provided better predictions of movement times compared to the conventional model.

Additionally, Fitts' law holds for pointing movements under conditions with restricted visual feedback (Wu, Yang, & Honda, 2010). Wu et al. (2010) found that pointing tasks with full vision corresponded to longer movement times due to an increase in voluntary adjustments to improve the accuracy of the movement, compared to conditions with restricted and no visual feedback. Linear relationships between movement time and ID were noted for conditions with full vision and with restricted vision. This finding indicated the influence of visual feedback in guiding the hand to the target and corresponding increases in movement time and accuracy.

1.3.3 Sequential Movements

Sequential or serial movements include a series of multiple relatively separate, independent movements performed in a sequence. The sequence may be known to the operator a priori or may be cued by stimuli while the task is performed. The movements may be of the same

type (e.g., typing on a keyboard, playing a piano) or different (e.g., manually replacing a flat tire, starting up a power plant). The former category comprising similar types of movements is relevant to the current context. A few studies have quantified the effects of target characteristics on movement time in sequential reach movements (Ricker et al., 1999; Smiley-Oyen, 1996). A sequential movement differs from a discrete movement as one must reach to consecutive targets, often varying in spatial tolerance, in a specific sequence. The focal research question in these studies was the role of preprogramming (vs. online programming) in a multi-segmental rapid aiming task with a stylus. Interestingly, the study findings indicated that later target characteristics (e.g., the 2nd target) influenced the timing of movements and movement time to earlier targets in a sequence (Ricker et al., 1999; Smiley-Oyen, 1996). For instance, Ricker et al. (1999) studied rapid two-component aiming movements, and with the second target being either larger, smaller or the same size at the first target. Ricker et al. (1999) found that movement times to the first and second target increased as the size of the second target decreased, suggesting preparation for the second movement component occurred even before reaching the first target. Further, vision prior to movement onset was used to form a movement plan to both targets in a sequence (Ricker et al., 1999). Smiley-Oyen and Worringham (1996) found similar evidence of additional programming occurring before initiation and during movement in a task that involved participants contacting 7 consecutive targets with a stylus in rapid succession. Collectively, these findings also imply that rapid sequential aiming movements violate Fitts' law, since the latter considers movement time to be independent of different amplitude and target precision in any preceding or successive reach segment.

1.3.4 Continuous Movements

Continuous movements involve continuous control or tracking of a certain type of movement with control adjustments made based on changing stimuli associated with the task. In contrast to discrete movements, continuous movements lack recognizable end-points where the hand must reach and maintain zero speed for a distinct period of time. Examples include such activities as operating the steering wheel of a car, tracing a path using a stylus or fingertip, and use a handheld object such as joystick to track a visual target.

To explain continuous movements, Craik (1947) introduced a theory of intermittent control in manual tracking tasks, which generally states humans use an intermittent control mechanism to perform corrective submovements when the tracking error exceeds a certain threshold. One implication of this theory is that intermittent control is dependent on visual feedback. In other words, in open-loop movements when there is no visual feedback, the system should no longer be able to generate error signals to produce corrective submovements. Researchers have tested this hypothesis in manual tracking tasks using a joystick to track a moving target (Miall, Weir, & Stein, 1993). Miall et al. (1993) concluded that control is indeed intermittent in visually guided tracking tasks, and that tracking was significantly smoother if no visual feedback of joystick position is available. Additionally, they found tracking remained intermittent when tracking a memorized target pathway suggesting intermittent control is a sign of feedback control in general, rather than just visual feedback.

Prior research has investigated error and variability in tracking velocity in continuous tracking tasks with and without visual feedback (Liu, Tubbesing, Aziz, Miall, & Stein, 1999). Liu et al. (1999) found an increase in tracking velocity error for conditions without visual feedback of the target and cursor, compared to conditions with visual feedback, and no changes

in tracking velocity among a sample of healthy control participants. This is further evidence suggesting the importance of visual feedback in tracking performance.

1.3.5 Reach Movement Control Models

Various control models attempt to explain the mechanisms underlying aiming movements and Fitts' law, most of which are based on feedback. The theory of intermittent sampling feedback with proportional correction was one of the first (Crossman & Goodeve, 1983; Keele, 1968). This theory proposes that a target-directed reach movement consists of an initial movement followed by a series of corrective movements, based on visual feedback, until the target is contacted. Therefore, movements with a large amplitude or to targets that have small size, have longer movement times because they require more corrections. Thus, the number of corrections the person makes until contacting the target determines the movement time. However, opponents to this theory claim that the time to process error information and form a new movement response is too long for the control of rapid-aimed movements (Schmidt et al., 1979). Alternatively, the impulse-variability theory (Schmidt et al., 1979) suggests variability in impulse forces lead to errors during rapid-aimed movements, where the source of variability could be from errors in motor program selection, the parameters in the motor program related to the index of difficulty, and from random noise.

The stochastic optimized-submovement model is widely cited for explaining the effects of Fitts' Law (Meyer et al., 1988), and is a hybrid between the Crossman-Goodeve model (Crossman & Goodeve, 1983) and the impulse variability model (Schmidt et al., 1979). According to the Crossman-Goodeve model, corrective movements would still occur in a correctly programmed movement to a target. However, studies have shown that corrective movements do not always occur (Langolf et al., 1976). The optimized-submovement model

proposes that an aimed movement toward a target is comprised of a primary submovement and an optional secondary corrective submovement. The initial portion of the aimed movement is controlled by principles of the impulse-variability theory and corrections can be applied to the limb trajectory after the initial movement.

More recently, optimal feedback control has proven to be the dominant model for explaining human motor behavior from a theoretical and practical perspective (Todorov, 2004; Todorov & Jordan, 2002). The optimal feedback control model postulates an underlying control strategy (or control law) for movement behavior that meets some specified performance criterion, with optimal performance being achieved by reducing motor variability in dimensions where accuracy is most needed and allowing variability to accumulate in dimensions that are redundant or task-irrelevant (Todorov & Jordan, 2002). Compared to typical optimal control models of movement behavior that minimize some cost function such as movement time, energy, variance, jerk, or muscle activity, the model of optimal feedback control suggests that the motor system exploits redundancy to achieve high-level goals in a reliable and repeated manner. Thus, redundancy within the motor system such as in terms of speed vs. positional control is not a problem but rather critical to achieving optimal performance on the task outcome.

1.3.6 Relevance to the Current Research

This dissertation research operationalized the sequential reach task as that of routing continuous thread through a system of pulleys that differ in spatial tolerance (e.g., pulley diameter, groove width), horizontal and vertical location (relative to the operator), and sequence (Figure 1.3). The specific contributions of target tolerances, reach movement direction and amplitude on hand trajectory shape and speed during this task are of interest. Further, the ability

of prior motor control models to explain mechanisms in sequential reaches with continuous material are explored.

Previous research investigating hand kinematics in rapid-aimed movements provides a foundation for examining how humans plan and coordinate hand movements in sequential reach tasks with continuous material. Notably, the current task involves aspects of both serial and continuous reaching movements. The motion of reaching to each consecutive target is similar to serial reach in that the hand reaches to successive target locations in a known sequence, with the goal of positioning the material in a pulley groove. However, the operator also needs to continually process information for maintaining tension in the material during the reach and when guiding the material along the groove path, as opposed to a discrete work object where the operator is only concerned with the control of the object in the hand.

Since successive targets differ in location and tolerance, the movement requires on-line control which has the potential to influence hand speed. Besides proprioceptive feedback, visual feedback through line of sight with the target could be hypothesized as important for generating accurate and efficient (i.e., smooth) tracking movements. Therefore, it is possible operators would utilize online control mechanisms in sequential reaches by continuously obtaining feedback about the material location and target position to conduct accurate movements. Routing the thread along the pulley groove is similar to continuous tracking in the sense that the hand movement directed by a specific pathway (e.g., arc-length or wrapping angle along the pulley groove). Thus, the reach movements could be hypothesized to have an accelerating open-loop phase and corrective closed loop phase to position the thread in the pulley groove, and transitioning to a continuous tracking movement of routing the thread along the pulley groove, followed by the next reach movement.

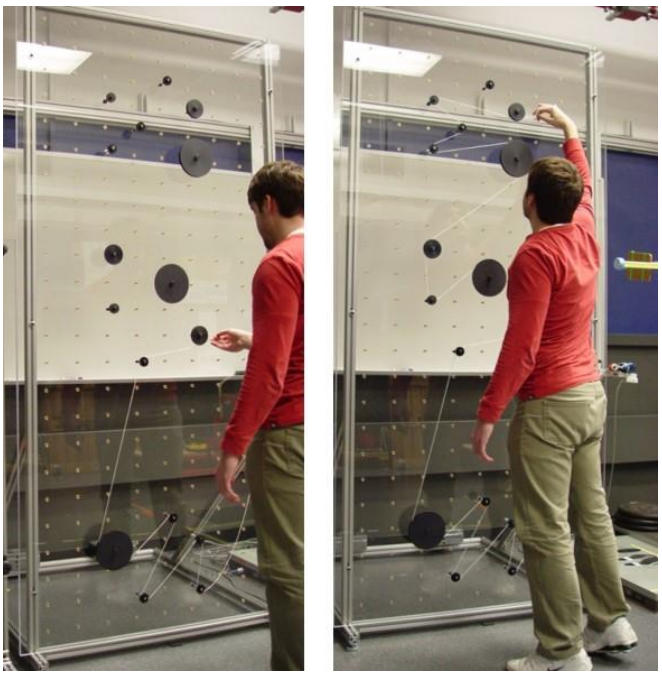

Figure 1.3. Sample images depicting the sequential reach task with continuous material operationalized as routing thread through a system of pulleys that differ in size, tolerance (e.g., groove width), horizontal and vertical location (relative to the operator), and sequence.

The accurate prediction of worker postures and task completion time using DHM tools, is valuable for improving the design of a workplace. Computer-aided ergonomic analysis using DHM and simulation rely on algorithms for predicting the reach motion trajectory in order to then determine pathway clearances, reachability of a target, as well as worker postures using inverse kinematics. Thus, this research is also focused on developing a model to predict reach trajectory shape during sequential reaches with continuous material. Trajectory shape combined with hand speed would allow for estimating task times. Specific to this task, since the hand is continuously in motion (in contrast to discrete reach tasks with zero terminal speed) the speed profiles would also be useful for understanding the underlying motor control mechanisms that

inform movement performance. Thus, an empirically-based model to predict reach movement speed profiles in this task is investigated.

1.4 Conceptual Model

Informed by prior research literature and properties of the task determined from field observations and communications with the industry partner, a conceptual model is proposed that summarizes factors hypothesized to influence performance in a sequential reach task with continuous material (Figure 1.4). Broadly, four categories of factors including the work environment, the material properties, the task parameters, and operator characteristics are considered to influence the operator's movement strategies and resulting task outcomes, namely, reach trajectory path, reach speed profile, and task completion time. For a simplified example, consider a standing, one-handed sequential reach task that involves threading three consecutive pulleys as depicted in Figure 1.4.

Environmental factors, such as the brightness level in the workplace, contrast between the material and work surface, and time pressure constraints placed on the worker, could potentially impact the outcome of the task. **Materials** of different shapes, sizes, elasticity, etc. could influence grasping methods and movement strategies for routing the material through the system of pulleys. However, to simplify the problem, these environmental factors and material properties will be held constant in the experiments throughout this dissertation.

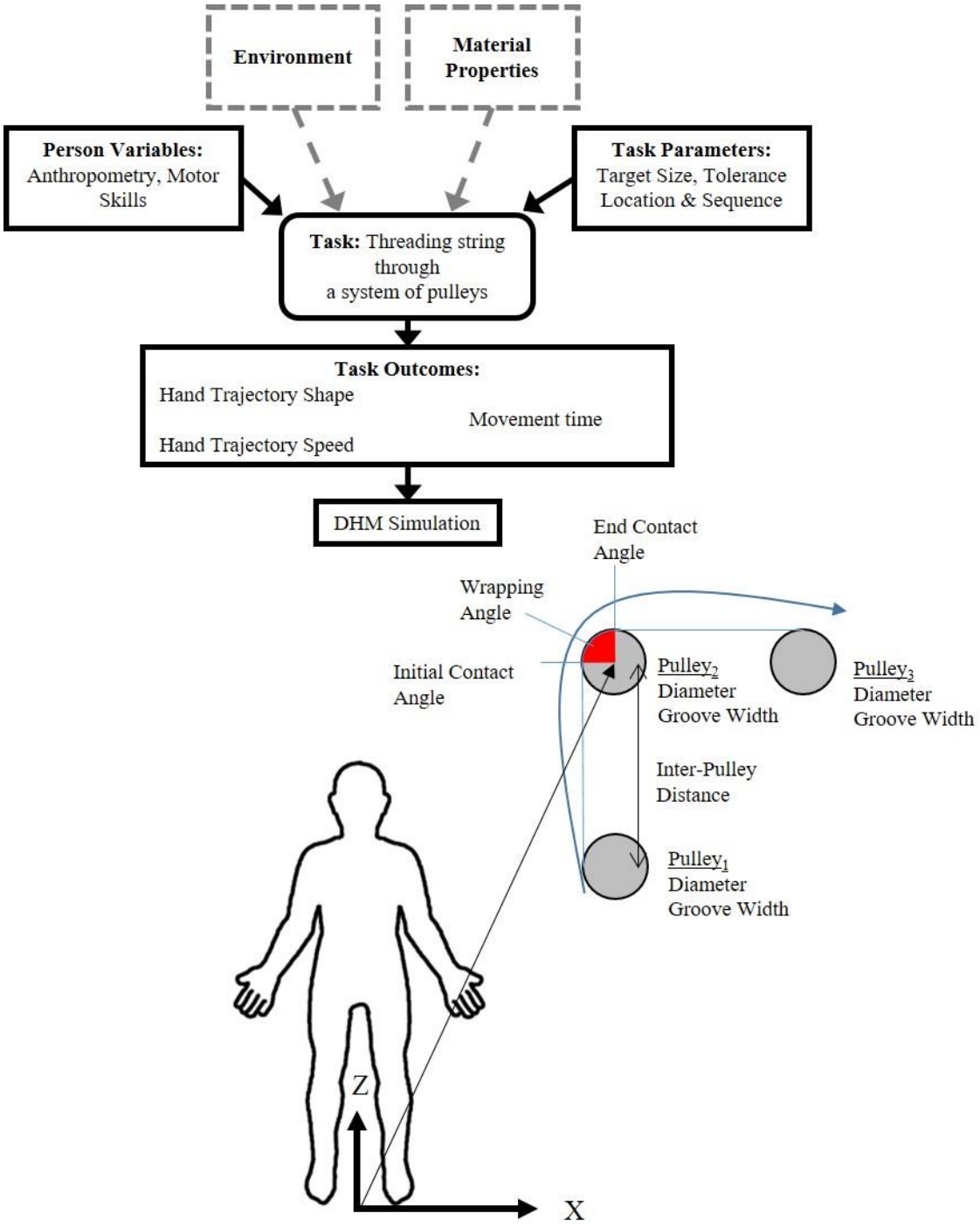

Figure 1.4. Conceptual model of a sequential reach task with continuous material.

Person characteristics, such as anthropometry and motor control skills, may affect how someone will perform the task. For instance, an operator of tall stature will likely have a longer

reach and require less time threading pulleys at extreme height locations than a person of short stature. Additionally, variability in motor skills across people is well known, and there is potential that it can have an impact on the task outcome.

Task parameters are divided into two categories. The first category includes design characteristics of the target. This includes the target tolerance which determines the precision demands, similar to the target width in the Fitts' Law model. The second category includes characteristics about the layout of the targets on the workstation and the threading sequence. Figure 1.4 portrays a schematic of the task setup for threading three consecutive pulleys and identifies task parameters that were hypothesized to influence task performance. The target tolerance correspond to the pulley design parameters (outer diameter and groove width), and the target pulley locations (relative to stature) are in reference to the global origin located at the midpoint of the feet. When threading a specific target pulley, the relative locations of the previous pulley and the next pulley, along with the threading direction, interact to determine the initial and end contact angles of the thread on the pulley groove. The initial contact angle is the included angle measured at the pulley center made by the point on the pulley circumference where the thread will *first* contact the pulley relative to the right-most point on the pulley circumference (i.e., zero degrees). A similar measure is computed for the point on the pulley circumference where the thread will *last* contact the pulley. In Figure 1.4, the second pulley has an initial contact angle of 180º and end contact angle of 90º. The wrapping angle corresponds to the difference between these two parameters. Based on previous research, line of sight or visual feedback availability has a significant effect on performance in target directed reach movement tasks. In this task, the level of visual feedback availability is a function of the initial contact

angle on the target pulley and the azimuth angle of the target pulley relative to the operators' eye location.

1.5 Research Objectives

The overall goal of this research is to model the spatial and temporal properties of a reach movement in a sequential reach task that involves handling continuous material. The outcomes of this research will be predictive models of hand trajectory shapes and a baseline model for predicting speed profiles with respect to specific task parameters. These models are being developed for the purpose of implementation within a DHM framework (Reed, Faraway, Chaffin, & Martin, 2006) as well as furthering our understanding of motor control and performance in sequential reach tasks with continuous material.

1.5.1 Specific Aims

Aim 1: ***Quantify the effects of pulley design parameters and reach movement direction on movement time.***

Hypothesis: Reaching to thread pulleys with smaller tolerances and reduced line of sight with the initial contact point of the thread and pulley groove will be associated with longer movement times and slower hand speeds.

The human factors literature is replete with studies investigating effects of target tolerance and reach movement on performance during discrete reach movements. An initial experiment was conducted to determine if manipulating target tolerance and reach movement influenced movement kinematics in sequential reaches with continuous material. A sample of right- and left-handed participants performed a task that involved threading string through a system of pulleys. Target tolerance was altered by manipulating the pulley diameter and groove width. Reach movement direction was altered by changing the destination pulley location.

Aim 2: ***Develop a model to predict (a) hand trajectory shape and (b) speed profiles in a sequential reach task with continuous material using task parameters as predictors.***

Hypothesis: Target tolerance, reach movement direction and amplitude, and line of sight to the target will influence the shape and speed of reach trajectories.

Factors influencing hand trajectory shape and speed in sequential reach tasks (i.e., where the hand is continually in motion) have not been previously investigated. Trajectory data from multiple experiments will be used to develop a statistical model of trajectory shape and speed with task parameters (target tolerances, target locations and sequence, etc.) as predictors.

Aim 3: ***Empirically validate the predictive model of hand trajectory shape, speed and task completion time in sequential reach tasks with continuous material.***

The ability to predict individual operator performance, in terms of hand trajectory shape, speed, and task completion times, is essential to evaluating and improving workstation design. Current models for predicting movement time and reach trajectory kinematics are limited to discrete aiming and positioning movements, and do not consider the effects of handling continuous material and reaching to sequential targets. The performance of the developed hand trajectory shape and speed model will be evaluated in a validation experiment. These models will allow workstation designers to simulate tasks that involve sequential reach movements with continuous material, and evaluate how the work setup and location of reach targets in novel user-defined configurations impacts task performance.

1.6 Dissertation Organization

This dissertation is comprised of four studies investigating the effects of task parameters on the spatial and temporal properties of hand motions in a sequential reach task with continuous material. **Chapter 2** presents an initial study examining the effects of target pulley design parameters and reach movement direction on movement time (**Aim 1**). **Chapter 3** summarizes 3 data collection experiments to develop and present a novel method for modelling hand trajectory shape in sequential reach tasks (**Aim 2a**). **Chapter 4** presents a method for modeling hand trajectory speed profiles in sequential reach tasks (**Aim 2b**). **Chapter 5** presents an algorithmic framework for combining hand trajectory shape and speed to estimate task completion times, with an empirical assessment of the presented algorithm (**Aim 3**). **Chapter 6** discusses the theoretical and practical contributions of this research and concludes with recommended directions for future research.

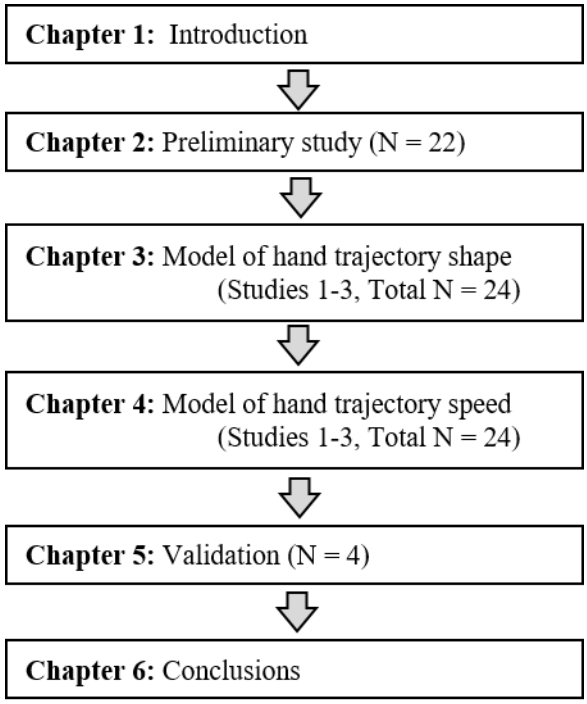

Figure 1.5. Overview of dissertation organization**.**

CHAPTER 2

An Initial Study of Target Precision and Location Effects on Movement Time and Speed in a Sequential Reach Task

Abstract

The human factors literature is replete with studies investigating speed and accuracy during discrete reach movements. Studies quantifying human performance in sequential precision reaches (i.e., the hand remains in motion) while manipulating continuous material are absent. The objective of this study was to determine the effect of target size and tolerance, and reach movement direction on hand speed and movement time in a sequential reach task with continuous material.

Twenty-two participants completed a full-factorial experiment that involved threading string through a sequence of pulleys of 5 radial locations in the frontal plane and in 2 threading directions. Three pulley diameters and 3 groove widths were used. Movement times, minimum hand speeds, and the reach distance past the target pulley during reach movements to each target pulley were analyzed using mixed effects models.

Results demonstrated that the design and location of individual targets in a sequential reach task produced systematic local effects on hand movement kinematics in sequential reaches. Movement time, hand speed and reach distance past the target were influenced by target tolerance and availability of line-of-sight with the initial contact point of the pulley groove. Target pulleys with narrower groove widths and located on the contralateral side of the body

were associated with longer movement times and slower hand speeds. Increasing pulley diameters resulted in longer movement times but did not influence minimum hand speed. Workplace design and locating of targets in sequential reach tasks can take advantage of the fact that certain reach movements can be performed more efficiently than others.

2.1 Introduction

Low force, high precision material handling is a staple of many manual assembly jobs in industry. Examples include the dexterous manipulating and routing of continuous material such as thread in textile manufacturing or electrical wire in automobile and wire harness assembly. Constraints in the work environment such as high precision, time pressure, occluded line of sight, hard to reach target locations, and limited hand clearance place additional demands on human performance, particularly on accuracy and speed (i.e., completion times). To date, a substantial amount of human factors research has focused on the effect of task parameters on movement times in one-handed discrete reach movements. To our knowledge, no study has investigated sequential reach movements that involve transporting light-weight continuous material. Improving workstation design for efficient routing of continuous material requires a systematic investigation of the impact of task demands on hand kinematics and completion times.

The motivation for this study was derived from textile manufacturing where operators manually route continuous material (e.g., threads, films or webbing) through a system of pulleys in order to prepare machinery for operation. The routing task involves operators performing sequential reach movements to multiple target locations in a particular sequence around a workstation. This task is performed routinely when loading new material stock at each assembly line, at startup, and during general maintenance tasks. Inefficiencies in this routing process (i.e.,

excessive time, missed targets) can cause line stoppages. In the case of routing thread, pulleys of different diameter and groove sizes that guide and tension the continuous material, serve as reach targets. From an operational viewpoint, pulley design characteristics have the potential to impact process efficiency. For instance, the groove width and depth must be sufficient to support the material under tension and avoid the material from slipping out of position. Increasing arc length contact will increase frictional force between the conveyor belt and pulley, which is important if traction is necessary. Understanding the effects of target tolerances (e.g., pulley diameters, groove widths, arc of contact) and layout (e.g., target locations, sequence) on operator performance (e.g., task completion time, reachability) while manually routing material through successive pulleys is critical for production planning and for improving equipment design.

Target tolerance defined by target size and precision requirement is known to influence movement time in discrete target-directed aiming tasks, as characterized by Fitts' law (Fitts, 1954). However, the effect of target tolerance on movement time in sequential reaching tasks with continuous material is not well understood. Sequential reach movements with continuous material differ from discrete pointing tasks due to other intrinsic task properties. In a sequential threading task, one must reach to multiple targets of different sizes and precision. Controlling the thread during the reach movement and positioning it within the target constraints increases the complexity of the task and requires visual feedback. The amplitude of the movement may vary depending on the target location and sequence in the operators workspace. Since the goal is to position material within the constraints of the target tolerance the task requires the operator to reach past the target pulley, which increases the effective reach distance for the task. This is very different from discrete reach tasks, where the end goal is to contact the target with a finger or stylus. Reach movement direction and threading direction can interact to cause line of sight

issues. The hand is continually in motion, hence initial and final hand speeds between two consecutive targets could differ across conditions.

The objective of this study was to quantify the effects of pulley groove width (GW) and outer diameter (OD), target location (azimuth angle), and threading direction (clockwise vs. counter-clockwise) on movement time (MT), minimum hand speed and effective reach distance during movements to each successive target pulley in a sequential reach task with continuous material. Pulley groove width and outer diameter were considered to affect target tolerance. Target pulley location was considered to influence reach movement direction. Threading direction was considered to affect the line of sight to the pulley groove at the point of contact with the thread. The study hypothesized longer movement times, slower hand speeds, and shorter reach distances when reaching to thread pulleys with smaller tolerances and reduced line of sight with the initial contact point of the thread and pulley groove.

As an initial investigation, this study proposed segmenting sequential reach tasks into discrete movements between two consecutive target locations in order to quantify and compare the effects of intermediate targets in a continuous movement. Demonstrating these effects were also considered important in order to prove the ability of the experimental set-up to elicit movement behaviors characteristic of sequential reaches, towards developing statistical models of reaching movement in subsequent chapters.

2.2 Experiment 1: Methods

2.2.1 Participants

Twenty-two young adults (12 right-handed and 10 left-handed) were recruited from the university student population to participate in a laboratory experiment. All participants were free of any neurological and musculoskeletal disorders, had normal or corrected 20/20 visual acuity,

and had no prior experience performing the task. The experiment was approved by the university's institutional review board and written informed consent was obtained from participants prior to the study.

2.2.2 Experiment Setup

Participants performed a one-handed sequential reach task that involved transferring thread between successive target pulleys in a predefined sequence and wrapping the thread along a groove on the circumference of each target pulley. Targets consisted of black nylon pulleys situated on a transparent acrylic panel (1.49 m x 1.49 m) oriented vertically so that all pulley axes were horizontal and parallel. The pulleys were custom-made to specific combinations of pulley outer diameters (i.e., 38-mm, 76-mm, and 152-mm) and groove widths (i.e., 3-mm, 6-mm, and 9-mm) (Figure 2.1). The pulleys had a constant groove depth of 6-mm.

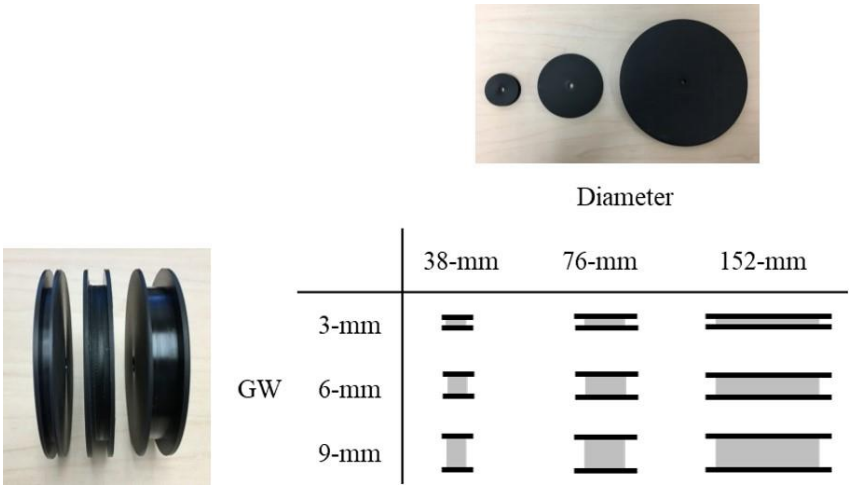

Figure 2.1. Cross-sectional view of the target pulleys depicting combinations of pulley outer diameter (OD) and groove width (GW) used in the experiment.

Figure 2.2 depicts the experiment set-up. Each threading sequence consisted of five target pulleys located on the perimeter of a semicircle with a radius of 46-cm at azimuths of 0° (right) ,

45° (upper-right) , 90° (up), 135° (upper-left), and 180° (left) relative to a constant origin pulley located at the center, which had a 30-mm OD and a 37-mm GW. The height of the origin pulley from the floor was normalized to each participants' standing elbow height. Participants stood at a comfortable distance away from the board with the midline of their torso aligned with the center origin pulley. They were allowed to self-select body postures and movements during the threading trials. The thread (100% polyester, Coats & Clark, Dual Duty XP Heavy Thread) was pulled from a fishing reel (Shakespeare Alpha Baitcasting Reel) clamped onto the right edge of the board. The reel was fixed to the "cast" setting to allow the thread to unspool freely with no drag during the threading task.

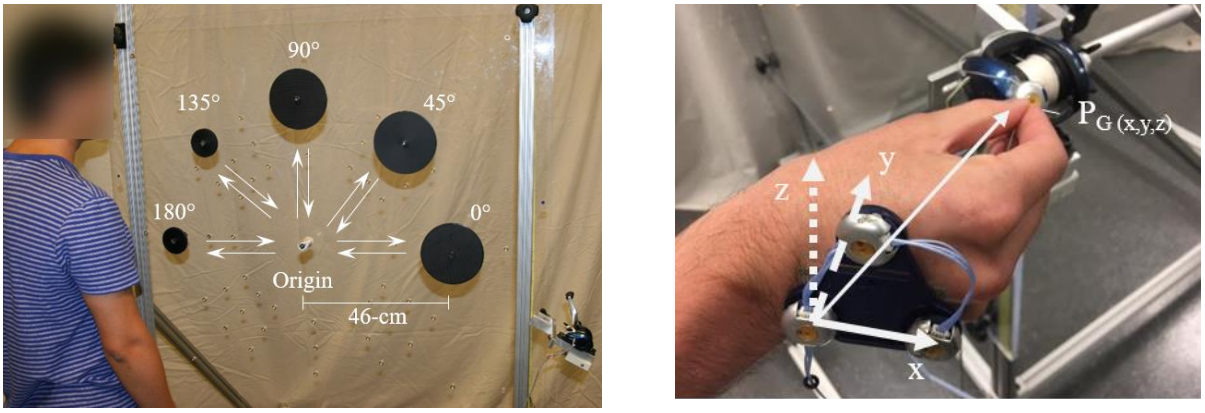

Figure 2.2. (Left) Experiment apparatus and setup for a right-handed participant. (Right) Pretest calibration pose to estimate the location of thread-fingertip contact position (P_G) using a motion capture marker triad.

2.2.3 Experiment Design

Four within-subject factors were varied in this experiment: pulley OD (3 levels: 38-mm, 76-mm, and 152-mm), pulley GW (3 levels: 3-mm, 6-mm, and 9-mm), target pulley location (5 levels: 0°, 45°, 90°, 135, and 180°), and threading direction around the pulleys (2 levels: CW and

CCW). Each participant performed three repetitions of the 90 (= 3 x 3 x 5 x 2) conditions yielding a total of 270 threading trials per participant.

2.2.4 Procedure

The threading sequence was constant throughout the experiment. The target pulley order depended on the participant's handedness, with the first target pulley corresponding to the target pulley located on the contralateral side of the body at elbow height. For right-handed participants, the sequence order by pulley location was origin-180°-origin-135°-origin-90°-origin-45°-origin-0°-origin (Figure 2.2). For left-handed participants, the sequence order by pulley location was origin-0°-origin-45°-origin-90°-origin-135°-origin-180°-origin. Participants were instructed to complete the task as quickly as possible but to primarily focus on accuracy, i.e., threading all of the pulleys successfully. The presentation order of the pulley OD and GW and the threading direction was counterbalanced to include every combination of these parameters. A 30sec interval between trials was provided for rest and change-up of pulleys. Six practice trials were provided (3 in the CW threading direction and 3 in the CCW threading direction) prior to data collection to familiarize participants with the task.

2.2.5 Instrumentation and Data Processing

An optical motion capture system (Qualisys, Göteborg, Sweden) was used to measure hand movements at a sampling frequency of 120 Hz. An active-marker triad located on the back of the participants' right hand (Figure 2.2) tracked hand motions during the threading task. Video of all trials was recorded from a sagittal and frontal anterior view of the participant using two conventional video camcorders. A qualitative video analysis was performed on the frontal and sagittal video recordings to give insights into any observable patterns in postural changes during the experiment task.

Each trial began with the participant grasping the end of the thread with their right/left hand using a thumb-forefinger pinch grip. The participant then performed a calibration pose by holding the thread end next to a motion capture marker on the reel for 3-seconds. Assuming a rigid grasp posture, the global position of the thread finger-tip contact point (P_G in Figure 2.2) during the trials was estimated from motion capture data using Equation 2.1:

$$\begin{bmatrix} P_{G,x} \\ P_{G,y} \\ P_{G,z} \\ 1 \end{bmatrix} = \begin{bmatrix} u_{x1} & u_{x2} & u_{z1} & origin_x \\ u_{y1} & u_{y2} & u_{z2} & origin_y \\ u_{z1} & u_{z2} & u_{z3} & origin_z \\ 0 & 0 & 0 & 1 \end{bmatrix} \begin{bmatrix} P_{L,x} \\ P_{L,y} \\ P_{L,z} \\ 1 \end{bmatrix}, \qquad [2.1]$$

where P_G represents the global position of the thread fingertip contact point, u is the unit vectors of the local coordinate system defined by the marker triad, *origin* is the global position of the marker triad's local coordinate system origin, and P_L is the position of the thread-fingertip contact with respect to the local coordinate system. P_L corresponds to the position of the marker located on the reel during the 3sec calibration pose.

Three-dimensional coordinate data were filtered using a 2nd-order zero-lag low-pass Butterworth filter with a 6-Hz cut-off frequency. Two-dimensional position data in the frontal plane (i.e., parallel to the panel) was computed and used in the analysis. Left-handed 2-D data was rotated 180° about the superior-inferior axis to align it with the right-handed participant coordinate system. For example, the 180° Location and CW threading direction condition for left-handed participants corresponded to the 0° Location and CCW threading direction after rotation. Data were processed using Matlab 2016b.

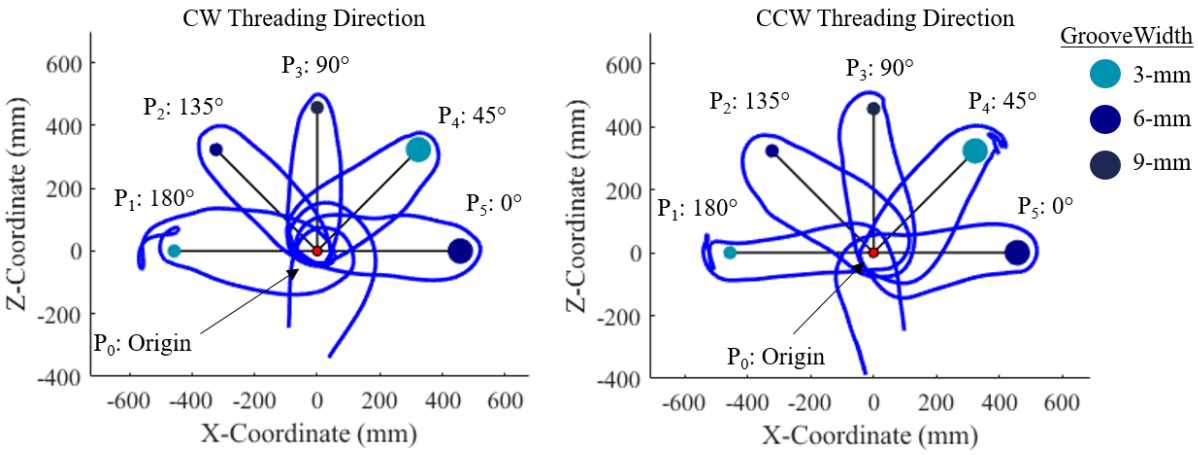

Figure 2.3. Exemplar measured finger-tip trajectory from a right-handed participant for one threading trial in the clock-wise (left panel) and counter-clockwise (right panel) direction at each target pulley.

2.2.6 Data Reduction

Each motion trial was segmented into five origin-target threading tasks based on the five pulley locations. Movement Time (*MT*) for reaching from each origin to target pulley corresponded to the time point at which the fingertip trajectory first crossed the tangent line connecting the pulleys at the origin and the last time it crossed the tangent line at the target (Figure 2.4). The straight-line distance (D_T) from the end of the reach movement to the target pulley center was calculated from the 2D position data to capture the overshoot distance unique to this threading task. The normalized distance $\%D_T$ (where, $\%D_T = D_T$ / target pulley radius x 100%) was used for data analysis. Initial speed (S_0) and absolute minimum speeds (S_{min}) were obtained from the resultant fingertip speeds calculated using finite differences on the 2D position data. Minimum speed, S_{min} was considered to be more informative of capturing movement kinematics at/near the target pulley, and aligned with the focal research question of this study. Maximum speed was intentionally excluded from the analysis. Further, a preliminary analysis showed that maximum speed did not vary across conditions because it was largely influenced by

the wide-groove pulley at the origin and movement amplitude (i.e., inter-pulley distance), both of which were held constant in this experiment.

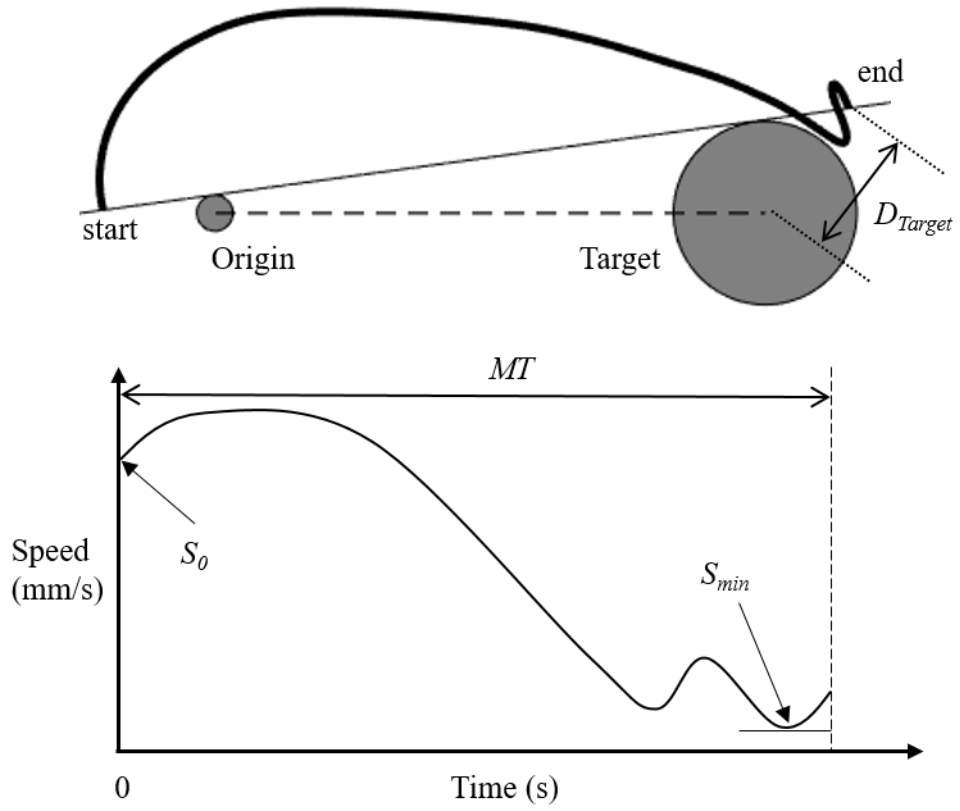

Figure 2.4. Schematic of the segmented trajectory and variables extracted for analysis. The sample trajectory shows a corrective movement at the end indicating a missed threading on the first attempt. Movement time corresponds to the instant the trajectory crosses the tangent line at the origin pulley to the last time the trajectory crosses the tangent line at the target pulley.

2.2.7 Statistical Data Analysis

All statistical analyses were performed with IBM SPSS version 24. Four mixed effects models were run to test for the main effects of Handedness (Right vs. Left), Location (0°, 45, 90°, 135°, 180°), GW (3-mm, 6-mm, 9-mm), OD (38-mm, 76-mm, 156-mm), Direction (CW vs. CCW), and all two-way interactions on dependent measures of *MT*, S_{min}, and $\%D_T$. Initial speed,

S_0, was included as a covariate in the models to account for differences in hand speed at the start of the reach movement. Significant main and interaction effects were investigated using Bonferroni pairwise comparisons. Statistical significance was set at $p < 0.05$.

2.3 Results

The mean (± SD) age, stature, and mass of participants in the study are listed in Table 2.1. Results of the mixed effect models for MT, S_{min} and $\%D_T$ are summarized in Table 2.2. The qualitative video analysis showed that participants remained aligned with the center origin pulley throughout the task. However, side-stepping and torso leaning were observed for threading the 180° Location in the CW direction.

Table 2.1. Mean (± SD) age, stature, and body mass for the study sample stratified by handedness.

Handedness	N (Men, Women)	Age, years (Mean ± SD)	Stature, cm (Mean ± SD)	Mass, kg (Mean ± SD)
Right	12 (5, 7)	22.5 ± 2.2	168.5 ± 8.6	72.0 ± 17.5
Left	10 (6, 4)	22.7 ± 2.2	172.4 ± 7.7	69.3 ± 13.0
Combined	22 (11, 11)	22.6 ± 2.2	170.2 ± 8.2	70.8 ± 14.3

Table 2.2. Mixed Effects model results for Movement Time (*MT*), Minimum Speed (S_{min}), and Normalized Distance from Target ($\%D_T$)

		MT		***S_{min}***		***$\%D_T$***	
Factor	DOF	F stat.	*p*-Value	F stat.	*p*-Value	F stat.	*p*-Value
Intercept	1	1086.3	< **0.001**	87.5	< **0.001**	961.977	< **0.001**
S_0	1	158.3	< **0.001**	66.9	< **0.001**	23.580	< **0.001**
Handedness	1	0.2	0.688	0.0	0.955	5.944	**0.023**
Location	4	50.4	< **0.001**	125.8	< **0.001**	117.754	< **0.001**
OD	2	27.3	< **0.001**	4.3	**0.014**	1617.624	< **0.001**
GW	2	175.4	< **0.001**	411.8	< **0.001**	7.461	**0.001**
Direction	1	293.0	< **0.001**	212.2	< **0.001**	0.325	0.569
Location * OD	8	2.4	**0.015**	3.3	**0.001**	16.438	< **0.001**
Location * GW	8	1.8	0.068	4.7	< **0.001**	0.891	0.524
Location * Direction	4	11.9	< **0.001**	17.3	< **0.001**	11.922	< **0.001**
OD * GW	4	14.4	< **0.001**	2.1	0.078	7.586	< **0.001**
OD * Direction	2	3.5	**0.029**	1.9	0.147	1.695	0.184
GW * Direction	2	2.6	0.077	4.1	**0.016**	1.465	0.231
	Note: Bolded *p*-values represent significant effects						

2.3.1 Movement Time, MT

Location, OD, GW, and Direction had a significant effect on *MT* (Table 2.2). *MT* was significantly shorter when threading pulleys in a counterclockwise direction (1667 ± 61 ms) compared to the clockwise direction (2010 ± 61 ms, $p < 0.001$). *MT* was significantly longer when reaching to locations at 180° (2079 ± 64 ms) and 135° (1929 ± 64 ms) compared to the 90° (1689 ± 63 ms, $p = 0.001$), 45° (1738 ± 63 ms, $p < 0.001$), and 0° (1757 ± 85 ms, $p < 0.001$) locations. *MT* at the 90°, 45°, and 0° locations were not significantly different.

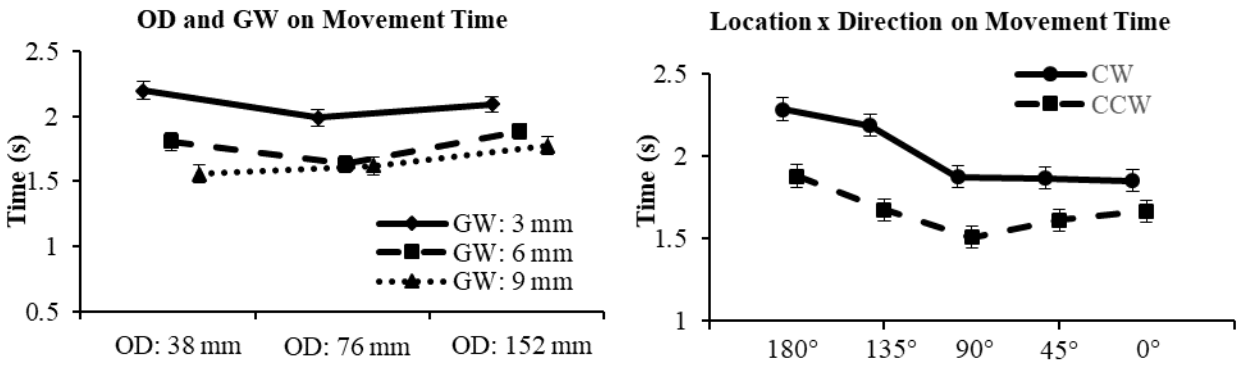

Figure 2.5. (Left) Estimated marginal means (± standard error) for movement times by OD and GW (left), and location and direction (Right), at average values of initial speed, S_0 = 557 mm/s.

The two-way interactions of OD by GW, Location by Direction, and OD by Direction on *MT* were statistically significant (Table 2.2). The trends in *MT* across Location for the clockwise and counter- clockwise Threading Direction are shown in Figure 2.5. For the clockwise direction, *MT* decreased as Location changed from 180° to 0°, i.e., contralateral to ipsilateral side. For the counter-clockwise direction, *MT* was shortest at the 90° Location and increased as Location changed from 90° to 180° and 90° to 0°. Overall, a wider GW corresponded to shorter *MT* (9-mm: 1649 ± 61 ms, 6-mm: 1775± 61 ms, 3-mm: 2092 ± 63 ms). An increase in OD corresponded to an increase in *MT* for the 9-mm GW. Average *MT* was shortest for the pulley with 38-mm OD and 9-mm GW. Average *MT* was longest for the pulley with 38-mm OD and 3-mm GW.

2.3.2 Minimum Speed, S_{min}

S_{min} differed significantly by main effects of Location, GW, OD, and Direction (Table 2.2). Pairwise comparisons showed that S_{min} was significantly faster for the 9-mm GW (194 ± 12 mm/s) compared to the 6-mm GW (155 ± 12 mm/s, $p < 0.001$), and in turn, faster for the 6-mm compared to the 3-mm GW (100 ± 11 mm/s, $p < 0.001$). S_{min} was significantly slower when

threading pulleys in the CW (128 ± 11 mm/s) vs. CCW direction (171 ± 11 mm/s, $p < 0.001$). S_{min} showed an increasing trend as location changed from the contralateral side to the ipsilateral side of the body (i.e., 180° to 0°) for both the CW and CCW Directions (Figure 2.6, left). S_{min} for target locations of 45° and 0° were not significantly different. S_{min} varied marginally by pulley OD. Pairwise comparisons showed that S_{min} was slower for the 38-mm OD (144 ± 11 mm/s) compared to the 76-mm OD (151 ± 12 mm/s, $p = 0.019$)

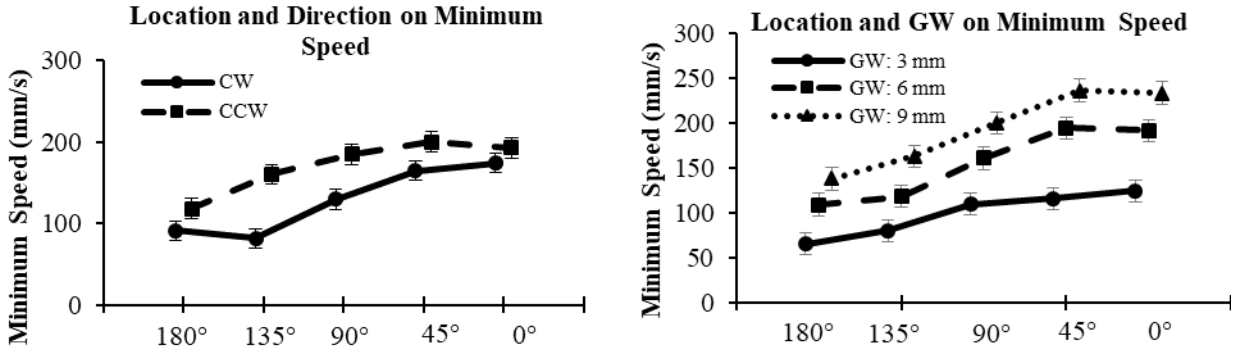

Figure 2.6. Estimated marginal means ± standard errors for minimum speed by Location and Direction (Left), and Location and Groove Width (right), at average values of initial speed, S_0 = 557 mm/s.

Analysis indicated significant interactions of Location by Direction, Location by GW, Location by OD, and GW by Direction on S_{min}. The interaction effects of Location by Direction and Location by GW interactions are shown in Figure 2.6. Though the Location by OD interaction effect was significant, the overall trends were similar as the individual main effects with the exception of no significant effect of OD on S_{min} at the 135° and 90° Locations.

2.3.3 Normalized Reach Distance from Target, $\%D_T$

$\%D_T$ differed significantly by Handedness, Location, OD, and GW (Table 2.2). Overall, $\%D_T$ significantly increased with decreasing OD (139 ± 6% at 38-mm OD < 204 ± 6% at 76-mm OD < 357 ± 7% at 152-mm OD). This trend was observed at all levels of GW.

There was a significant interaction between Location and Direction on $\%D_T$ (Table 2.2). $\%D_T$ was largest for the CCW Direction at the 180° Location (300 ± 8%). In general, $\%D_T$ decreased as Location changed from 180° to 0°, i.e., contralateral to ipsilateral (Figure 2.7). $\%D_T$ significantly increased in the CW vs. CCW Direction at 135° ($p = 0.003$) and significantly less at 180° ($p < 0.001$).

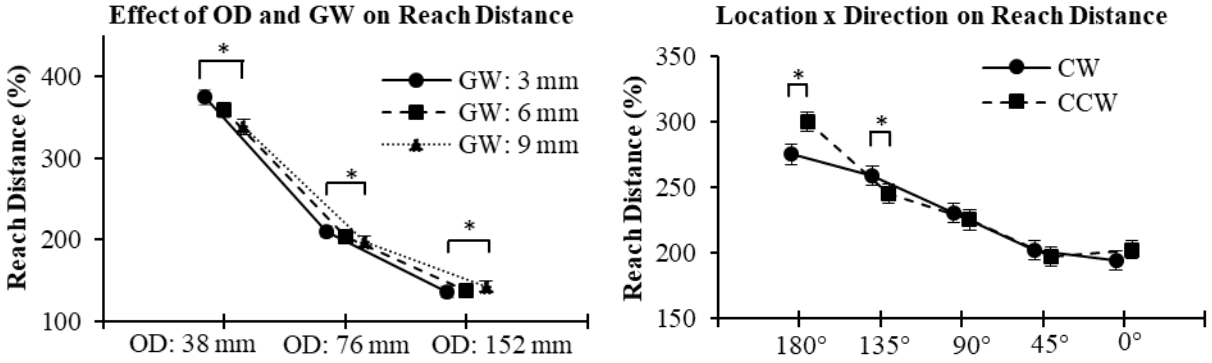

Figure 2.7. Estimated marginal means ± standard errors for Reach Distance by Diameter and Groove Width (Left), and Location and Direction (right), at the average initial speed, S_0 = 557 mm/s.

2.4 Discussion

This study examined the effects of pulley groove width and diameter, reach movement direction, and threading direction on hand kinematics and movement times in a sequential reach task with continuous material. Notably, the findings indicate that target pulley parameters had systematic local effects on movement kinematics even as the hand was continually moving.

Shorter movement times were obtained when reaching to target pulleys with wider groove widths and smaller diameters, and when reaching to pulleys located on the ipsilateral side of the body (i.e., 0° and 45°) compared to the contralateral side (i.e., 180° and 135°). Likewise, minimum hand speeds were higher when reaching toward pulleys with a wider groove width and when located on the ipsilateral side of the body. Unique to this task, participants had to reach past the target pulley to ensure visibility with the pulley-thread point of initial contact. As a proportion of pulley diameter, participants reached further past pulleys with smaller diameters and when pulleys were located on the contralateral side of the body.

Overall, the study findings were consistent with research on discrete positioning tasks in the Fitts law paradigm wherein average movement times increase with lower target tolerance and larger movement amplitude, with their combined effect represented in the dimensionless Index of Difficulty (Fitts, 1954; Langolf et al., 1976). In the present study, reach amplitude (i.e., inter-pulley distance) was held constant, while target tolerance characterized by pulley groove width was manipulated with narrower groove widths representing lower target tolerances. However, the present study findings indicated that the relationship between movement time and target tolerance was modified by additional task parameters such as pulley diameter, location, and threading direction intrinsic to this sequential threading task.

In this study, movement time was longer for reach movements to pulleys located on the contralateral side. The results showed reach movements to the 180° pulley location and threading in a CW direction proved to be the most difficult condition. For this condition, participants did not have a direct line of sight with the initial contact point of the pulley groove. Video analysis gave insight into postural changes in the task. Participants used compensatory strategies, such as trunk rotation, contralateral torso leaning, or side-stepping, to improve visual and manual access

to the pulley groove. When line of sight was initially available, such as when threading pulleys located at 0° in a CW direction, movement times were comparatively shorter and the hand was able to achieve a higher speed. These findings align with findings from a study by Murata and Iwase (2001) on the effect of movement azimuth direction on movement time in a 3D pointing task. Murata and Iwase (2001) reported longer movement times for reach movements directed toward targets located on the contralateral side compared to the ipsilateral side. However, in their study, the movements directed vertically upward (90° azimuth angle) took the longest time. In the current study, transferring and positioning thread within the groove at the target destination increased the precision demands of the task compared to simple pointing and may explain this difference in findings.

In a different study on pointing tasks, Bertucco et al. (2013) found increases in movement time to a target located on the contralateral side, 100-cm from the midline, compared to 65-cm away. They concluded that pointing movements performed while rotating the trunk were associated with Coriolis forces that perturbed planned hand trajectories leading to longer movement times. In this experiment, reaches to the target locations on the contralateral side required trunk rotations, which could explain the longer movement time when reaching toward targets on the contralateral side compared to the ipsilateral side.

Reach distance past the pulley provided additional evidence of participants' attempt to obtain line of sight with the pulley-thread point of initial contact, particularly when the hand or forearm may occlude the target pulley. Specifically, participants opted to reach further past the pulley at locations on the contralateral side compared to the ipsilateral side. This reach distance measure has direct implications for hand clearances during threading, and further supports the

need to model hand trajectories in sequential threading tasks with continuous material since actual reach distances may only partially be influenced by inter-pulley distance and pulley OD.

Similar modifying effects of task parameters on performance were obtained on minimum speed when approaching the target pulley. The effect of groove width on minimum speed was prominent on the contralateral side of the body. Minimum speed was higher on the ipsilateral side, compared to the contralateral side, for the wider groove widths but not the narrowest. This suggests narrow groove widths hinder performance regardless of proximity to threading hand. Pulley diameter had less of an effect on movement time and hand speed. We found increases in movement time with an increase in diameter and no difference in minimum speed. The increase in movement time could be explained by the increase in reach distance between the tangent line crossings for the largest pulley diameter.

This study provides preliminary insights into motor control methods for handling continuous material in sequential reach movements. Previous motor control models have focused largely on rapid-aiming movements in discrete reach tasks (Meyer et al., 1988; Schmidt et al., 1979). Consistent with these models, findings in the present study provide evidence of a speed-accuracy tradeoff when performing the reach movement. Woodworth (1899) first proposed that discrete reach movements are controlled by an initial impulse phase, under open-loop control, followed by a second current control phase, i.e. “homing” phase that is under feedback-based control. Analysis of minimum speed in this study indicated systematic decelerations occurring when approaching the target pulley. Determining if sequential reach movements are comprised of a combination of open-loop and closed-loop motor control phases would require analysis of speed profiles. It is possible the hand may operate under closed-loop control throughout the threading task. For instance the participants may try to maintain a certain level of tension in the

thread as they transfer it causing variations in speed. This topic is investigated in more detail in Chapter 4.

2.4.1 Practical Implications

Findings from this study have implications for workstation design for tasks that involve continuous material handling. The reach distance parameter (i.e., distance past the target pulley during threading) provides valuable information about the amount of clearance space around the pulley should be provided. The study provided initial insight into how task parameters effect movement times, and guidance for subsequent studies on the task parameters (e.g., reach direction, line of sight) that might influence predictions of hand trajectory shape, speed, and movement times. Understanding the influence of task parameters on movement kinematics and task completion time is beneficial from a workstation design perspective. Workplace design and locating of targets in sequential reach tasks can take advantage of the fact that certain reach movements can be performed more efficiently than others. Workstation designers can make decisions about target precision requirements, target locations, and the extent of hand clearance space needed to increase operator performance (i.e., time-efficiency, reachability) while also satisfying operational needs and constraints.

2.4.2 Methodological Limitations

This study was limited by a few factors. First, the study did not manipulate the diameter and groove width of the origin pulley and it had a very low precision requirement, which partially explains the differences in initial speeds across the task conditions. Participants were able to quickly wrap their hand around the pulley without slowing down. Therefore, the hand reaches a peak speed at an earlier moment at the beginning of the reach movement and then gradually slows down. Secondly, the study does not directly track the location of the thread-

fingertip contact point because we were unable to place a reflective marker on the fingertip without interfering with the task. Instead, fingertip location was estimated from a pre-trial calibration pose with the assumption that participants maintained a grasp similar to the pretest calibration pose throughout each threading trial. While it is possible for the operation to change their hand posture, video observations in this study did not provide evidence of any re-grasping during the threading trial. In this study, the distance between consecutive pulleys (46-cm) was the same for each participant. Therefore, participants of short stature and/or short arm length may have experienced a slight disadvantage. Lastly, this study segmented the continuous hand trajectories in a sequential reach task into discrete components. Subsequent chapters investigate methods for retaining to continuous nature of the movement data in the analysis of trajectory shape (Chapter 3) and speed (Chapter 4).

2.5 Conclusion

This study investigated the effects of pulley groove width and diameter, reach movement direction, and threading direction on task performance in a one-handed standing sequential reach task. These factors has systematic effects on the time to reach to and thread a target pulley. The pulley tolerance, defined by the groove width and diameter, and line of sight availability with the pulley groove were the primary factors that influenced movement time. Participant's performed faster movements for conditions that had a wider groove width and smaller diameter and when visual feedback was initially available. In other conditions, participants were observed to adapt their posture by leaning to the side or taking a side step, in order to obtain a line of sight to the target pulley groove. Importantly, for the purposes of subsequent modeling of sequential reaches the study findings demonstrated that task performance in sequential reaches is influenced locally

by individual target precision demands, reach direction (i.e., laterality), and line of sight demands.

CHAPTER 3

Hand Trajectory Shape: Model Development and Assessment

Abstract

The effects of target characteristics and target sequence on hand trajectory shape in a sequential reach task with continuous material have not been previously quantified. This chapter presents a statistical model for predicting continuous hand trajectory shapes in a sequential reach task with continuous material using task parameters (e.g., target characteristics, target locations and sequence) as predictors. Three data collection experiments were conducted yielding hand trajectory data for 9396 motion trials that involved threading target pulleys across combinations of task parameters representing pulley characteristics, reach direction and line of sight availability. The modeling approach proposed involved segmenting the continuous hand trajectory to sequential targets into two alternating phases: (1) a *transition* phase when the hand is reaching between two consecutive target pulleys, and (2) an *interaction* phase when the hand is engaged in threading a target pulley. B-splines were fit to the segmented data from each phase. Multiple regression was used to predict b-spline control point coordinates using task parameters as predictors. Root mean squared errors (RMSE) between predicted and measured trajectories were analyzed to assess model performance (31 ± 16 mm).

Study findings demonstrate the feasibility of modeling sequential reaches as a series of alternating transport and target interaction phases. The regression models developed quantify the

effects of task parameters on spatial properties of sequential reach trajectories, and are compatible for integration into a digital human modeling framework.

3.1 Introduction

Predicting reach motion trajectory is important in computer-aided ergonomic analyses for determining pathway clearances and reachability to a target. Accurate prediction of reach postures using digital human modeling (DHM) tools allows engineers to assess worker postures and task completion times toward identifying ergonomics problems, improve the design of equipment, and developing work performance standards. Sequential reach tasks are a common component of manual assembly jobs that involve handling continuous material, such as thread or wire. Sequential reaches involve reaching to multiple target locations in a particular sequence around a workplace. However, DHM currently lack the capability of simulating tasks that require manipulating continuous material limiting the ability of engineers to evaluate such jobs for pathway clearances, reachability, and task completion times. Developing data-driven models for simulating reach motion trajectories is a critical step to improving such analysis capabilities.

3.1.1 Research Background

Different methods for predicting operator postures and motions in dynamic reach movement tasks exist, including methods based on inverse kinematics (Jung, Kee, & Chung, 1995; Wang, 1999; Wang & Verriest, 1998), differential inverse kinematics (Zhang & Chaffin, 2000), and optimization techniques (Flash & Hogan, 1985). In these models, the final position of the hand is constrained and optimization techniques are used to minimize specific characteristics about the movement to solve the kinematic redundancy problem, which occurs when the number of degrees of freedom of a biomechanical system exceeds what is needed to perform the movement. For example, Flash and Hogan (1985) proposed minimizing jerk, defined as the rate

of change of acceleration. This produces a straight line hand trajectory between the initial position and target location. However, hand trajectories are generally curved over movements of larger amplitude. Similarly, Uno, Kawato, and Suzuki (1989) proposed minimizing change in torque throughout the movement.

Another technique for modeling reach movements is using motion capture technology to measure hand motions, and fitting basis-splines (b-splines) to the observed trajectories (Faraway, 2000; Faraway & Reed, 2007; Faraway, Reed, & Wang, 2007). B-splines have been used to model hand trajectories in various seated reach tasks (Faraway, 2000; Faraway et al., 2007) and for trajectories of the head, spine, and pelvis in low- speed automatic impacts (Samuels, Reed, Arbogast, & Seacrist, 2016). B-splines use control points to determine the shape of a curve. The degree of the fitted curve and number of control points determine goodness of fit to the observed trajectory. Statistical analysis is performed to make estimations on control point locations given a variety of input parameters (e.g. subject anthropometry, target location, and other task parameters).

However, previous studies implementing this method were limited to modeling trajectories in discrete reach movement tasks where the end of the reach movement has a distinct location and the end effector is stationary at the start and end of the reach movement (i.e., zero speed). In the current study, the sequential nature of the reach task presents a unique challenge because the task has multiple phases and with the hand continually moving with varying speed. The previous Chapter 2 provided preliminary evidence of such differences in movement time and speed associated with target characteristics and reach direction. Further, the effects of target characteristics and target sequence on hand trajectory shape in such sequential reach tasks with handling continuous material have not been previously quantified.

3.1.2 Objective

This chapter presents a methodology for predicting hand trajectory shape using b-splines in a sequential reach task with task parameters as predictors. The sequential reach task was operationalized as a threading task with participants threading pulleys with continuous thread in a defined sequence. The study hypothesized target tolerance, reach movement direction and amplitude, and line of sight to the target to influence the shape of reach trajectories. In order to obtain a generalizable reach trajectory shape model, multiple task parameters were systematically manipulated in 3 data collection experiments to obtain a diverse data set of reach motions measured using optical motion capture.

3.2 Data Collection Methodology

Based on a literature review (Chapter 1) and preliminary work (Chapter 2), this study hypothesized multiple task parameters to have an effect on hand trajectory movements including target characteristics (e.g., pulley diameter, groove width, and wrapping angle), reach direction and amplitude (i.e., target location relative to the operator, co- vs. counter rotating threading direction between pairs of pulleys, inter-pulley distance) and availability of line of the sight to the target (e.g., initial contact angle on the pulley groove).

Given the large number of potential task parameters three data collection experiments were conducted, each experiment focusing on a sub-set of task parameters, and the data subsequently aggregated for model development. Table 3.1 provides an overview of the task variables operationalized as parameters or independent variables in each experiment. Figure 3.1 provides a graphic representation of these task parameters.

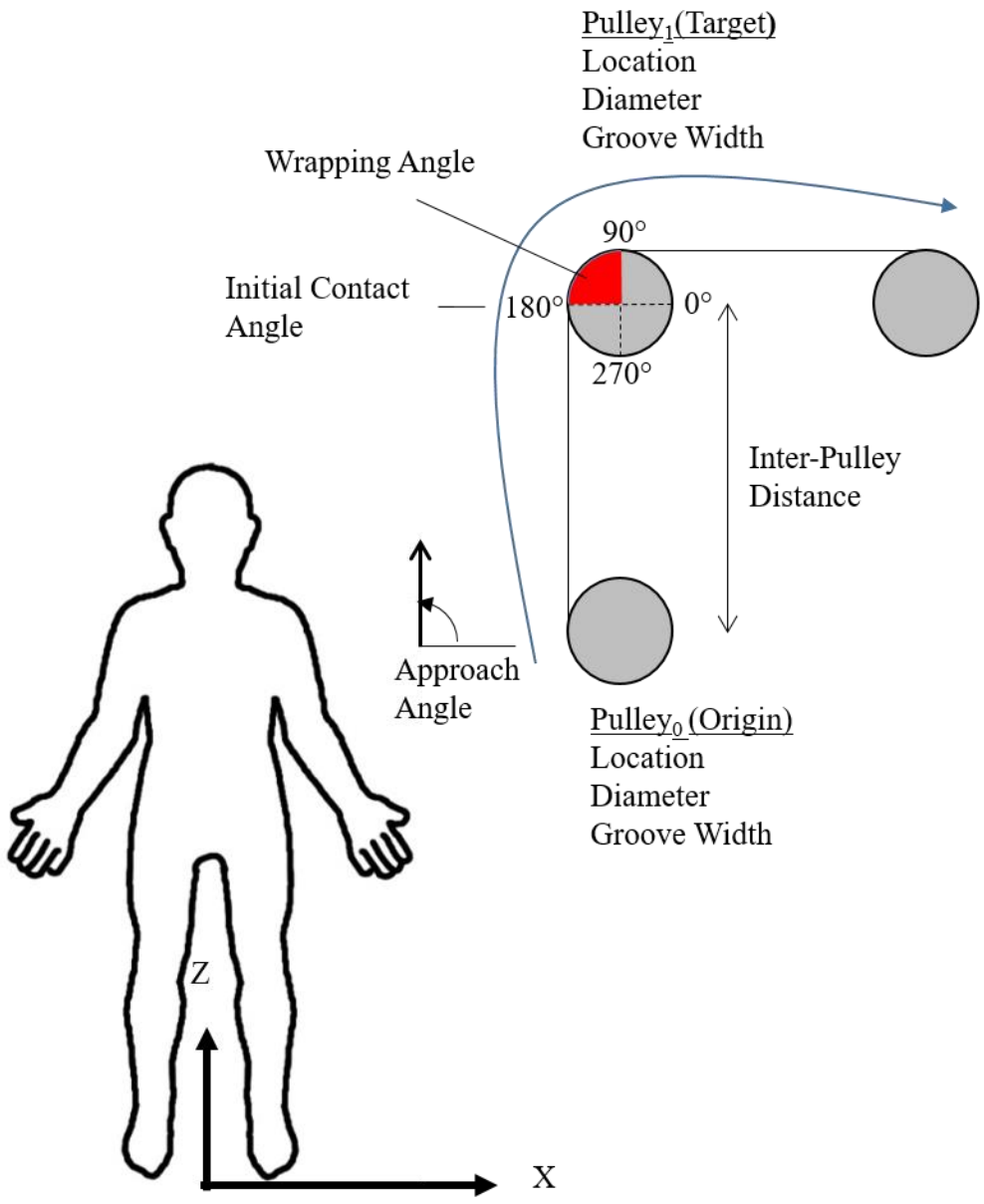

Figure 3.1. Graphical representation of the task parameters manipulated in the 3 experiments.

Table 3.1: Summary of the underlying task variables and associated parameters or independent variables manipulated in Experiments 1, 2, and 3. Cells highlighted in grey indicate fixed levels (constants) in the experiment.

Task Variable	Independent variable	Experiment-1	Experiment-2	Experiment-3
Target Tolerance	Groove Width, mm (in.)	3 (1/8”)	6 (1/4”)	3 (1/8”) , 6 (1/4”), 9 (3/8”)
	Pulley Diameter, mm (in.)	38 (1.5”)	38 (1.5”), 76 (3”), 152 (9”)	38 (1.5”), 152 (6”)
	Wrapping Angle	45°, 90°, 135°	45°, 90°, 135°	45°, 90°, 180°
Reach Distance	Inter-pulley distance, mm (in.)	229 (9”), 318 (12”), 381 (15”)	229 (9”), 318 (12”), 381 (15”)	229 (9”), 343 (13.5”), 457 (18”)
Reach Direction	Target Approach Angle	0°, 90°, 180°, 270°	0°, 45°, 90°, 135°, 180°, 225°, 270°, 315°	45°, 135°
	Origin to Target Threading Direction	Co-rotating pairs (CW to CW, or CCW to CCW)	Counter- rotating pairs (CW to CCW, or CCW to CW)	Co-rotating pairs (CW to CW, or CCW to CCW)
Reach Direction & Line of sight	Threading location (region)	Center Top – Right Bottom – Right Top – Left Bottom – Left	Center Top – Right Bottom – Right Top – Left Bottom – Left	Azimuth angle: Upper right, 45° Upper left, 135°
	Initial Contact Angle	0°, 90°, 180°, 270°	0°, 45°, 90°, 135°, 180°, 225°, 270°, 315°	45°, 135°, 225°, 315°

The general experiment set-up and procedures are discussed next, and is followed by details about the test conditions specific to each Experiment 1, 2 and 3. Participants across the 3 experiments (n = 6, 8, and 10, respectively) were all right-handed, free of any neurological and musculoskeletal disorders, had normal or corrected vision, and had no prior experience performing the task conducted in the experiment. The study was approved by the university's institutional review board and written informed consent was obtained from all participants prior to participation.

3.2.1 General Experiment Setup and Procedures

Across the 3 experiments, participants had to perform one-handed sequential reach movements that involved transferring thread between successive target pulleys in a predefined sequence while wrapping the thread along a groove on the circumference of each target pulley. Targets consisted of black nylon pulleys situated on a transparent acrylic panel (1.49 m x 1.49 m) oriented vertically so that all pulley spindle axes were horizontal and parallel. The pulleys were custom-made to specific combinations of pulley outer diameters (i.e., 38-mm, 76-mm, and 152-mm) and groove widths (i.e., 3-mm, 6-mm, and 9-mm). The pulleys had a constant groove depth of 6-mm. Target characteristics, their locations, and the threading sequence differed by experiment.

During the threading trials participants stood at a comfortable distance away from the work-panel and could self-select body postures and movements. The thread material (100% polyester, Coats & Clark, Dual Duty XP Heavy Thread) was pulled from a fishing reel (Shakespeare Alpha Baitcasting Reel) clamped onto the right or left edge of the work-panel. The reel was fixed to the "cast" setting to allow the thread to unspool freely with minimal drag during the threading task. Each trial began with the participant grasping the end of the polyester thread

from the spool with their right hand using a thumb-forefinger pinch grip. The participant then moved their hand end effector over to a motion capture marker located on the spool for a static 3-second calibration pose after which the threading task could commence. Participants were instructed to complete the task as quickly as possible but to primarily focus on threading all of the pulleys successfully. Side steps and torso learning were allowed if they were necessary to reach the pulley location. A 30 second interval between trials was provided for rest and change-up of pulleys. Six practice trials were provided prior to data collection to familiarize participants with the task.

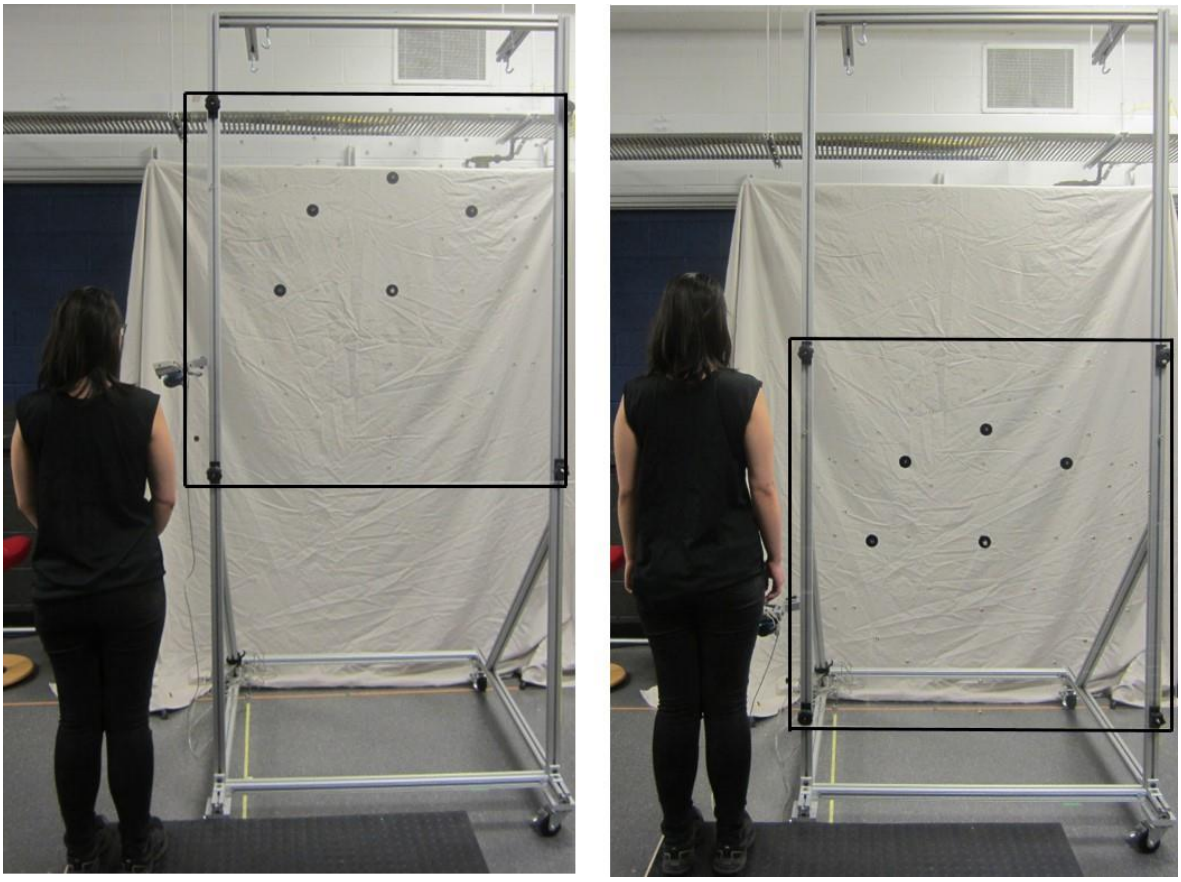

Figure 3.2: Apparatus used for the experiment consisting of a vertically oriented transparent acrylic panel (1.49 m x 1.49 m) with multiple locations for positioning pulleys mounted on spindles. The image shows a sample configuration of pulleys. The thread was unspooled from a fishing reel clamped on the left edge of the board.

3.2.2 Experiment-1

Experiment Design: Independent variables for Experiment-1 (Table 3.1) consisted of wrapping angle (3 levels), threading location (5 levels), inter-pulley distance (3 levels), and initial contact angle (α_{IC}; 4 levels) (Figure 3.3 and Figure 3.4). Pulleys in this experiment had a constant OD of 38-mm, and groove width of 3-mm.

Experiment Setup: Independent variables were organized to generate 8 unique threading sequences (Figure 3.4). Within each sequence, the location of the origin pulley (PL_0) and target pulley (PL_1) were constant resulting in a unique value of initial contact angle (i.e. the included angle at the target pulley center based on the point at which the thread first contacts the pulley groove). The wrapping angle at the target pulley was manipulated within each sequence by altering the location of a tertiary pulley ($PL_{1A\text{-}C}$) at increments of 45°. The wrapping angle value corresponded to the included angle at the target pulley over the arc-length of thread contact with the pulley groove (i.e. the absolute difference between the initial and final contact angles). The origin and tertiary pulleys were located on the perimeter of a circle of radii representing the inter-pulley distance. Three inter-pulley distances of 23-cm, 32-cm, and 38-cm were investigated.

Five threading locations were investigated and defined by the location of the target pulley relative to the mid-sagittal plane and stature of the participant, namely:

1) Center: eye height and mid-sagittal,
2) Top – right: standing height and 508-mm (20”) to the right,
3) Bottom – right: hip height and 508-mm to the right,
4) Top – left: standing height and 508-mm to the left, and
5) Bottom – left: hip height and 508-mm to the left.

Conditions with and without line of sight were determined by the interaction between initial contact angle and target pulley location (Figure 3.3). Participants performed all 8 threading sequences at the center-eye height quadrant. In addition, Sequences 1 to 4 were performed at the Top – Left and Bottom – left locations. Sequences 5 to 8 were performed at the Top – Right and Bottom – Right locations. The target pulley threading order for each sequence was $PL_0 \rightarrow PL_1 \rightarrow PL_{1A} \rightarrow PL_0 \rightarrow PL_1 \rightarrow PL_{1B} \rightarrow PL_0 \rightarrow PL_1 \rightarrow PL_{1C} \rightarrow PL_0$.

Sample size: Six young, right-handed adults participated in this experiment. Each participant completed a total number of 216 trials (= [4 quadrants x 4 initial contact angle threading sequences x 3 wrapping angles) + (1 quadrant x 8 initial contact angle threading sequences x 3 wrapping angles)] x 3 repetitions). Inter-pulley distance was blocked by participant. Two participants performed the threading task at each of the three inter-pulley distances.

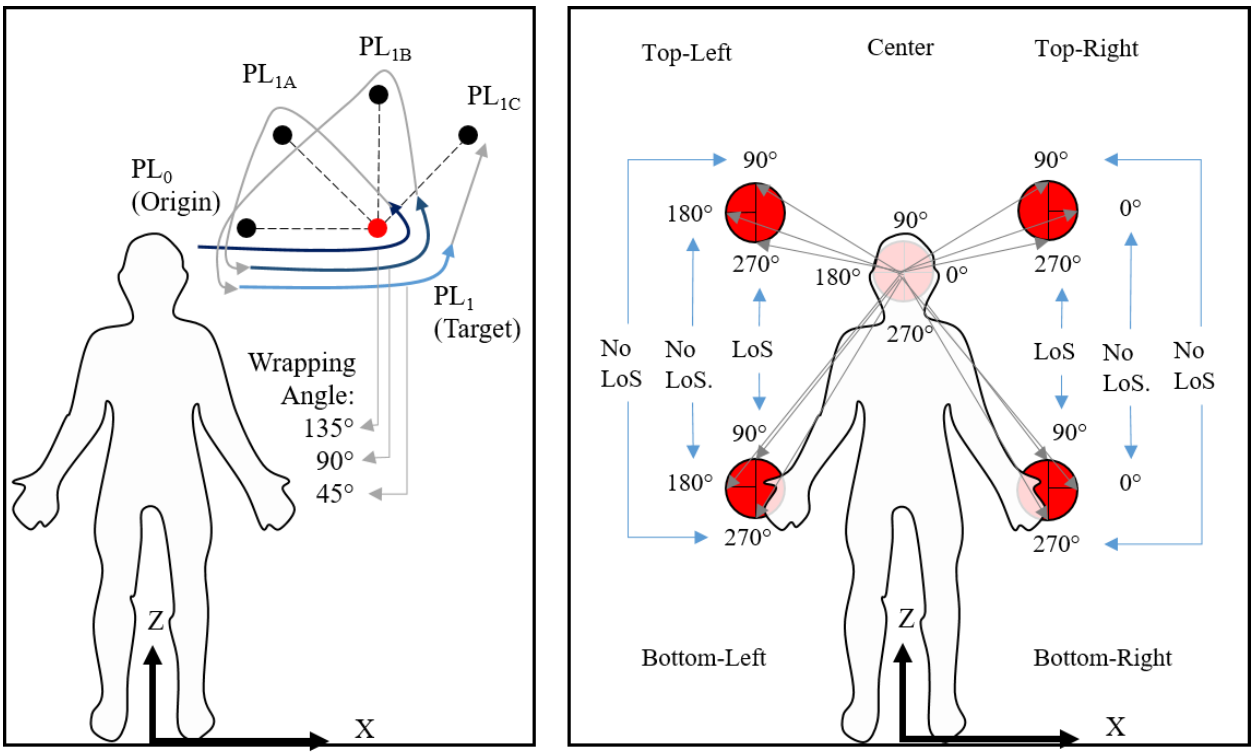

Figure 3.3. (Left) Schematic of the pulley configuration and example threading sequence with different wrapping angles at the target pulley (PL_1, shown in red) at the Top-Right region. (**Right**) The target pulley location was normalized to the quadrant condition. Line of sight (LoS) was determined by the interaction between initial contact angle and target pulley location.

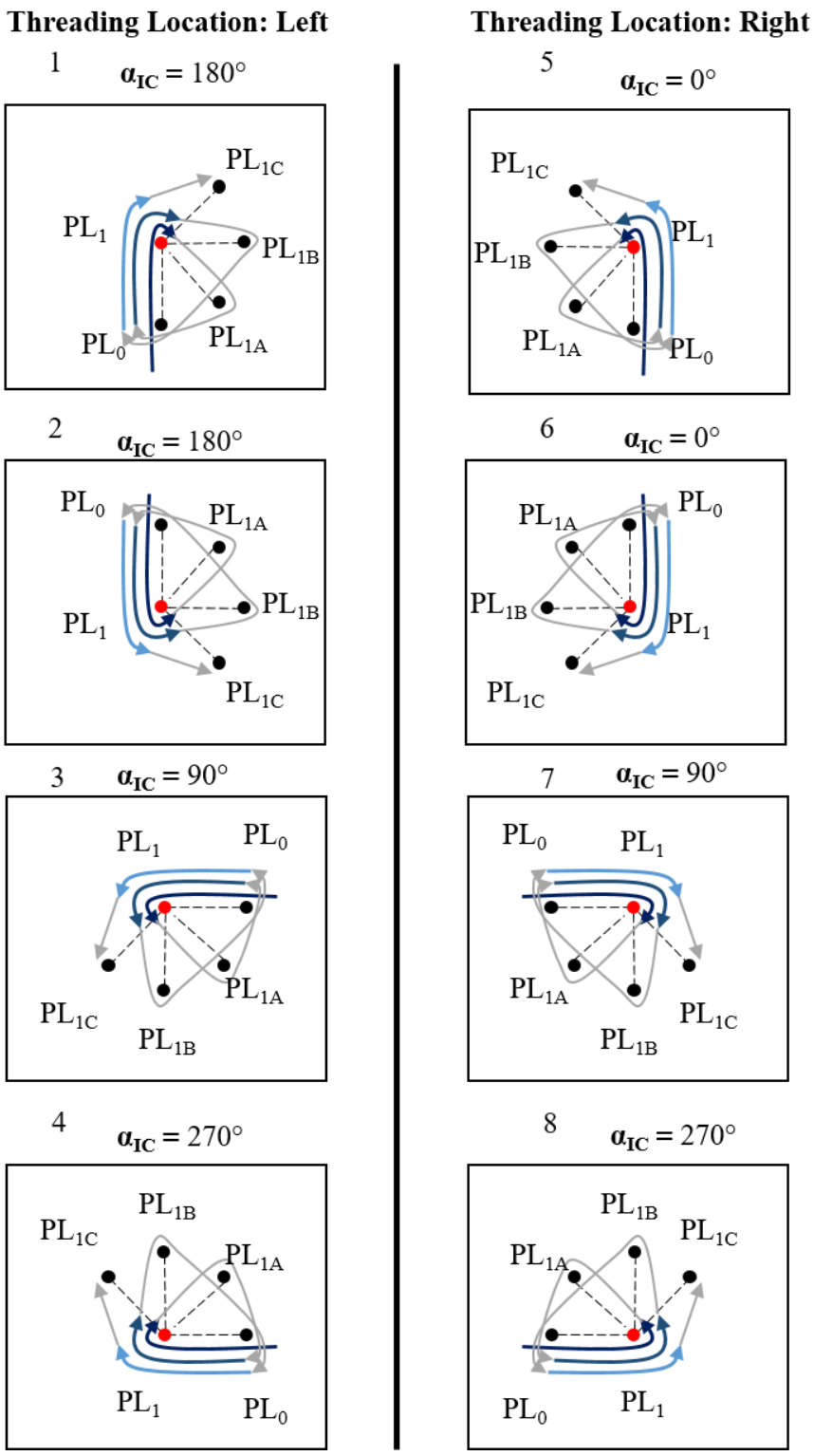

Figure 3.4. Threading sequences for Experiment 1. Each sequence involved 3 origin (PL_0) to target (PL_1) pulley reach movements that varied in wrapping angle (135°, 90°, and 45°) based on location of tertiary pulleys PL_{1A}, PL_{1B}, and PL_{1C}. The target pulley location and initial contact angle (α_{IC}) were constant within each sequence.

3.2.3 Experiment-2

Experiment Design: The independent variables consisted of pulley outer diameter (OD; 3 levels), threading location (5), inter-pulley distance (3 levels), initial contact angle (8 levels), and origin-target threading direction (2 levels). All target pulleys had a 6-mm groove width (GW). The origin pulleys had a 38-mm OD and a 3-mm GW.

Experiment Setup: Eight unique threading sequences were generated by manipulating the initial contact angle (α_{IC}: 0°, 45°, 90°, 135°, 180°, 225°, 270°, 315°) at the target pulley and threading direction between origin-target pairs (Figure 3.5). Each participant performed one of the eight threading sequences, across different combinations of OD (38-mm, 76-mm, and 152-mm) and inter-pulley distances (23-cm, 32-cm, and 38-cm), and threading location (Center, Top – Right, Bottom – Right, Top – Left, Bottom – Left). Threading locations were operationalized identical to the definitions in Experiment-1. All 8 sequences were completed at the Center location. Sequences 1 to 4 were performed at the Top – Left and Bottom – Left locations, with a target pulley threading order of $PL_{0A} \rightarrow PL_1 \rightarrow PL_{1A} \rightarrow PL_{0B} \rightarrow PL_1 \rightarrow PL_{1B} \rightarrow PL_{0C} \rightarrow PL_1 \rightarrow PL_{0A}$. Sequences 5 to 8 were performed at the Top – Right and Bottom – Right locations with a target pulley threading order of $PL_{0A} \rightarrow PL_1 \rightarrow PL_{1A} \rightarrow PL_{0B} \rightarrow PL_1 \rightarrow PL_{1B}$.

Sample size: Eight young, right-handed adults participated in this experiment. Participants assigned to sequences 1,2,5, and 6 completed a total of 243 trials (= [3 quadrants x 3 target diameters x 3 inter-pulley distances x 3 initial contact angle x 3 repetitions]). Participants assigned to sequences 3,4,7, and 8 completed a total of 162 trials (= [3 quadrants x 3 target diameters x 3 inter-pulley distances x 2 initial contact angle x 3 repetitions]). Reach movements from the origin pulley to the target pulley were extracted for data analysis.

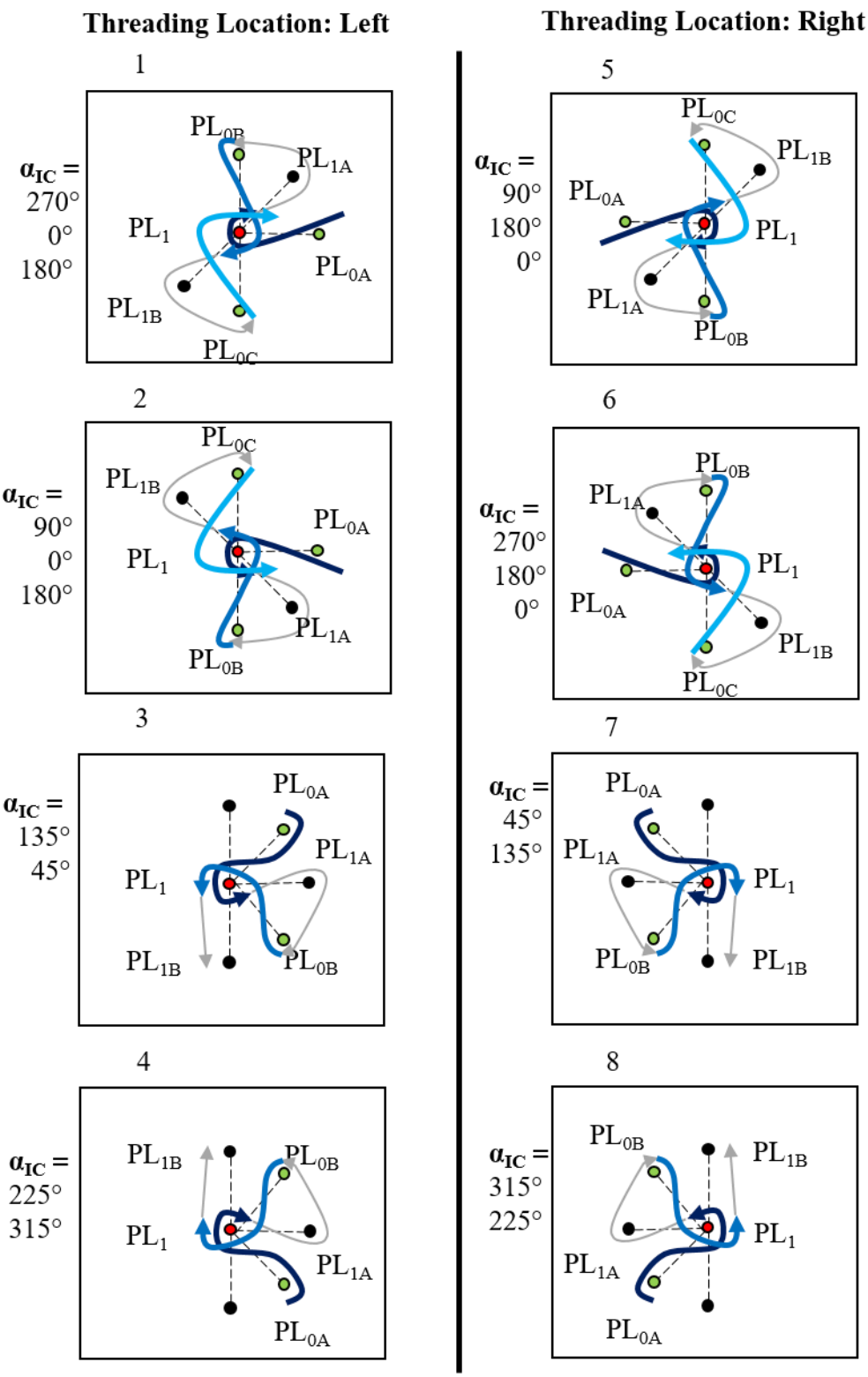

Figure 3.5. Threading sequences for Experiment-2. The target pulley location (PL_1) was constant within each threading sequence, while the origin pulley (PL_0) and initial contact angle (α_{IC}) varied.

3.2.4 Experiment-3

Experiment Design: The independent variables consisted of pulley groove width (GW; 3 levels), outer diameter (OD; 2 levels), wrapping angle (3 levels), initial contact angle (2), threading locations (2 levels), and inter-pulley distances (3 levels).

Experiment Setup: Pulleys were arranged to create a threading sequence which manipulated wrapping angle (Figure 3.6). This threading configuration was rotated and/or inverted to created 4 variations for different target pulley locations and initial contact angles. Sequence 1A and 1B were conducted within the same threading trial, likewise for Sequence 2A and 2B. Each threading sequence consisted of one origin pulley (of 38-mm OD and a 3-mm GW) located in the center of the configuration and normalized to the participants' standing elbow height. Two target pulleys were located at azimuths of 45° and 135° relative to the origin pulley. The target pulleys differed in pulley OD (38-mm and 152-mm), groove width (3-mm, 6-mm, 9-mm), and inter-pulley distance (23-cm, 34-cm, and 46-cm), and were presented in random order.

Sample size: 10 young, right-handed adults participated in this experiment. The experiment had a full-factorial design. Participants completed a total of 648 trials (= [2 sequences x 2 diameters x 3 groove widths x 3 wrapping angles x 2 target pulley locations x 3 inter-pulley distances] x 3 repetitions).

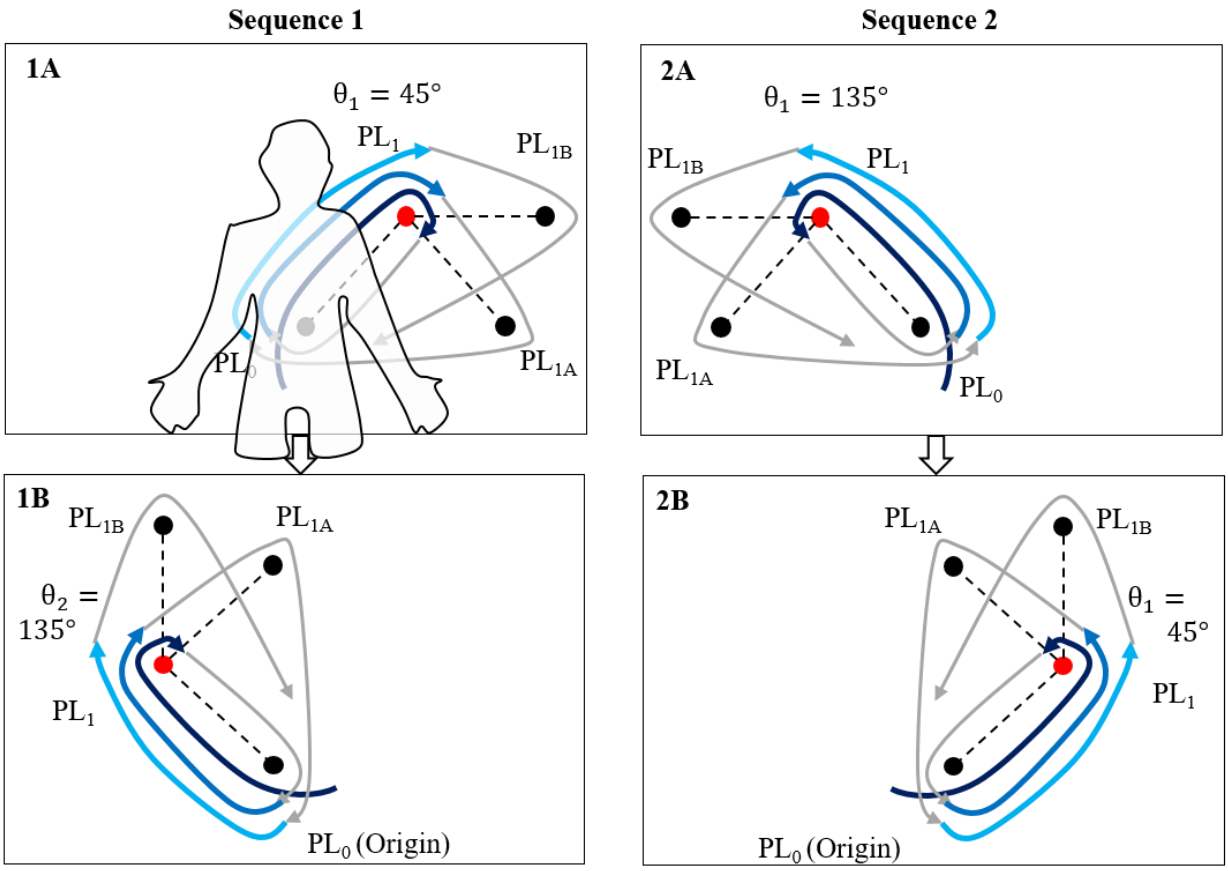

Figure 3.6. Threading sequences for Experiment 3. The origin pulley location (PL_0) was constant within each sequence, while the target pulley location (PL_1: azimuths of 45° and 135°) and wrapping angle (45°, 90°, and 180°) was manipulated. Each sequence involved 6 origin to target pulley reach movements (2 target pulley locations x 3 wrapping angles).

3.2.5 Instrumentation and Data Processing

A conventional web-camera was used for video recording all trials from a frontal anterior view of the participant. An optical motion capture system (Qualisys, Göteborg, Sweden) was used to record hand movements at a sampling frequency of 120 Hz. A passive-marker triad located on the dorsum (i.e., back) of the participants' right hand estimated the position of the thumb-forefinger pinch grip based on the pretest calibration measurement. Three-dimensional coordinate data from the motion capture system were filtered using a 2nd-order low-pass Butterworth filter with a 6-Hz cut-off frequency. Two-dimensional hand (thumb-forefinger)

position data in the frontal plane (i.e., parallel to work-panel) were computed using data from the static 3-second calibration pose recorded at the start of each threading trial. Data processing and analysis was performed in Matlab R2018 (The Mathworks Inc., Natick, MA).

3.3 Model for Trajectory Shape Prediction

Figure 3.7 provides an overview of the model developed for predicting trajectory shape using the aforementioned empirical data. The model consisted of 5 general steps. Each step is described subsequently in detail.

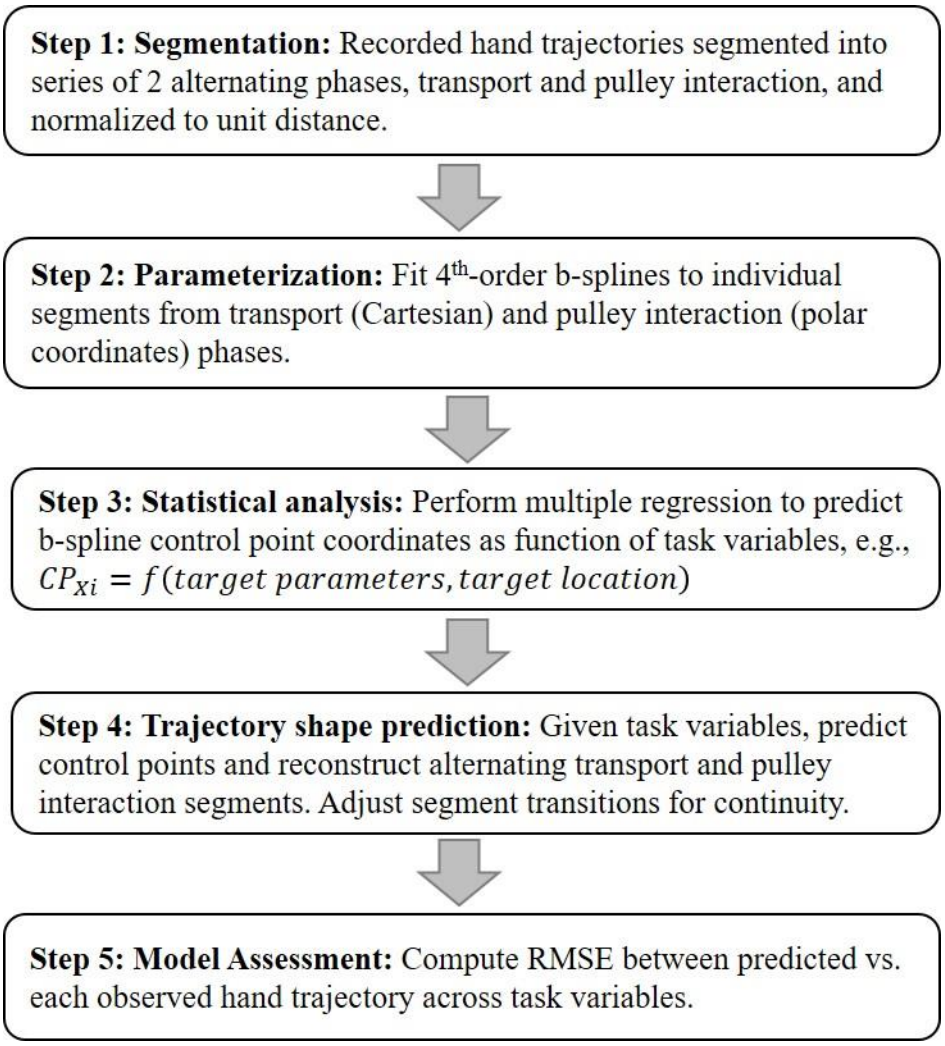

Figure 3.7. Overview of the proposed model for trajectory shape prediction and assessment.

3.3.1 Step 1: Trajectory Segmentation Scheme

The modeling approach proposed involved segmenting the continuous hand trajectory to sequential targets into two alternating phases: (1) a *transition* phase 'P_T' when the hand is reaching between two consecutive target pulleys, and (2) an *interaction* phase 'P_{PI}' when the hand is engaged in threading a target pulley (Figure 3.8). Transition points between phases were identified based on pulley geometry. Specifically, the start of the pulley interaction phase corresponded to the instant the trajectory first crossed a line segment passing through the target pulley center perpendicular to the centerline between the target pulley and the previous pulley in the sequence. To determine the end of the pulley interaction phase, the derivative of the resultant distance between the trajectory and target pulley edge was calculated. The end corresponded to the final instant the derivative changed signs from negative to positive within a distance equal to a pulley diameter away from the pulley center, i.e., signifying that threading was completed and the hand starts to move away from the pulley (and towards the next pulley in the sequence).

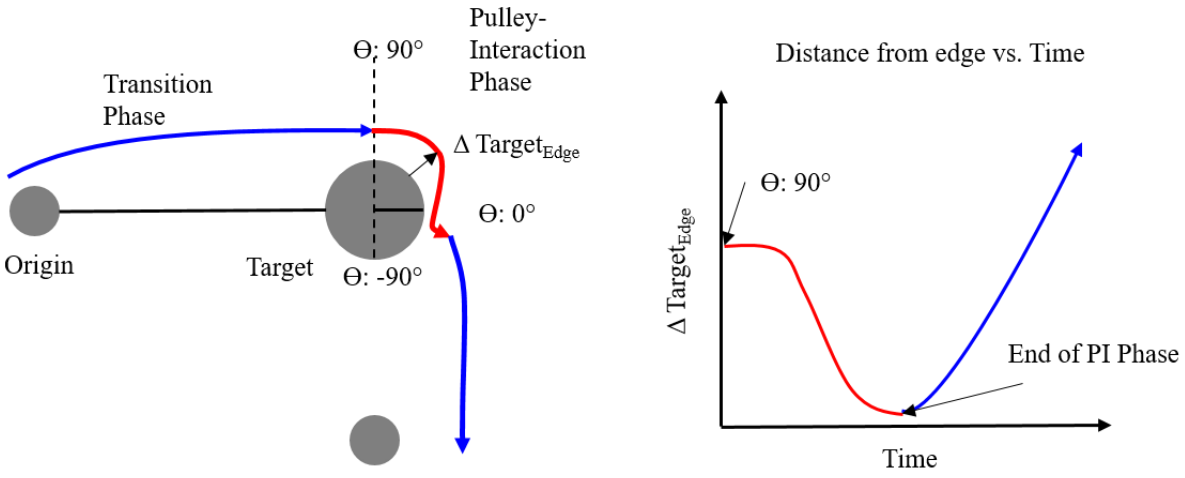

Figure 3.8. Schematic of trajectory segmentation scheme. Transition points between the transition phase (blue) and pulley-interaction phase (red) were based on pulley geometry.

3.3.2 Step 2: Trajectory Parameterization

First, the transition and pulley interaction segment data were normalized. For the transition phase, trajectory coordinates were rotated about the anterior-posterior (Y) axis and normalized to an inter-pulley distance of unit length, such that the origin pulley location had Cartesian horizontal (X) and vertical (Z) coordinates of (0, 0) and the target pulley had coordinates of (1, 0). For the pulley interaction phase, trajectory data were normalized to the center of the target pulley, and rotated about the anterior-posterior axis to align at the start point.

Next, a cubic (fourth-order) b-spline was fitted to each normalized 2-D hand trajectory in the frontal plane for the transition phase 'P_T' and pulley interaction phase 'P_{PI}' separately. A k^{th} order b-spline curve *C(u)* is composed of a linear combination of n+1 control points *P* and basis functions *f(u)*:

$$C(u) = \sum_{i=0}^{n} P_i f_i^k(u), \text{ where } 0 \le u \le 1. \tag{3.1}$$

The b-spline is evaluated along the non-decreasing input parameter $u \in [0, 1]$. B-spline basis functions are polynomials that are joined end-to-end by a set of interval boundaries, referred to as knots. The knot vector *U* consists of $n + k + 1$ non-periodic knots that control the shape of the curve:

$$U_j = \begin{cases} 0, & j < k \\ \frac{j-k-1}{n-k+2}, & k \le j \le n \\ 1, & j > n \end{cases}, \text{ where } 0 \le j \le n + k. \tag{3.2}$$

The repeated knots at the beginning and end of the knot vector create a clamped curve which causes the curve to pass through the endpoints of the measured data, in this case the start and end of the transition phases. The b-spline functions are constructed using a recursive algorithm that utilizes the knot vector:

$$N_i^1 = \begin{cases} 1, & U_i \le u \le U_{i+1} \\ 0, & otherwise \end{cases}, \tag{3.3}$$

$$N_i^k(u) = \frac{u - U_i}{U_{i+k-1} - U_i} \cdot N_i^{k-1}(u) + \frac{U_{i+k} - u}{U_{i+k} - U_{i+1}} \cdot N_{i+1}^{k-1}(u) \quad (3.4)$$

The coordinates of the measured trajectory *K* over parameter *t* are approximated by using linear least squares regression to obtain the set of $n + 1$ control points *P*:

$$P = (N^T N)^{-1}(N^T K). \quad (3.5)$$

In this study, fourth order cubic b-splines were fitted to the transition phase P_T using 6 control points (i.e., $n = 5$ in Equation 3.1), and to the pulley interaction phase P_{PI} using 4 control points (i.e. $n = 3$ in Equation 3.1). An example of a b-spline fit for the transition and pulley-interaction phases from sample trajectory data is shown in Figure 3.9. Separate analysis of the root mean square error (RMSE) between the fitted b-splines and measured trajectory were conducted to identify the fewest number of control points required to adequately represent the shape of the transition and pulley interaction phases. B-spline fits in the transition phase generally had lower RMSE values compared to the pulley-interaction phase. For instance, the mean (± SD) RMSE of the fitted b-splines and the measured trajectories from all experiment trials combined was 1.95 ± 1.64 mm for the transition phase fitted with 6 control points, and 3.06 ± 4.24 mm for the pulley-interaction phase fitted with 4 control points.

The difference in RMSE between phases was largely due to movement corrections during pulley- interaction in about 30% of trials when participants missed the target pulley groove resulting in irregular trajectory shapes. Two examples are shown in the bottom panel of Figure 3.9, namely, without (bottom-left) and with a movement correction (bottom-right). The use of 4 control points in the pulley interaction phase implied that most of these irregularities in trajectory shape would smoothed out in the spatial domain, however the durations are captured when modeling speed profiles in the subsequent Chapter 4. Lastly, the Cartesian coordinates of the pulley-interaction phase were converted to polar coordinates (R, θ) referenced to the target pulley

center to facilitate interpretation. The radial (*R*) dimension of the pulley-interaction phase control points were skewed right so control point values were log-transformed to create a normal distribution about the mean.

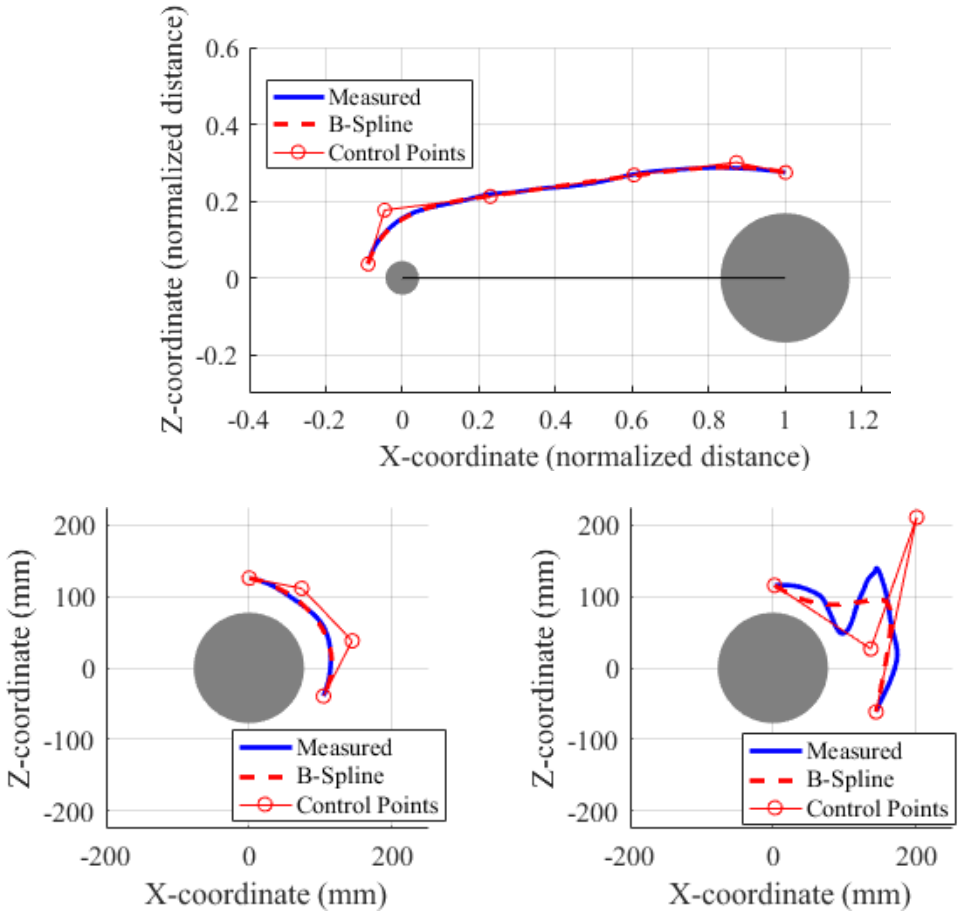

Figure 3.9. Top: Exemplar b-spline fit to a measured trajectory in the transition phase. Bottom: Exemplar b-spline fit to a measured trajectory in the pulley-interaction phase with a relatively low error (Bottom-Left) and high error due to presence of a movement correction during pulley interaction (Bottom-Right). The task condition for the examples depicted involved reaching to a target pulley of 152-mm diameter, 3-mm groove width, and CW threading direction located towards the upper right (45°) with an inter-pulley distance of 457-mm.

3.3.3 Step 3: Statistical Analysis

Multivariate regression analyses were performed on control point coordinates for $P_T(X, Z)$ and $P_{PI}(R,\ \theta)$. A total of 11 regression equations were constructed for the control points in the transition phase in Cartesian coordinates, i.e., P_{TXi} and P_{TZi} where i = 0 to 5. (Note: P_{TX5} was of constant value equal to the unit distance between pulley centers). Likewise, 7 regression equations were constructed for the pulley interaction phase control points in polar coordinates, i.e., P_{PIRi} and $P_{PI\theta i}$ where i = 0 to 3. Note: $P_{PI\theta 0}$ was set to 90°).

A generic form of the regression equations is shown in Table 3.2. Forward stepwise regression was used to select parameters based on statistical significance criteria of $p < 0.05$ for inclusion in the final regression models to predict control point locations. For the transition phase, the predictors represent differences in target tolerance (e.g., pulley diameter, groove width, wrapping angle at the origin and target pulleys), reach direction and amplitude (e.g., inter-pulley distance, origin and target pulley locations), and line of sight (e.g., initial contact angle at and approach angle to the target pulley, threading direction at the origin and target pulleys, interaction between target location coordinates X and Z). Threading directions at the origin and target pulley (CW: 0, CCW: 1) and their two-way interaction were included to differentiate between co- vs. counter rotating pulleys. Pulley location coordinates and inter-pulley distance were normalized to stature. Pulley location was in reference to the global coordinate system origin located at the midpoint of the starting feet position. Approach Angle (0-315°) was defined as the angle of the vector pointing from the origin pulley to the target pulley in reference to the horizontal.

For the pulley interaction phase (i.e., at the target pulley), the predictors represent differences in target tolerance (e.g., pulley diameter, groove width, wrapping angle), reach

direction and approach speed (e.g., inter-pulley distance, pulley location), and line of sight (e.g., initial contact angle, approach angle, threading direction, interaction between target location coordinates X and Z).

The Results sections summarizes the obtained regression models. The explained variance using adjusted R^2 values were tabulated and compared to assess model fit.

Table 3.2. Generic form of the regression models for computing control points for the transition and pulley interaction phases.

Control Points for Transition Phase, P_T	Control Points for Pulley Interaction Phase, P_{PI}
$P_{TX0-4}, P_{TZ0-5} =$ $\beta_0 +$ $\beta_1(Origin\ Diameter) +$ $\beta_2(Origin\ Groove\ Width) +$ $\beta_3(Target\ Diameter) +$ $\beta_4(Target\ Groove\ Width) +$ $\beta_5(Target\ Location\ X) +$ $\beta_6(Target\ Location\ Z) +$ $\beta_7(Origin\ Threading\ Direction) +$ $\beta_8(Target\ Threading\ Direction) +$ $\beta_9(Target\ Initial\ Contact\ Angle) +$ $\beta_{10}(Inter-Pulley\ Distance) +$ $\beta_{11}(Origin\ Wrapping\ Angle) +$ $\beta_{12}(Target\ Wrapping\ Angle) +$ $\beta_{13}(Approach\ Angle) +$ $\beta_{14}(Target\ Threading\ Direction)$ $\times\ (Origin\ Threading\ Direction)$ $+$ $\beta_{15}(Target\ Location\ X)$ $\times\ (Target\ Location\ Z) +$	$P_{PIR0-3}, P_{PI\theta 1-3} =$ $\beta_0 +$ $\beta_1(Target\ Diameter) +$ $\beta_2(Target\ Groove\ Width) +$ $\beta_3(Target\ Location\ X) +$ $\beta_4(Target\ Location\ Z) +$ $\beta_5(Target\ Threading\ Direction) +$ $\beta_6(Target\ Initial\ Contact\ Angle) +$ $\beta_7(Inter-Pulley\ Distance) +$ $\beta_8(Approach\ Angle) +$ $\beta_9(Target\ Wrapping\ Angle) +$ $\beta_{10}(Target\ Wrapping\ Angle)$ $\times\ (Target\ Diameter) +$ $\beta_{11}(Target\ Location\ X)$ $\times\ (Target\ Location\ Z)$

3.3.4 Step 4: Trajectory Shape Prediction

In this step, for a given set of predictor values, the trajectory shape was constructed using control point locations (b-spline coefficients) estimated using equations in Table 3.2. Trajectory shapes were predicted for one transition phase and one pulley interaction phase to represent one origin-to-target reach movement. To combine the two trajectory phases, the last control point for

the first transition phase, P_T, was replaced with the first control point for the pulley interaction phase, $P_{PI,0}$. This is necessary to assure the trajectories are co-located, i.e., pass through the same point when transitioning between phases. Additionally, to obtain continuity in gradient at the transitions between the two trajectory phases, the locations of the control points before and after the transition point were adjusted to be collinear (Appendix A). This approach allows for connecting consecutive pairs of predicted transition and pulley interaction phase trajectories to obtain one continuous reach trajectory for any number of pulleys given each pulleys' characteristics, location, and threading sequence.

3.3.5 Step 5: Model Assessment

Goodness of fit for the statistical regression models was assessed by examining the RMSE of the resultant distance between predicted and measured reach trajectories (i.e., $RMSE_{P\text{-}M}$) obtained from Experiments 1, 2 and 3 by condition. Predicted trajectories were constructed for each trial condition using equation 3.1. $RMSE_{P\text{-}M}$ was computed as the error at each frame on the predicted trajectory matched to the closest point on the measured trajectory, as follows:

$$RMSE_{P-M} = \sqrt{\frac{1}{k}\sum_{i=1}^{k}(S_i - K_i)^2} \tag{3.6}$$

where k is the length of *t*, the measured trajectory *K*, and predicted trajectory *S*.

Additionally, to obtain a measure of the within-person variability the RMSE between measured trajectories across the 3 repetitions for the same task conditions was computed, i.e., $RMSE_{M\text{-}M}$. The error corresponded to the maximum error at each time point between the three repetitions.

3.4 Results

This section presents the study results pertaining to participant characteristics, regression models for transition and pulley interaction control points, and assessing the goodness of fit of the fitted shape trajectories.

3.4.1 Participant characteristics

The mean (± SD) age, stature, and mass of participants in the study sample used for model development by Experiment 1, 2, and 3 and combined are listed in Table 3.3.

Table 3.3. Mean (± SD) age, stature, and mass for participants in Experiments 1, 2, and 3 and combined.

Experiment	N (Men, Women)	Age, years (Mean ± SD)	Height, cm (Mean ± SD)	Mass, kg (Mean ± SD)
1	6 (2, 4)	21.5 ± 2.1	166.0 ±10.9	64.9 ± 14.1
2	8 (5, 3)	21.1 ± 1.1	173.5 ± 7.9	71.1 ± 7.3
3	10 (6, 4)	23.5 ± 4.2	170.9 ± 9.1	73.1 ± 23.2
Combined	24 (13, 11)	22.2 ± 3.1	170.5 ± 9.3	70.4 ± 22.8

3.4.2 Regression Models: Explained Variance and Significant Effects

Table 3.4 and Table 3.5 summarize the regression results in terms of standardized beta coefficients for statistically significant predictors and the explained variance using adjusted R^2 values ($\hat{R}^2_{adj}$) for each of the control point coordinates in the transition and pulley interaction phases. The average (± SD) $\hat{R}^2_{adj}$ from the regression analyses for control point coordinates in the transition and pulley interaction phases were 0.32 ± 0.16 and 0.36 ± 0.14 , respectively. Tables containing unstandardized beta coefficients for the control point coordinates in the transition and pulley interaction phases are provided in Appendix B.

Given the different units used for each predictor resulting in differently scaled unstandardized partial coefficients, the standardized partial coefficients are preferred when

comparing effects of predictors to each other. Standardized partial coefficients can be interpreted as the number of standard deviations the outcome increases for every standard deviation increase in the predictor, holding all other predictors constant. For the transition phase, the inter-pulley distance (standardized partial coefficient, β ranged from -0.31 to 0.05), the origin wrapping angle (β: -0.36 to 0.21), and the two-way interaction between the origin and target threading directions (β: -0.40 to 1.90) attributed to most of the explained variance.

Generally, for control point locations in the pulley interaction phase, the target wrapping angle (β: -0.50 to 0.13), the interaction between target OD and wrapping angle (β: -0.36 to 0.11), and the medial-lateral target pulley location coordinate (Target Location X; β: -0.16 to 0.24) attributed to most of the explained variance. The radial dimension (R) of the control point locations increased with increasing target diameter, target wrapping angle, and for target pulleys located on the contralateral side of the body. The angular dimension (θ) of control point locations was negatively influenced by target wrapping angle (i.e. there was greater change from the starting value of 90° with an increase in wrapping angle).

Table 3.4. Standardized beta coefficients for significant predictors ($p < 0.05$) of control point coordinates (X, Z) in the transition phase. A blank cell indicates a non-significant effect. The total row provides a measure of explained variance using the $\hat{R}^2_{adj}$ values for each regression model. Note: $P_{T5,X}$ is not predicted.

	Transition Phase Control Points											
	P_{T0}		P_{T1}		P_{T2}		P_{T3}		P_{T4}		P_{T5}	
Predictors	***X***	***Z***	***X***	***Z***	***X***	***Z***	***X***	***Z***	***X***	***Z***	***X***	***Z***
Intercept (Unstandardized)	0.18	0.34	0.28	0.31	0.26	0.34	0.12	0.46	0.12	0.58		0.59
Origin Diameter	0.21	0.40	0.19	0.40	0.16	0.28	0.17	0.16	0.12	0.09		0.07
Origin Groove Width	-0.11		-0.10		-0.08	0.08	-0.07	0.07	-0.05	0.06		0.06
Target Diameter	-0.02	-0.02	-0.06		-0.07	0.06	-0.05	0.12	-0.11	0.18		0.23
Target Groove Width	-0.04	-0.02	-0.06		-0.08	0.06	-0.05	0.07	-0.05	0.06		0.04
Target Location X							0.02	-0.07		-0.07		-0.08
Target Location Z	0.02	-0.02		-0.01	0.03	-0.05		-0.05		-0.05		-0.05
Origin Threading Direction	0.13	-0.11	0.19	-0.21	0.18	-0.48	0.08	-0.78	-0.04	-0.99		-0.98
Target Threading Direction	0.10	-0.16	0.16	-0.26	0.18	-0.53	0.09	-0.81		-1.01		-1.02
Target Initial Contact Angle	-0.02	-0.08	-0.05	-0.08	-0.08		-0.02	0.05	-0.04	0.05		0.06
Inter-pulley Distance		-0.21		-0.24	0.05	-0.28	0.03	-0.31	0.04	-0.26		-0.27
Origin Wrapping Angle	-0.27	-0.15	-0.36	-0.06	-0.34	0.21	-0.22	0.17	-0.20	0.09		0.06
Target Wrapping Angle	0.10		0.14	-0.04	0.13	-0.14	0.08	-0.09	0.09	-0.07		-0.07
Approach Angle	-0.04	-0.05	-0.04	-0.03		-0.02		-0.04	-0.05	-0.04		-0.03
Origin x Target Threading Direction	-0.26	0.20	-0.38	0.41	-0.40	0.99	-0.21	1.52		1.89		1.90
Target Location X x Z				-0.04	0.02	-0.06			0.02			
$\hat{R}^2_{adj}$	.18	.34	.28	.31	.26	.34	.12	.46	.12	.58		.59
Mean (± SD) $\hat{R}^2_{adj}$	.32 ± 0.16											

Table 3.5. Standardized beta coefficients for significant predictors ($p < 0.05$) of control point coordinates (θ, R) in the pulley interaction phase. Cell values represent standardized beta coefficients. The total row provides a measure of explained variance using the $\hat{R}^2_{adj}$ values for each regression model. Note: $P_{I0,\theta}$ is not predicted.

	Pulley-interaction phase control points							
	P_{PI0}		P_{PI1}		P_{PI2}		P_{PI3}	
Predictors	θ	R	θ	R	θ	R	θ	R
Intercept (Unstandardized)		4.27	61.54	4.25	44.94	4.30	30.10	4.20
Target Diameter		0.55	-0.06	0.52	0.16	0.57		0.57
Target Groove Width		0.08	0.14	0.02	0.08	-0.03	0.08	
Target Location X			0.06	-0.15	0.23	-0.16	0.24	-0.14
Target Location Z		-0.13		-0.11		-0.10	0.03	-0.09
Target Threading Direction		-0.17	-0.02	-0.10		-0.05	0.06	
Target Initial Contact Angle		0.06	-0.05	0.04		0.04	-0.03	0.03
Inter-pulley Distance		-0.05		-0.09	0.07	-0.08	0.08	-0.07
Approach Angle			-0.04	0.05		0.06	-0.03	0.06
Target Wrapping Angle		-0.11	-0.27	0.10	-0.33	0.13	-0.50	-0.06
Target Wrapping Angle x Diameter		0.05	0.11	0.10	-0.36		-0.23	
Target Location X x Z		-0.09			-0.12		-0.13	
$\hat{R}^2_{adj}$		0.44	0.07	0.45	0.33	0.40	0.47	0.37
Mean (± SD) $\hat{R}^2_{adj}$	0.36 ± 0.14							

Figure 3.10 graphically depicts the effect of target groove width and diameter for the transition and pulley-interaction phase together. As seen in Figure 3.10 (top), target groove width had a statistically significant but relatively small influence on overall trajectory shape in the transition and pulley-interaction phases. Predicted hand trajectory shapes were visibly more curved or rounded when reaching towards pulleys with a wider compared to narrower groove width (e.g., 9-mm vs 3-mm). Increasing target pulley diameter caused the predicted trajectory shape to be more flat in the second half of the transition phase and more rounded in the pulley-interaction phase (Figure 3.10, bottom).

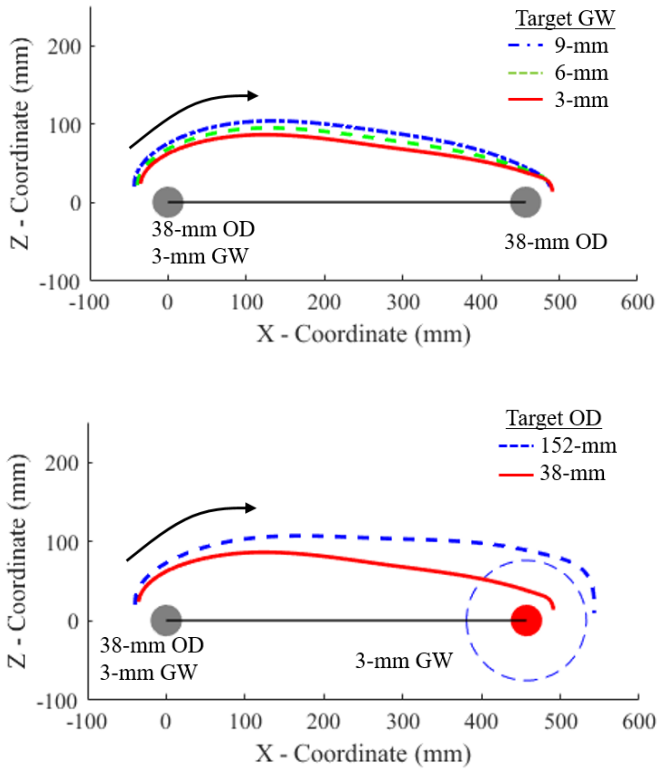

Figure 3.10. Exemplar predicted trajectory shapes depicting the main effect of target groove width (top), target outer diameter (bottom), for a target pulley location to the upper right (Azimuth: 45°) and CW threading direction. Trajectories are rotated 45° about the Y-axis and centered to the origin pulley location.

Figure 3.11 graphically depicts the effects of inter-pulley distance (top) and diameter (for counter-rotating pulleys) on trajectory shape predictions. Generally, the height of the trajectory from the origin-target pulley centerline increased with an increase in inter-pulley distance. For counter-rotating pulleys, trajectory shapes were visibly more rounded in the second half of the transition phase and pulley-interaction phase, and there was a larger excursion from the pulley edge during the pulley interaction phase

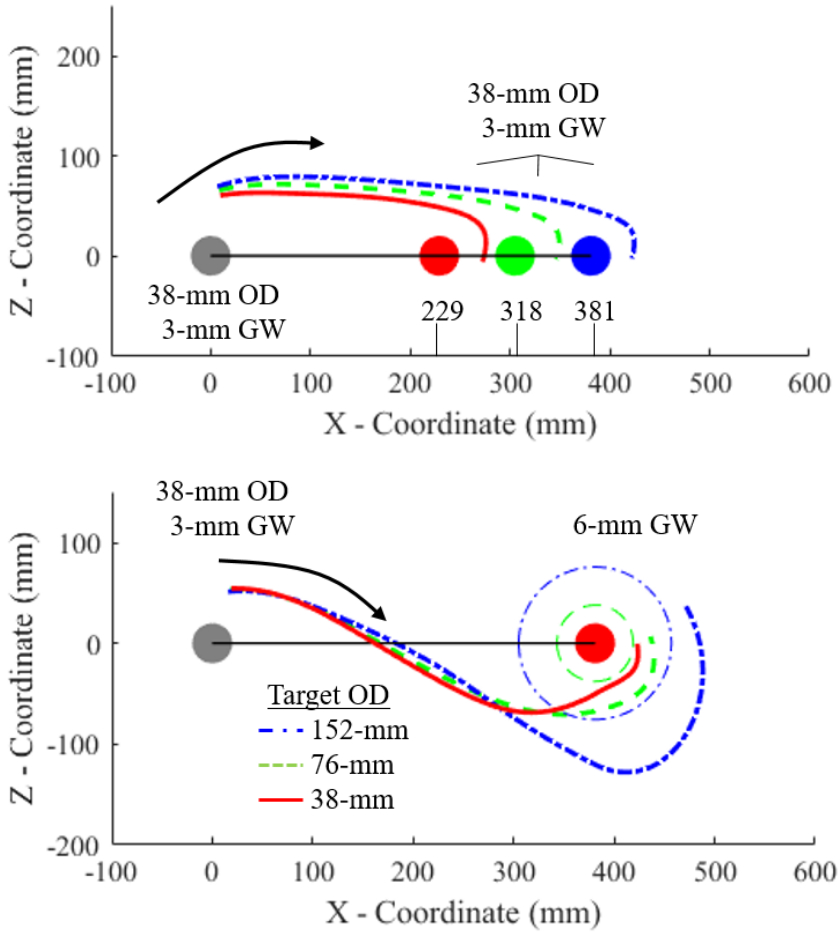

Figure 3.11. Exemplar predicted trajectory shapes depicting the main effect of inter-pulley distance (top) and diameter for counter-rotating pulleys (bottom) for the Bottom - Right target pulley location region with an approach angle of 180°. Predicted trajectory shapes are centered to the origin pulley location.

Figure 3.12 graphically depicts the predicted trajectory shape for a person with a stature of 1725-mm when reaching to target pulleys located at stature vs. hip height on the contralateral and ipsilateral side of the body. For the conditions shown, the origin and target pulleys had a constant 38-mm diameter and a 3-mm groove width, the inter-pulley distances of 381-mm, and the target wrapping angle of 135°. Approach angles were 180° and 0° (both horizontal) for reach movements on the contralateral and ipsilateral side, respectively. The combinations of predictors, create conditions with (dotted) and without (solid) line of sight. Target pulley location had a visibly substantial impact on trajectory shape depending on a directly direct line of sight with the initial contact point at the target pulley was available relative to the reference standing location (i.e., aligned with the mid-sagittal plane of X = 0).

In general, hand trajectories for horizontal reach movements to target pulleys located at stature height tended to be more flat, or have less excursion from the inter-pulley centerline, compared to target pulleys located at hip height. Reach movement trajectories to target pulleys located on the contralateral side, at stature and hip height, tended to extend further past the pulley edge, compared to target pulleys located on the ipsilateral side.

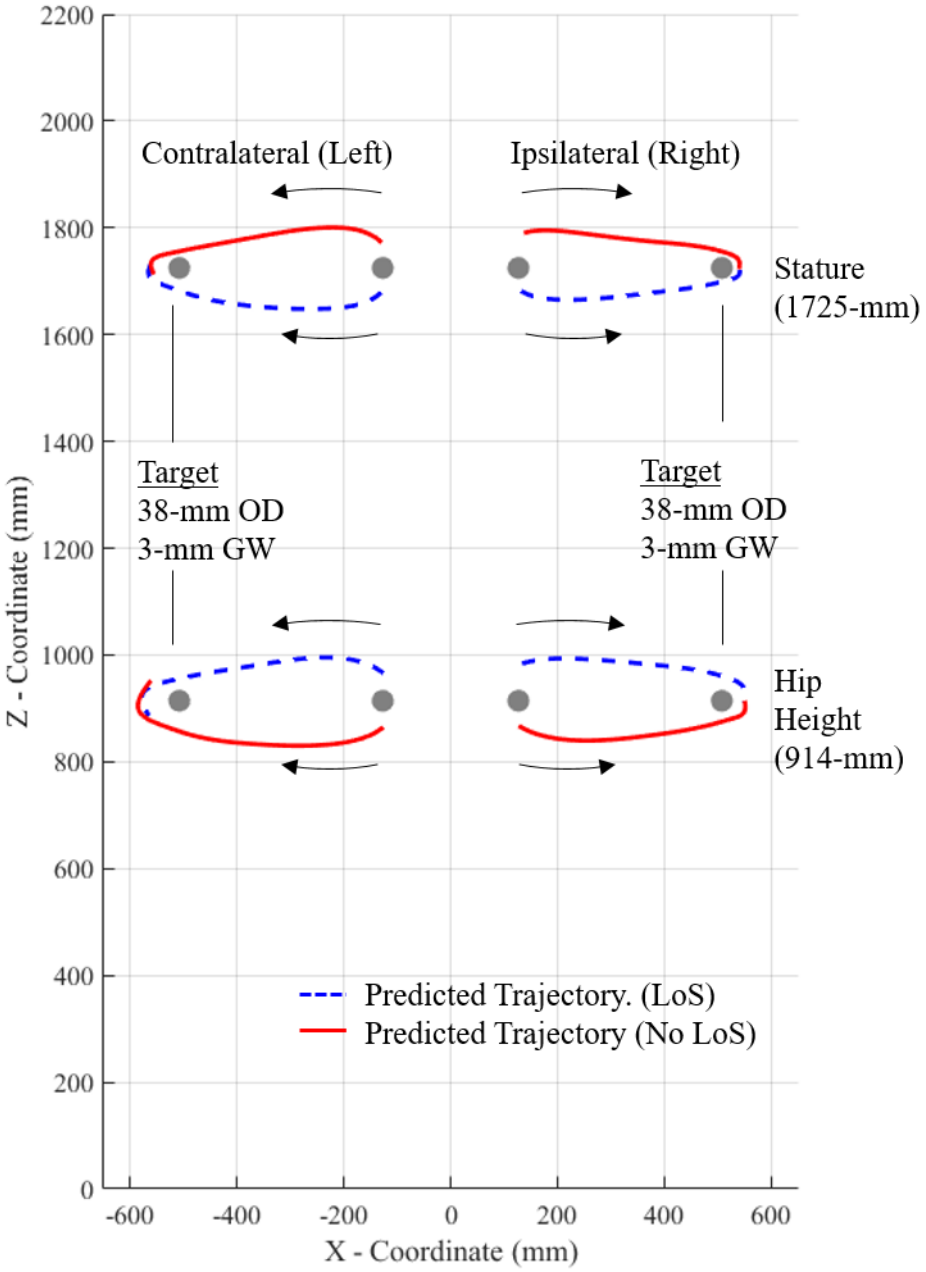

Figure 3.12. Exemplar predicted trajectory shapes demonstrating the effect of target pulley location for conditions with (dotted) and without (solid) line of sight (LoS) and laterality (i.e., ipsilateral vs. contra-lateral reaches). Predicted trajectory shapes are for a right-handed person of 1725 mm stature, and origin and target pulleys of 38-mm diameter (OD) and 3-mm groove width (GW).

3.4.3 Assessment of Trajectory Shape Model

Goodness of fit of the models was assessed by comparing the RMSE between predicted and measured trajectories (i.e., over combined pairs of transition and pulley interaction phases). Table 3.6 provides the overall mean, standard deviation, and the 95th percentile of $RMSE_{P\text{-}M}$ and $RMSE_{M\text{-}M}$ pooled across all of the measured conditions. RMSE's between the average predicted and measured trajectories were lower than the inherent within-person variability in measured trajectories. This indicates that the prediction models capture the variance in *average* trajectory shape associated with task conditions more compared to variance associated with within-person variability in measured trajectory shape.

Table 3.6. Summary statistics for overall model performance.

	Mean (± SD)	95th Percentile	Total # of trials
Predicted vs. Measured $RMSE_{P\text{-}M}$	31 ± 17 mm	63 mm	9396
Measured vs. Measured $RMSE_{M\text{-}M}$	62 ± 43 mm	158 mm	3132

To better understand the effects of task parameters on model goodness of fit, ANOVA was used to separately assess the $RMSE_{P\text{-}M}$ for reach movements varying in target diameter, target groove width, and inter-pulley distance. Figure 3.13 provides a graphical comparison of the $RMSE_{P\text{-}M}$ within each level of these task parameters. In summary, goodness of fit degraded with an increase in target diameter ($p < 0.001$), increasing target groove width ($p < 0.001$), and increasing inter-pulley distance ($p < 0.006$). However, as seen from Figure 3.13, the difference in mean $RMSE_{P\text{-}M}$ within each task parameter was relatively small (less than 5-mm).

Additionally, $RMSE_{P\text{-}M}$ values across line of sight conditions, in terms of line of sight with the initial contact angle on the pulley groove, was compared for conditions with and without line of sight by target pulley region (Figure 3.14). Variance in the error between predicted and

measured trajectories tended to increase for reach movements conditions without line of sight compared to those with line of sight. Additionally, mean $RMSE_{P\text{-}M}$ and variance tended to increase for reach movements located on the contralateral side of the body, compared to the ipsilateral side.

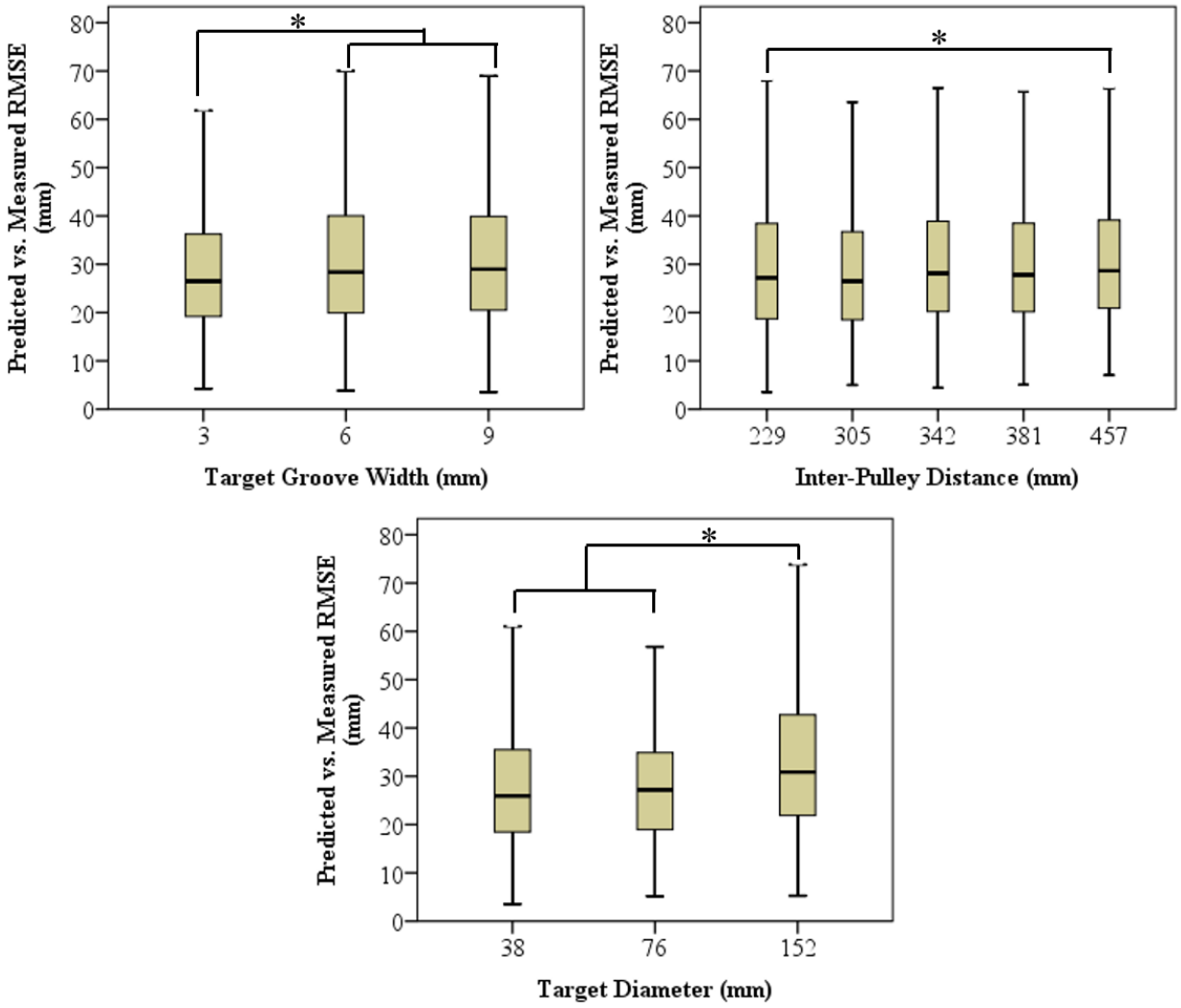

Figure 3.13. Comparison of model goodness of fit in terms of RMSE between predicted and measured trajectories by target outer diameter, target groove width, and inter-pulley distance.

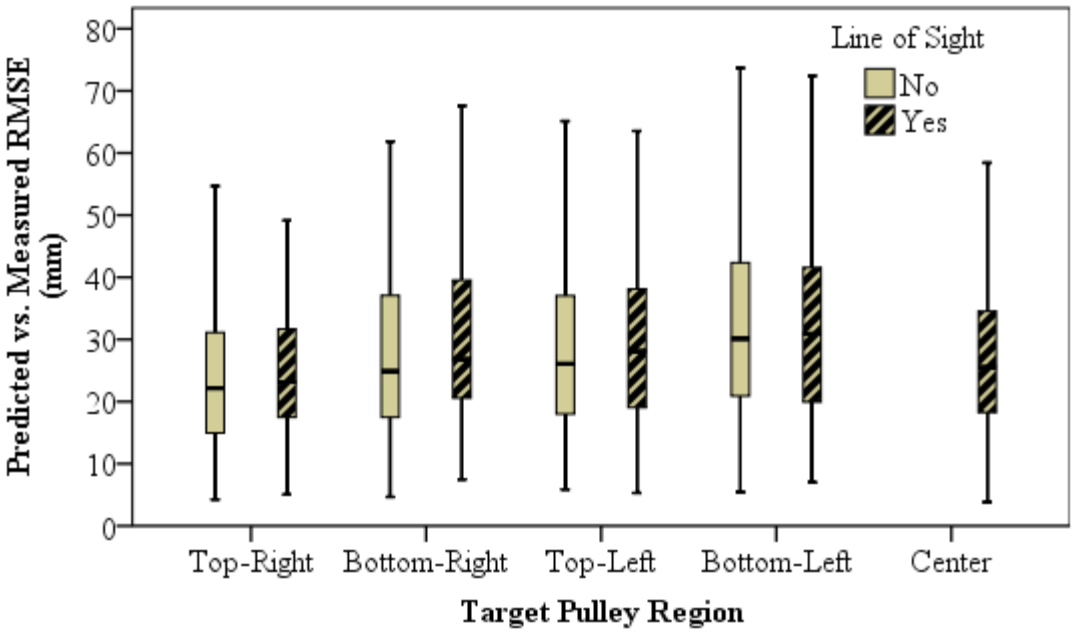

Figure 3.14. Comparison of model goodness of fit in terms of RMSE between predicted and measured trajectories by target pulley region for conditions with and without line of sight of the initial contact point on the pulley groove.

Figure 3.15 shows a graphical comparison between the predicted trajectory (average for the entire sample) and 3 measured repetitions from one sample participant for a reach movement to a target pulley located at hip height, initial contact angle of 270°, approach angle of 180°, inter-pulley distance of 381-mm, 38-mm target diameter, and a 3-mm target groove width. For this participant and specific condition, the $RMSE_{P\text{-}M}$ values between the predicted and measured trajectories were 50mm, 11mm, and 23mm respectively. This figure provides an example of the within-person variability for reach movements that have the same task parameters. The lack of visual feedback due to the target pulley region and initial contact angle interaction potentially increases the variability in measured trajectories.

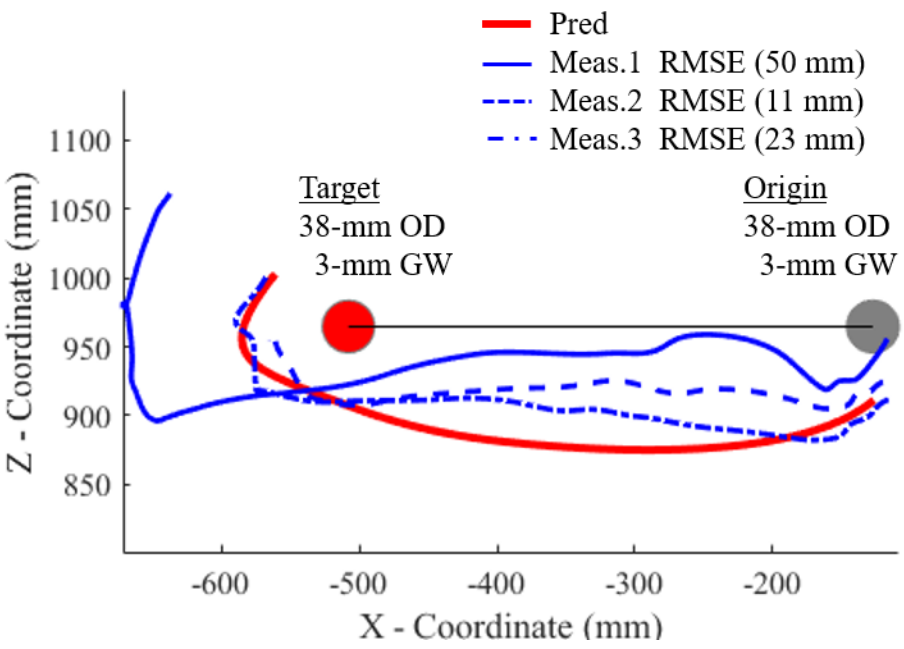

Figure 3.15. Predicted (Red) vs. three measured trajectories (Blue) from a sample participant, for a target pulley located at hip-height on the contralateral side of the body.

3.5 Discussion

This chapter presents a statistical model using b-splines and functional regression analysis for predicting hand trajectory shape in a sequential reach task with continuous material. The low RMSE of the fitted b-splines provides evidence that cubic b-splines adequately represent average hand trajectory shape for this task. Use of functional analysis methods allowed for both compression and smoothing of the trajectory shape and incorporating of this information into a statistical prediction model. Use of b-splines clamped at the ends (i.e., using repeated knots) allowed for combining predicted trajectory segments associated with transition and pulley interaction phases, while maintaining continuity in position and gradient between segments. This feature was essential to support our hypothesis of modeling a sequential reach tasks as alternating transition and pulley interaction phases. To our knowledge, this is the first such

model to predict reach trajectories to sequential targets wherein the hand does not come to rest at individual targets (i.e., the hand is continually in motion).

In contrast to typical approaches that examine scalar properties of reach trajectories (e.g., curvature, maximum deviation or excursion), the presented model provides a means for analyzing the effects of different task parameters on continuous trajectory shape. The model successfully predicted trajectory shape based on a diverse set of task parameters, accounting for an average of 32% of the variance in the control point locations for the transition phase and 36% for the pulley interaction phase. Inter-pulley distance and the two-way interaction between origin and target threading directions attributed to most of the explained variance, whereas the target wrapping angle and the two-way interaction between target diameter and wrapping angle attributed to most of the explained variance of the pulley interaction phase control point locations. Though the model captured a small portion of the variance, errors between predicted and measured trajectories were relatively low (31 ± 16 mm on average). Model performance degraded for conditions that had a wider origin pulley groove width, longer inter-pulley distances, larger target pulley diameters, and when target pulleys were located on the contralateral side of the body. Despite these differences, the mean error was lower than the mean within participant variability (62 ± 43 mm), computed as the maximum error between repeated trials with the same task conditions.

An interesting finding was that target groove width has a small effect on trajectory shape, despite having a large influence on movement time, as found in the previous chapter 2. This suggests that target tolerance only has an effect on hand movement trajectories in terms of speed and not the spatial domain. Hand trajectories tended to be more flat for movements with a larger amplitude, defined by the inter-pulley distance, and for reach movements that were

directed towards target pulleys located at standing height on both the contralateral and ipsilateral side of the body. These extreme locations forced the participant to fully extend their arms and approach their maximum reach envelope while attempting to remain aligned with the midline of the threading panel. The resulting constrained reach posture yielded little variability in reach movement trajectory.

Generally, the largest prediction errors occurred for reach movements located on the contralateral side of the body. Multiple factors may have contributed to this, including the inherently increased difficulty when reaching across the body as participants modify their movement to obtain line of sight to the reach target and fingertip resulting in increased variability in trajectory shape. Additionally, contralateral reach movements require contributions from multiple body segments shape (e.g., involves twisting of the torso and pelvis) which introduce a higher potential for movement error (Bertucco et al., 2013).

3.5.1 Study limitations

A few study limitations are worth emphasizing. This study was limited to modeling the fingertip trajectory path in a 2D frontal plane. As such, the model assumes hand grip configuration remained unchanged during the reach movements. Video observations did not provide evidence of any re-grasping during the threading task. However, corrections during the pulley interaction were observed when participants missed the groove during initial contact (i.e., positioning). Fitting b-splines with a fixed number of control points implies that the model predicts the average shape of trajectories with and without such corrections. From a theoretical perspective, there may be value in investigating shape trajectories separately for trials with vs. without such corrections, however, this may be relegated to future work.

The study investigated a specific set of task parameters related to hypothesis about target tolerance, reach distance and amplitude, and line of sight. The range of values for parameters were limited and largely informed by the specific applied context (i.e., field-based observations at the Sponsor's worksite) and prior research. Certain task parameters were easier to operationalize than others. Specifically, the model did not directly parameterize line of sight. Line of sight was initially parameterized by the three way interaction between the initial contact angle, and the X-, Z- coordinates of the target pulley location. However, it was not included in the final model due to collinearity issues. Line of sight was eventually parameterized in terms of target pulley location, initial contact angle, approach angle, and threading direction. This parameterization scheme might not be sufficient to completely characterize issues related to line of sight because often the arm and hand also blocks one's vison with the target. However, results demonstrate that the model was still capable of capturing differences in trajectory shape across reach movements with and without line of sight as parameterized.

The post prediction adjustment of control point locations to force continuity at the phase transitions is another limitation of this model. However, this was necessary in order to construct smooth trajectory shapes. Additionally, the model was only able to capture an average of 34% of the variability in the control point locations associated with task parameters. It is likely that naturally occurring variability in human movement attributes to a portion of the unexplained variance in this task, as evidenced by the large error within repeated conditions.

The presented model is limited to predicting the average shape change for the measured sample. Other than stature used for normalizing the pulley locations, the model does not account for factors influence between-person variability (e.g., manual dexterity, hand-eye coordination). This remains a topic of future investigation.

Reach trajectory shape is also influenced by temporal characteristics of the end effector, i.e., the speed of the hand movement, characterized by speed-accuracy tradeoffs akin to Fitt's law. For example, one might surmise that a faster hand movement during the transition phase (perhaps with increasing amplitude or inter-pulley distance) would result in a more rounded reach shape trajectory. Analysis of movement speeds during the transition and pulley interaction phases is the focus of the subsequent chapter 4.

3.6 Conclusions

To summarize, the work presented in this chapter is the first model to predict hand trajectory shape in sequential reach tasks with continuous material. Overall, the trajectory shape was influenced globally by target location. However, the presented model provides a way to quantify local effects of task parameters (e.g., target tolerances, reach direction and amplitude, and line of sight availability) that influence global hand trajectory shape. These findings align with and expand upon our understanding of movement behaviors from discrete reaches to continuous reaches. For instance, results from this study provide evidence to support prior studies demonstrating that humans update their central motor program (more open loop) in response to local task demands requiring feedback (e.g., changes in groove width, wrapping angle). Importantly, the results indicate that target tolerance and target directed reach movements to the contralateral side of the body have the largest influence on trajectory shape. Implementation of this model in digital human modeling software will allow workstation designers to simulate and analyze sequential reach tasks with continuous material for access (e.g. hand clearances, reachability) across diverse task parameters and operator anthropometry. These new capabilities would allow engineers to make informed decisions about equipment design (e.g., target characteristics and locations) for improving operator access and task efficiency.

CHAPTER 4

Hand Trajectory Speed: Model Development and Assessment

Abstract

This chapter presents a statistical model for predicting the average speed profile of hand movement in a sequential reach task with continuous material using task parameters (e.g., target characteristics, target locations and sequence) as predictors. Model development used hand trajectory data measured in 3 data collection experiments that involved threading target pulleys across combinations of task parameters representing pulley characteristics, reach direction and line of sight availability. The model generates continuous speed profiles using b-splines for two alternating movement phases: (1) a *transition* phase when the hand is reaching between two consecutive target pulleys, and (2) an *interaction* phase when the hand is engaged in threading a target pulley. Multiple regression was used to predict b-spline control point coordinates using task parameters as predictors. Goodness of fit assessed using root mean squared errors (RMSE) between predicted and measured speed profiles (average RMSE 124 ± 68 mm/s) and differences in the average predicted vs. measured speed in the transition phase (2 ± 91 mm/s) indicated that the model captured average trends in speed profiles, but did not capture variability in speed about the mean. Implications of the model results and variability in measured speed in terms of motor control mechanisms specific to handling continuous material are discussed.

4.1 Introduction

Research on hand movement control in manual assembly jobs has largely focused on tasks requiring discrete reaches. Examples include studies investigating hand kinematics during object transfer and positioning tasks, and in prehension tasks that involve reaching for and grasping an object (Bootsma & Van Wieringen, 1992; Hoff & Arbib, 1993; Jeannerod, 1984; Marteniuk, Leavitt, MacKenzie, & Athenes, 1990). Reaching movements in such tasks are often modeled as an initial open loop movement phase followed by a closed loop phase with feedback, with the transition timing affected by the target precision requirements.

Movement times and speed profiles are common performance metrics in object transfer and positioning tasks, often with an explicit linkage to the terminology of the classic reciprocal tapping/aiming tasks (Fitts, 1954; C. L. MacKenzie, Marteniuk, Dugas, Liske, & Eickmeier, 1987). In these tasks, the speed profile of a landmark on the hand/wrist is analyzed for determining the task start and end events, where the onset and end of a movement correspond to the instances when the landmark speed crosses a predetermined speed threshold. This method is sufficient for discrete reach tasks that begin and end with the hand in a stationary position (i.e., zero speed). However, defining the start- and end-points is more challenging in sequential reach tasks when the hand is reaching to multiple locations in quick succession and hence is continually in motion. In this scenario, the initial and final speed of the hand may differ between multiple locations and not always cross some predetermined threshold.

4.1.1 Prior Approaches to Modeling Speed Profiles

Quantitative modeling of speed profiles can provide useful insights into the underlying motor control mechanisms and strategies used for generating the movement, and hence of substantial interest to motor control theorists. Many researchers have reported hand speed

profiles of rapid-aimed movements to be approximately bell-shaped and symmetric (Atkeson & Hollerbach, 1985; Beggs & Howarth, 1972; Georgopoulos, Kalaska, & Massey, 1981; Morasso, 1981). Additionally, the bell-shaped profile is approximately superimposable after normalization cross reach movements that vary in duration, distance, and peak velocity (Atkeson & Hollerbach, 1985). One explanation for the symmetric bell-shaped speed profile is the minimum jerk model (Flash & Hogan, 1985) on hand and arm coordination in voluntary movements. This model posits that human's attempt to minimize the jerk during a reach motion to produce the smoothest possible movement of the hand. The bell-shaped speed profile also holds for the curvilinear velocity in movements made in handwriting (Plamondon, Yu, Stelmach, & Clément, 1991). The invariance in the speed profiles suggests the CNS takes into account speed for movement planning and control. Plamondon (1991) proposed that the invariance in the speed profiles was a result of the global stochastic properties of the different networks (e.g. neural and muscle fibers) involved in speed control and movement generation. Hence, according to Plamondon (1991), the bell-shape results from a global self-organization in the cumulative action by a set of speed processors (e.g. neural and muscle fibers) acting sequentially (Plamondon, 1991).

Plamondon, Alimi, Yergeau, and Leclerc (1993) reviewed different mathematical functions (e.g., logarithmic, Gaussian, and sigmoidal functions) used in prior literature for modeling typical bell-shaped speed profile of rapid hand movements tasks that start and end at zero-speed. These include models of asymmetric bell-shaped speed profiles of hand motions in rapid hand movement tasks. Plamondon (1993) found asymmetric bell-shaped models perform better when compared to symmetric bell-shaped models of predicting hand speed in handwriting. Some examples include the lognormal model and the support-bounded lognormal model, both of which take in consideration the displacement of the hand, the movement time, and the mean (μ)

and dispersion (σ^2) of the impulse response of the neuro-muscular-system involved in the generation of the movement. The support-bounded lognormal model forces the speed to reach zero at the beginning and end of the movement proving to be a better fit compared to others. Another technique for modeling speed in rapid hand movements involves using piecewise functions to model the acceleration and deceleration phases separately, such as the Plamondon Gaussian model (Plamondon et al., 1991), which considers the peak speed throughout the movement, the time to peak speed, and time constants of curves fit to the acceleration and deceleration phases. One benefit of this model, is that the time and magnitude of the peak speed of the model output and observed trajectory is equivalent.

Related to the current study, hand speed in sequential reach movements with continuous material have two unique intrinsic properties which cause traditional approaches to modeling speed profiles to be inadequate. First, is that the hand speed differs at the start and end of each movement phase depending on the task parameters. The second challenge is that hand speed at the end of each movement phase progresses into the start of the next movement phase in the sequence. Thus, any attempt at modeling the speed profile would need to allow for such continuity in speed magnitude and gradient (i.e., acceleration) between multiple reach segments (e.g., target 1 to 2 vs. target 2 to 3), especially for implementation in digital human modeling software.

4.1.2 Study Objective

The previous chapter 3 presented a methodology for predicting continuous hand trajectory shape using b-splines in a sequential reach task with task parameters (e.g., target characteristics, target locations and sequence) as predictors. It involved predicting b-spline control points fit to alternating phases of transition and pulley interaction, followed by a process

of combining consecutive segments to form a continuous trajectory while maintaining continuity in position and gradient at transition points between segments. This chapter addresses the modeling of average hand speed profiles for the transition and pulley interaction phase during each segment of the sequential reach task. The study objective was to develop a model to predict the temporal properties of hand movments in terms of average speed profiles in a sequential reach task using task parameters (i.e., target characteristics, target locations and sequence) as predictors. Predicted speed profiles were combined with path length (using predicted hand trajectory shape in Chapter 3) to estimate task completion times. The study hypothesized task parameters associated with target tolerance, reach movement direction and amplitude, and line of sight to the target to jointly influence changes in hand speeds during the task.

4.2 Methodology

This study used hand trajectory data obtained from Experiments 1, 2, and 3 described in the previous Chapter 3 to develop and assess a statistical model for predicting average speed profile. A description of the data collection procedures for each the experiments was provided in Section 3.2. Table 4.1 summarizes the task parameters that were manipulated in the data collection experiment. Across the 3 experiments, participants had to perform one-handed sequential reach movements that involved transferring thread between successive target pulleys in a predefined sequence while wrapping the thread along a groove on the circumference of each target pulley.

Table 4.1. Summary of the underlying task variables and associated parameters or independent variables manipulated in Experiments 1, 2, and 3. Cell highlighted in grey indicate fixed levels (constants) in the experiment.

Task Variable	Independent variable	Experiment-1	Experiment-2	Experiment-3
Target Tolerance	Groove Width, mm (in.)	3 (1/8”)	6 (1/4”)	3 (1/8”) , 6 (1/4”), 9 (3/8”)
	Pulley Diameter, mm (in.)	38 (1.5”)	38 (1.5”), 76 (3”), 152 (9”)	38 (1.5”), 152 (6”)
	Wrapping Angle	45°, 90°, 135°	45°, 90°, 135°	45°, 90°, 180°
Reach Distance	Inter-pulley distance, mm (in.)	229 (9”), 318 (12”), 381 (15”)	229 (9”), 318 (12”), 381 (15”)	229 (9”), 343 (13.5”), 457 (18”)
Reach Direction	Target Approach Angle	0°, 90°, 180°, 270°	0°, 45°, 90°, 135°, 180°, 225°, 270°, 315°	45°, 135°
	Origin to Target Threading Direction	Co-rotating pairs (CW to CW, or CCW to CCW)	Counter- rotating pairs (CW to CCW, or CCW to CW)	Co-rotating pairs (CW to CW, or CCW to CCW)
Reach Direction & Line of sight	Threading location (region)	Center Top – Right Bottom – Right Top – Left Bottom – Left	Center Top – Right Bottom – Right Top – Left Bottom – Left	Azimuth angle: Upper right, 45° Upper left, 135°
	Initial Contact Angle	0°, 90°, 180°, 270°	0°, 45°, 90°, 135°, 180°, 225°, 270°, 315°	45°, 135°, 225°, 315°

4.2.1 Instrumentation and Data Processing

An optical motion capture system (Qualisys, Göteborg, Sweden) was used to record hand movements at a sampling frequency of 120 Hz. A passive-marker triad located on the dorsum (i.e., back) of the participants' right hand estimated the position of the thumb-forefinger pinch grip based on the pretest calibration measurement. Three-dimensional coordinate data from the motion capture system was filtered using a 2nd-order low-pass Butterworth filter with a 6-Hz cut-off frequency. Two-dimensional hand (thumb-forefinger) position data in the frontal plane (i.e., parallel to work-panel) was computed using data from the static 3-second calibration pose recorded at the start of each threading trial.

Speed profiles were generated from the filtered position data using finite differences. The data were then segmented into alternating phases of transition and pulley-interaction based on specific event-criteria in the position data as described in Chapter 3. The transition phase 'P_T' represented segments when the hand was reaching between two consecutive target pulleys. The interaction phase 'P_{PI}' represented segments of the movement when the hand was engaged in threading a target pulley.

Overall, the measured hand speed profiles were observed to have high variability in both the transition and pulley interaction phases. Figure 4.1 shows an exemplar measured hand trajectory path and corresponding speed profile obtained from one participant in a sequential threading trial (sequence 1A in Experiment – 3) with a target diameter and groove width equal to 152-mm and 9-mm, respectively. The trajectory and speed profile is segmented and color-coded into transition (blue) and pulley-interaction phases. The speed profile for transitions from the origin pulley (PL_0) to target pulley (PL_1) roughly resemble a bell-shaped curve containing the peak speeds but with notably different speed magnitudes at the start vs. end of the transition

phase. However, speeds fluctuated in both the transition and pulley-interaction phases. Potential sources of these variabilities are postulated in the Discussion section.

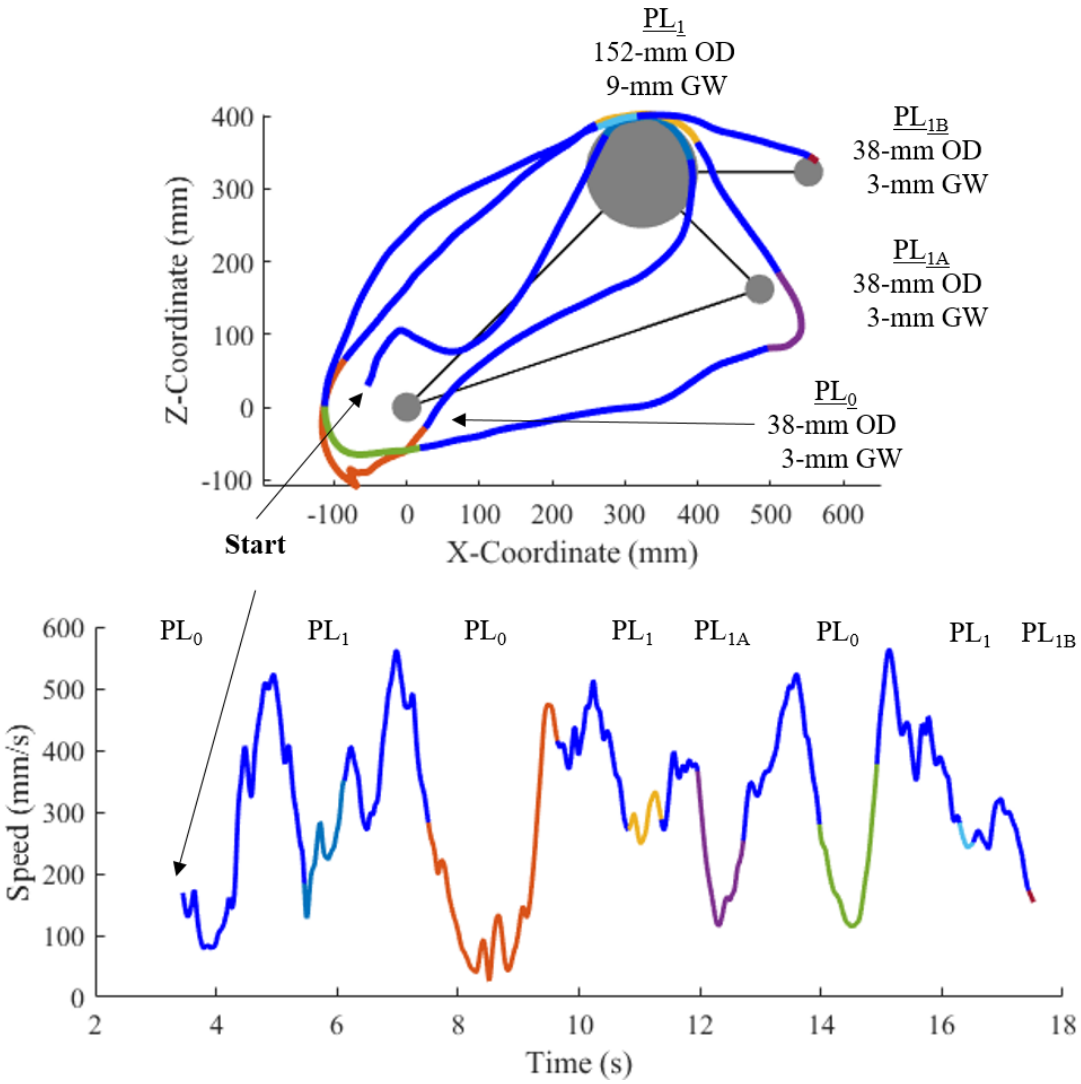

Figure 4.1. Exemplar speed profile and corresponding hand trajectory segmented into transition (blue) and pulley-interaction (other colors) phases for a continuous threading sequence. The origin pulley was located on the midline at elbow height. Note: The hand is already in motion at the start of the threading trial.

Figure 4.2 depicts exemplar hand trajectory paths (top panel) and corresponding speed profiles (bottom panel) for 10 participants for a pair of transition (in blue) and pulley-interaction

(in red) phase data for a sample test condition in Experiment – 3 with a target diameter and groove width equal to 152-mm and 6-mm, respectively. The speed phases are time normalized. Patterns in the normalized speed profiles start to emerge, specifically in terms of an approximately bell-shaped speed curve in the transition phase (in blue) and inverted bell-shaped speed curve in the pulley-interaction phase (in red). The subsequent section describes a method for predicting the *average pattern* of such continuous speed profiles as a function of task parameters.

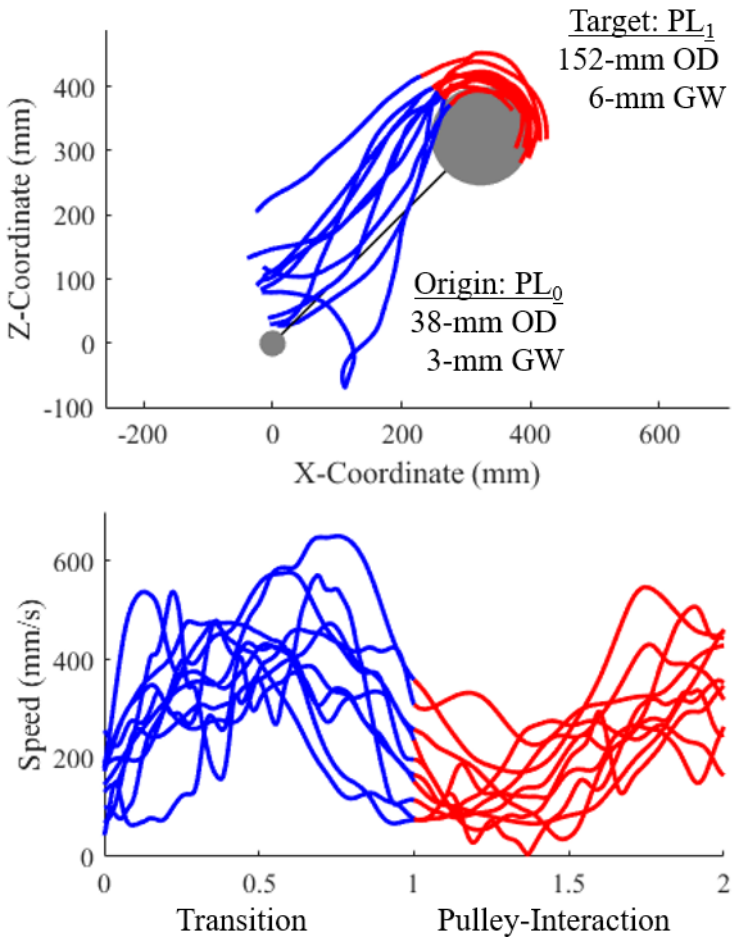

Figure 4.2. Exemplar measured hand trajectories (top panel) and speed profiles (bottom panel) from 10 participants segmented into transition (blue) and pulley-interaction (red) phases for hand movements between a pair of origin pulley PL_0 and target pulley PL_1 extracted from a sequential threading task. Speed profiles are time normalized by the length of the respective phases. The origin pulley PL_0 was located on the midline at elbow height.

4.3 Model for Predicting Speed Profiles and Task Completion Time

Figure 4.3 provides an overview of the method that was developed for predicting average speed profiles across different motion trials using task parameters as predictors. Task completion times for the entire sequential reach task were estimated using predicted speed profiles and path length of the reach movement trajectory.

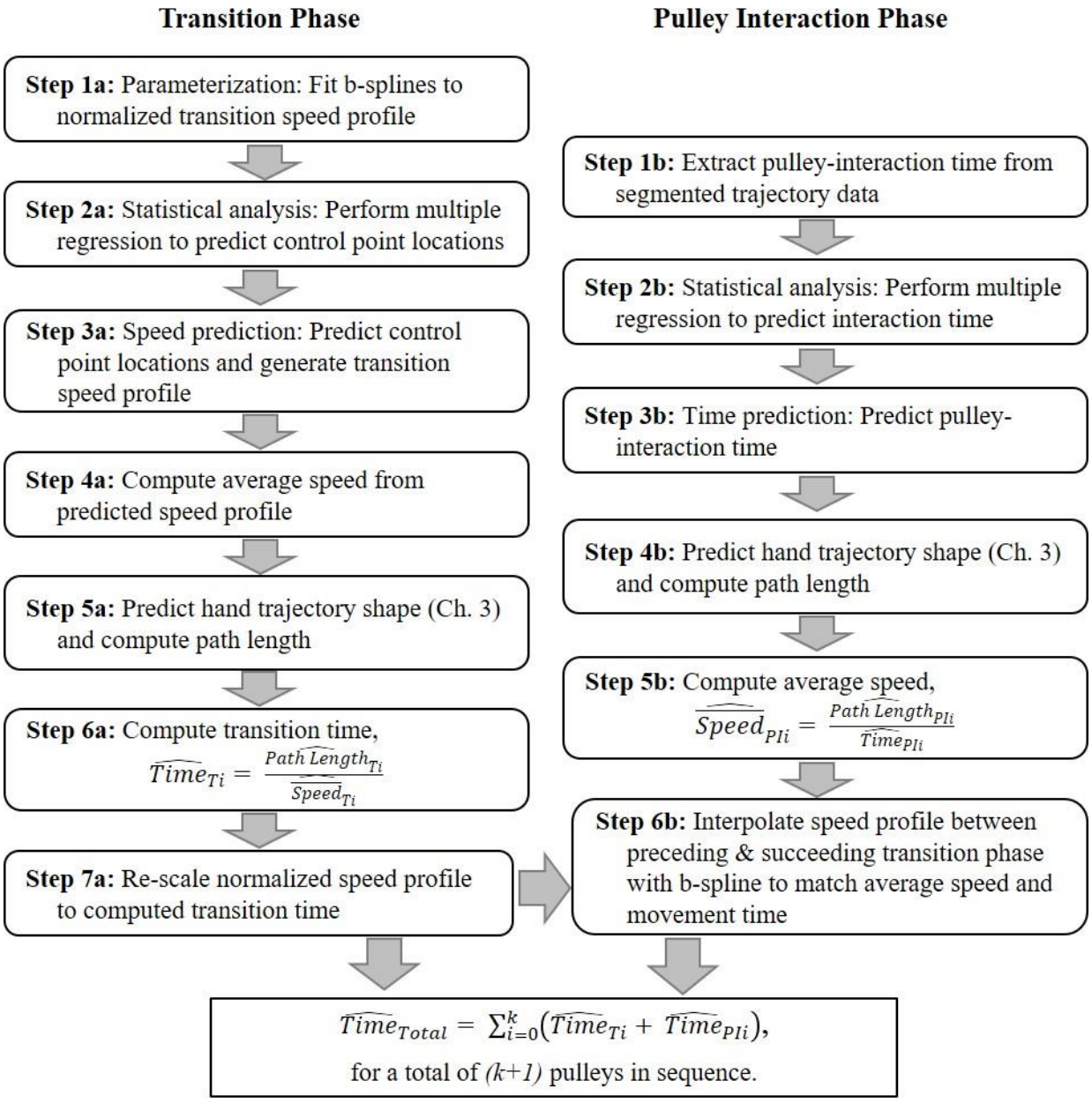

Figure 4.3. Overview of the proposed model for predicting hand speed profiles and task completion based on segmented transition and pulley interaction phases.

4.3.1 Transition Phase: Step 1a - Speed profile parameterization

B-splines were used to model the hand trajectory speed profiles in the frontal plane for each transition phase. Initially the transition phase speed profile was normalized to unit time. Next, 4th-order b-splines were fit to each of the measured speed profiles with 5 control points (speed mm/s, % time) using the methodology described in chapter 3 for fitting hand trajectory shape with b-splines. The timing dimension of the control points was constant (i.e. 0.0, 0.17, 0.5, 0.83, and 1.0, respectively), resulting in a five 1-dimensional control point coordinates capturing the variations in speed (P_{T0} *to* P_{T4}). Example b-spline fitted to normalized transition phase speed profiles are shown in Figure 4.4. Even though hand speeds showed high variability, 5 control points were used to perform a smoothing function while also achieving the objective of capturing the general underlying shape of the speed profiles. Across all motion trials, the average RMSE between the fitted b-splines and measured speed profiles was 38 ± 28 mm/s.

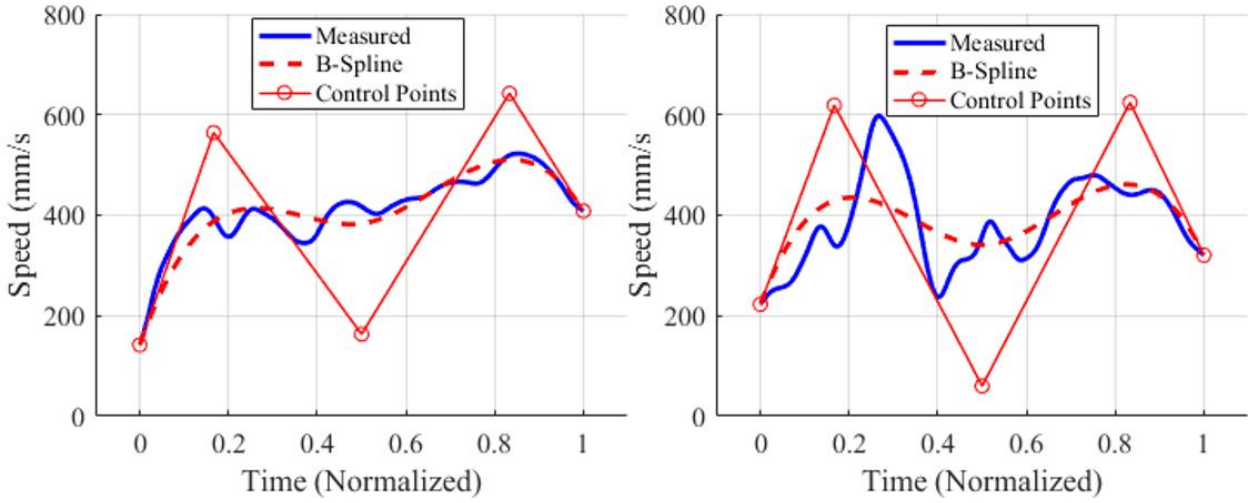

Figure 4.4. Exemplar b-splines fitted to measured hand speed profiles in the transition phase (normalized to unit time) for 2 participant motion trials with an inter-pulley distance of 457-mm, 152-mm target diameter, and 9-mm groove width. The b-spline fits provide a smoothing of the speed profile while capturing the general underlying shape of the speed profiles.

4.3.2 Transition Phase: Step 2a – Statistical Analysis

Five linear regression analyses were performed on the fitted 1-dimensional speed profile control points, P_{T0} *to* P_{T4}. A generic form of the regression equations are presented in Table 4.2. Forward stepwise regression was used to select predictors based on statistical significance criteria of $p < 0.05$ for inclusion in the final regression models to predict the 1-dimensional control point coordinates. Pulley diameter and groove width represent the target size and tolerance, and the inter-pulley distance represents the movement amplitude. Threading direction (CW vs. CCW) at the origin and target pulleys and their two-way interaction were included to differentiate between co- vs. counter rotating pulleys. Pulley location coordinates and inter-pulley distance were normalized to stature. Pulley location was in reference to the global coordinate system origin located at the midpoint of the starting feet position. Approach Angle (0-315°) was defined as the angle of the vector pointing from the origin pulley to the target pulley in reference to the horizontal.

Table 4.2. Generic form of the multiple regression equations for predicting control points for the transition speed profile (left column) and log-transformed pulley interaction time (right column).

Control Points for Transition Phase, P_T	**Pulley Interaction Time, log-transformed**
$P_{T0}\ to\ P_{T4} =$	$\mathrm{LN}(Time_{PI}) =$
$\beta_0 +$	$\beta_0 +$
$\beta_1(Origin\ Diameter) +$	$\beta_1(Target\ Diameter) +$
$\beta_2(Origin\ Groove\ Width) +$	$\beta_2(Target\ Groove\ Width) +$
$\beta_3(Target\ Diameter) +$	$\beta_3(Target\ Location\ X) +$
$\beta_4(Target\ Groove\ Width) +$	$\beta_4(Target\ Location\ Z) +$
$\beta_5(Target\ Location\ X) +$	$\beta_5(Target\ Threading\ Direction) +$
$\beta_6(Target\ Location\ Z) +$	$\beta_6(Target\ Initial\ Contact\ Angle) +$
$\beta_7(Origin\ Threading\ Direction) +$	$\beta_7(Inter-Pulley\ Distance) +$
$\beta_8(Target\ Threading\ Direction) +$	$\beta_8(Approach\ Angle)\ +$
$\beta_9(Target\ Initial\ Contact\ Angle) +$	$\beta_9(Target\ Wrapping\ Angle) +$
$\beta_{10}(Inter-Pulley\ Distance) +$	$\beta_{10}(Target\ Wrapping\ Angle) \times$
$\beta_{11}(Origin\ Wrapping\ Angle) +$	$(Target\ Diameter) +$
$\beta_{12}(Target\ Wrapping\ Angle)\ +$	$\beta_{11}(Target\ Location\ X) \times$
$\beta_{13}(Approach\ Angle)\ +$	$(Target\ Location\ Z)$
$\beta_{14}(Target\ Threading\ Direction) \times$	
$(Origin\ Threading\ Direction) +$	
$\beta_{15}(Target\ Location\ X) \times$	
$(Target\ Location\ Z)$	

4.3.3 Transition Phase: Step 3a – Speed Profile Prediction

In this step, for a given set of predictor values, 1-dimensional control points for transition speeds could be predicted using the regression equation Table 4.2. Predicted speed profiles were constructed for the transition phase from one origin to target pulley location reach movement across all of the measured trial conditions.

4.3.4 Transition Phase: Step 4a to 6a

The main goal of these steps were to rescale the predicted transition speed profile from normalized time to absolute time units. This rescaling was performed by computing the movement time for each transition phase ($\widehat{Time}_{Ti}$) using equation 4.1, where $\widehat{Path\ Length}_{Ti}$ is the scalar path length of the corresponding predicted transition phase trajectory, and $\overline{\widehat{Speed}}_{Ti}$ is the scalar average speed of the predicted speed profile obtained in the previous step 3a.

$$\widehat{Time}_{Ti} = \frac{\widehat{Path\ Length}_{Ti}}{\widehat{Speed}_{Ti}} \quad [4.1]$$

$\widehat{Path\ Length}_{Ti}$ was computed by a finite integration of the predicted hand trajectory shape for the corresponding segment of the sequential reach task (i.e., previous Chapter 3). The timing dimension of the normalized transition speed profile (i.e. 0.0, 0.17, 0.5, 0.83, and 1.0, respectively) was rescaled to $\widehat{Time}_{Ti}$ resulting in a transition speed profile expressed in absolute units of time (i.e., seconds).

4.3.5 Pulley Interaction Phase: Steps 1b to 3b: Predict Interaction Time

Pulley-interaction phase speed profiles were analyzed separate from the transition phase, due to the short durations and irregularity of speed profile shape. The latter resulted largely due to the pulley-interaction phase containing speed fluctuations during corrective movements when participants missed the pulley groove and had to re-thread the pulley. Figure 4.5 shows a sample trial with multiple corrective movements and a measured $Time_{PI}$ of 7.03 seconds.

A multiple regression model was constructed to predict pulley-interaction phase duration (LN($Time_{PI}$)), based on the task parameters (Table 4.2). This approach accounted for durations that were influenced by movement corrections. Since the distribution of time durations had positive skewness due to the aforementioned movement corrections, the data were log-transformed prior to regression analysis. Figure 4.6 depicts the distribution before and after transformation.

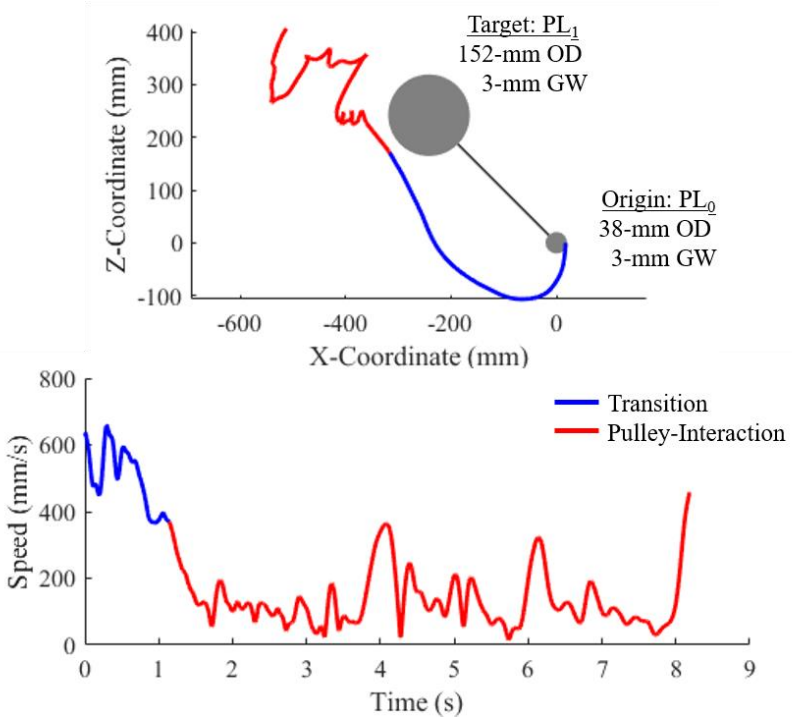

Figure 4.5. Exemplar measured hand trajectory (Top) and speed profile (Bottom) for the transition (blue) and pulley interaction (red) phases in a motion trial with multiple corrective movements. The movement trajectory is normalized to the origin pulley location aligned with the participant's mid-sagittal plane at elbow height.

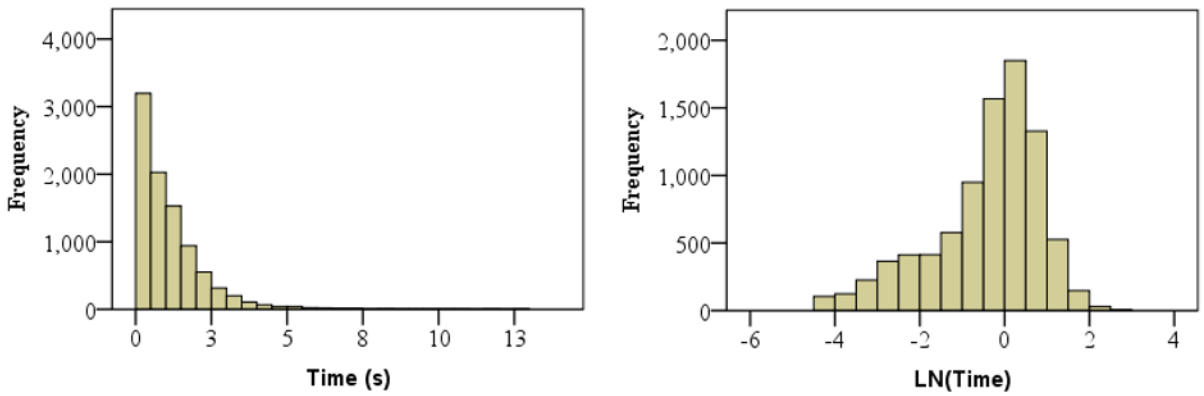

Figure 4.6. Distribution of measured times (left) and log-transformed times (right) for the pulley interaction phase across all measured motion trials (N = 9396).

4.3.6 Pulley Interaction Phase: Steps 4b to 6b – Interpolate Interaction Speed Profile

Predicted pulley-interaction phase speed profiles are interpolated using b-splines between two consecutive predicted transition phase speed profiles. The interpolation was performed with the objective of maintaining integrity between path length ($\widehat{Path\ Length}_{PIi}$), duration ($\widehat{Time}_{PIi}$), and resulting average speed ($\widehat{\overline{Speed}}_{PIi}$) of the pulley-interaction phase. First, the average speed in the pulley-interaction phase was calculated using equation 4.2.

$$\widehat{\overline{Speed}}_{PIi} = \frac{\widehat{Path\ Length}_{PIi}}{\widehat{Time}_{PIi}} \quad [4.2]$$

where $\widehat{Path\ Length}_{PIi}$ is the path length of the predicted pulley-interaction phase trajectory (Chapter 3), and $\widehat{Time}_{PIi}$ is the predicted pulley-interaction phase time (Step 3b).

Figure 4.7 shows a schematic of the interpolation process. Three control points P_{PI1} to P_{PI3} were used to interpolate the speed profile. Control points P_{PI1} and P_{PI3} were positioned to be collinear with last two control points in the preceding transition phase and the initial two control points of the succeeding transition phase, respectively, in order to force continuity in speed magnitude and gradient (i.e., acceleration). The step also accounts for different magnitudes of initial and terminal speed in the interaction phase. The control point P_{PI2} was adjusted along the vertical axis such that the average speed of the interpolated b-spline matched the desired average $\widehat{\overline{Speed}}_{PIi}$ obtained in Equation 4.2. In some rare cases, if the interpolated speed profile contained negative values, a post-prediction algorithm was run (Appendix B).

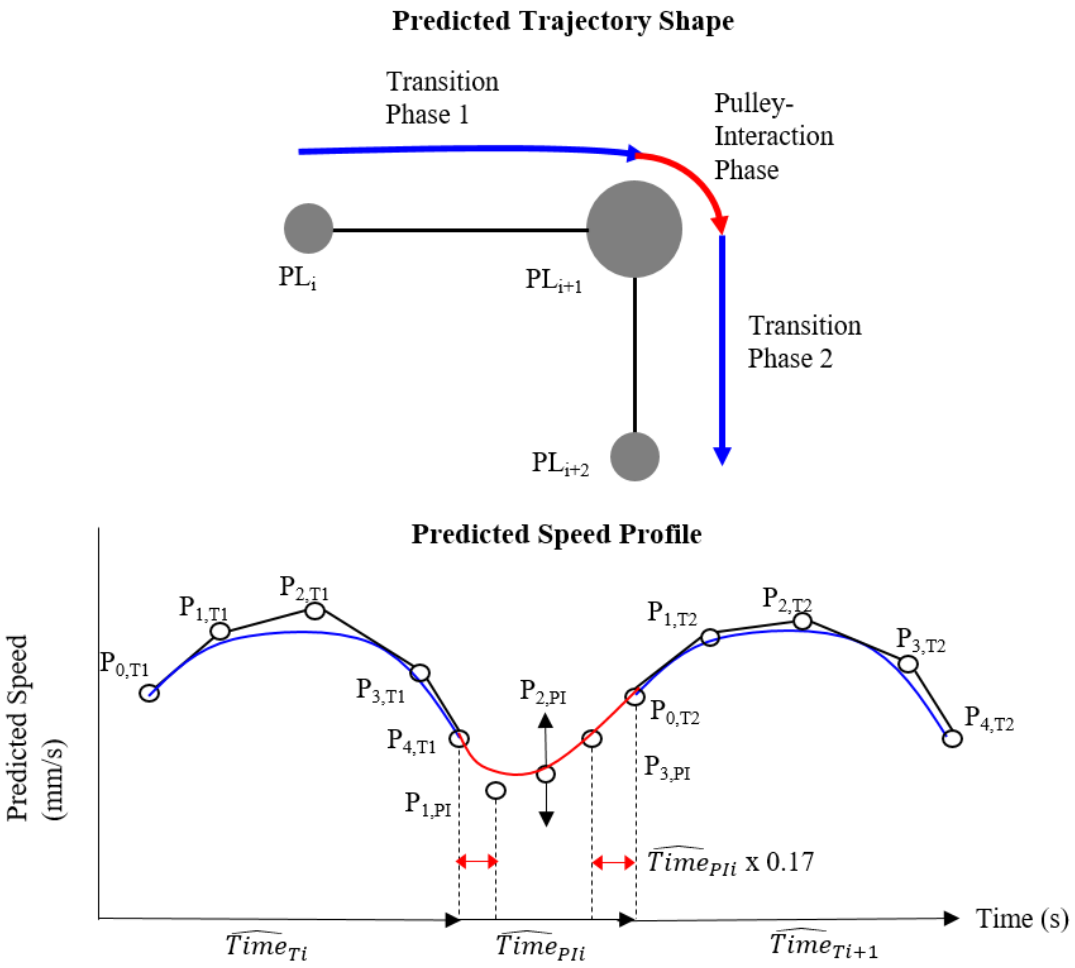

Figure 4.7. Schematic representation of the process for interpolating the speed profile (bottom panel) in the pulley interaction phase (red) between two transition phases (blue) for a hand trajectory movement from an origin pulley to two successive target locations (shown in top panel).

The interpolation process described above produces a continuous speed profile between alternating transition and interaction phases in absolute time, and can be extended to any number of pulleys in a threading sequence. Figure 4.8 shows an exemplar predicted trajectory shape and speed profile for a sample task condition that involved a sequential reach movement from an origin pulley to pulley PL_1 and back to pulley $PL_0 = PL_2$. The origin pulley, PL_0 (= PL_2) was located at 1100 mm (about elbow height) in line with mid-sagittal plane and has a 38-mm

diameter and 3-mm groove width, while the first target pulley PL_1 has a 152-mm diameter and 9-mm groove width. The segmented transition and pulley-interaction phases are shown in blue and red, respectively. The subsequent chapter 5 provides a more systematic and detailed validation of such continuous trajectory shapes and speed profiles.

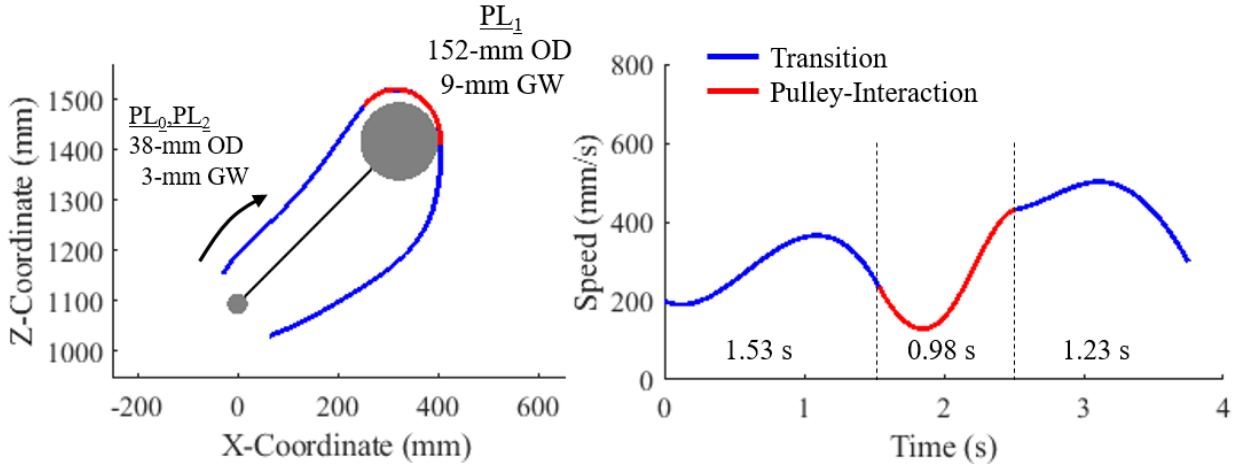

Figure 4.8. Exemplar predicted trajectory shape (left) and predicted speed profile (right) for a hand trajectory movement from an origin pulley to two successive target locations. The origin pulley PL_0 is located in line with the mid-sagittal plane at elbow height (1100 mm). Predicted trajectory shape and speed are segmented into the transition (blue) and pulley-interaction phases (red).

4.3.7 Total Task Completion Time

From the above, task completion time for the entire sequential reach task could be computed as the linear sum of movement times for alternating phases of transition and pulley interaction and for consecutive pairs of origin to target pulleys. Equation 4.3 provides a general form of the equation for computing task completion time,

$$\widehat{Time}_{Total} = \sum_{i=0}^{k} \left(\widehat{Time}_{Ti+1} + \widehat{Time}_{PIi+1} \right) \quad [4.3]$$

where, $\widehat{Time}_{Ti+1}$ is the transition phase duration when reaching from pulley *(i)* to pulley *(i+1)*, and computed using equation 4.1; $\widehat{Time}_{PIi+1}$ is the duration of the interaction phase at pulley

(i+1) obtained from Step 3b, and *i* = 0 to *k*, where '*k'* is the total number of pulleys in a sequence. Chapter 5 evaluates this step in more detail.

4.3.8 Model Assessment

The model presented was assessed for goodness of fit by transition phase and pulley interaction separately using multiple measures.

***Transition Phase**:* Goodness of fit of the predicted average speed profiles was assessed by computing:

(1) The root mean squared error between time normalized predicted and observed speed profiles for each trial ($RMSE_{P\text{-}M}$) in the transition phase obtained from Experiments 1, 2 and 3 by condition. $RMSE_{P\text{-}M}$ was computed as the difference in speed at each frame on the normalized predicted trajectory matched to the corresponding frame on the normalized measured trajectory, as follows:

$$RMSE_{P-M} = \sqrt{\frac{1}{k}\sum_{i=1}^{k}(S_i - K_i)^2} \qquad [4.4]$$

where, *S* and *K* are the predicted and measured speed profiles in the transition phase, respectively, and *k* is the length of the normalized time vector *t*.

(2) The root mean squared error between measured speed profiles ($RMSE_{M\text{-}M}$) across repetitions for the same task conditions, in order to obtain a measure of the within-participant variability. The repetitions were normalized by time prior to computing the root mean squared error using equation 4.4 between pairs of the three measured repetitions (i.e. Repetitions 1 vs. 2, Repetitions 1 vs. 3, and Repetitions 2 vs. 3).

(3) Difference between the average predicted speed profile and average measured speed ($\overline{Speed}_{\text{Error}}$) in the transition phase obtained from Experiments 1, 2 and 3 by condition. One

sample t-tests with a significance criteria of $p < 0.05$ were used to test for statistically significant differences in $\overline{Speed}_{\text{Error}}$ across key task parameters.

Pulley-Interaction Phase*:* Predictions of pulley interaction duration, $Time_{PI}$ (from Step 3b) was assessed by comparing the mean difference in predicted minus measured times ($Time_{PI,Error}$) across task parameters that were found to have the largest effect on $Time_{PI}$. One sample t-tests with statistical significance set at $p < 0.05$ were conducted to assess statistical significance.

4.4 Results

The mean (± SD) age, stature, and mass of participants in the study sample used for model development by Experiment 1, 2, and 3 and combined are listed in Table 4.3. The remainder of the results section is devoted to model assessment at the transition and pulley interaction phases.

Table 4.3. Mean (± SD) age, stature, and mass for participants in Experiments 1, 2, and 3.

Experiment	N (Men, Women)	Age, years (Mean ± SD)	Height, cm (Mean ± SD)	Mass, kg (Mean ± SD)
1	6 (2, 4)	21.5 ± 2.1	166.0 ±10.9	64.9 ± 14.1
2	8 (5, 3)	21.1 ± 1.1	173.5 ± 7.9	71.1 ± 7.3
3	10 (6, 4)	23.5 ± 4.2	170.9 ± 9.1	73.1 ± 23.2
Combined	24 (13, 11)	22.2 ± 3.1	170.5 ± 9.3	70.4 ± 22.8

4.4.1 Transition Phase - Regression Results

Table 4.4 summarizes the results from the regression analysis for the speed profile control point locations in the transition phase in terms of standardized beta coefficients for significant predictors and the explained variance using adjusted R^2 values ($\hat{R}^2_{adj}$). The average (± SD) $\hat{R}^2_{adj}$ for the five models was 0.12 ± 0.03. Given the different units used for each predictor resulting in differently scaled unstandardized partial coefficients, the standardized partial

coefficients are preferred when comparing effects of predictors to each other. Standardized partial coefficients can be interpreted as the number of standard deviations the outcome increases for every standard deviation increase in the predictor, holding all other predictors constant. The unstandardized beta coefficients are provided in Appendix D.

Table 4.4. Standardized beta coefficients for significant predictors ($p < 0.05$) of the 1-dimensional control point coordinates in the transition phase. A blank cell indicates a statistically non-significant effect. The total row provides a measure of explained variance using the $\hat{R}^2_{adj}$ values for each regression model.

Predictor	Transition Phase Speed Profile Control Points from datasets 1-3				
	$\boldsymbol{P_{T0}}$	$\boldsymbol{P_{T1}}$	$\boldsymbol{P_{T2}}$	$\boldsymbol{P_{T3}}$	$\boldsymbol{P_{T4}}$
Intercept	168.55	108.68	202.74	254.89	248.82
Origin Diameter	0.15	0.15	-0.06	-0.08	
Origin Groove Width	0.14	0.07	0.10	0.07	0.10
Target Diameter	-0.02	-0.04	-0.05	-0.09	-0.06
Target Groove Width	0.07	0.02		0.14	0.18
Target Location X			0.07	-0.08	-0.25
Target Location Z	-0.08		-0.03	-0.05	-0.09
Origin Threading Direction	0.08	0.06	0.26		
Target Threading Direction	0.09	0.07	0.28		
Target Initial Contact Angle	0.09	0.07	0.08		
Inter-pulley Distance	0.03		0.17	0.19	
Origin Wrapping Angle	0.23	0.23	0.15	0.06	0.09
Target Wrapping Angle	-0.13	-0.09	-0.09	-0.05	-0.08
Approach Angle					0.05
Origin x Target Threading Direction	-0.13	-0.19	-0.52		
Target Location X x Z	0.08	0.09			0.13
$\hat{\mathbf{R}}^2_{\mathbf{adj}}$	0.16	0.12	0.13	0.09	0.08
Mean (± SD) $\hat{\mathbf{R}}^2_{\mathbf{adj}}$	0.12 ± 0.03				

Generally, most of the explained variance in control point locations was attributable to the origin pulley wrapping angle (standardized partial coefficient, β ranged from 0.06 to 0.23), inter-pulley distance (β: 0.03 to 0.19) and groove width at the target pulley (β: 0.02 to 0.18). The

wrapping angle at the origin pulley had a large effect on the speed profile at the beginning of the transition phase (β = 0.23). Additionally, increases in inter-pulley distance and target pulley groove width corresponded to higher speeds towards the end of the transition phase.

Figure 4.9 shows two example effects of wrapping angle at the origin and target pulley on predicted speed profile shape for one transition and pulley-interaction phase. In Figure 4.9, the blue curve depicts the average speed profile for a wrapping angle of 180º at the origin pulley and 90º at the target pulley. The red curve depicts the average speed profile for a wrapping angle of 45º at the origin pulley and 180º at the target pulley. In general, the average speed profiles in the transition phase tended to resemble a symmetric bell-shape with a prominent acceleration followed by a deceleration component approaching the pulley interaction phase. A larger wrapping angle at the origin pulley (solid red curve) was associated with a higher peak speed and higher average speed during the transition phase, compared to conditions with a smaller origin wrapping angle (solid blue curve) which indicated a longer rise to peak speed. For the specific task condition shown in Figure 4.9, the predicted average speeds for the 45° and 180° origin wrapping angle conditions were 289 mm/s and 408 mm/s, respectively.

Wrapping angle at the target pulley influenced the duration of pulley-interaction. The minimum speeds in the pulley-interaction phase were of similar magnitude irrespective of wrapping angle at the target pulley. The deceleration in the pulley interaction phase occurred more gradually i.e., over a longer duration, for target pulleys with the larger wrapping angle (dotted red curve) compared to smaller wrapping angle (dotted blue curve).

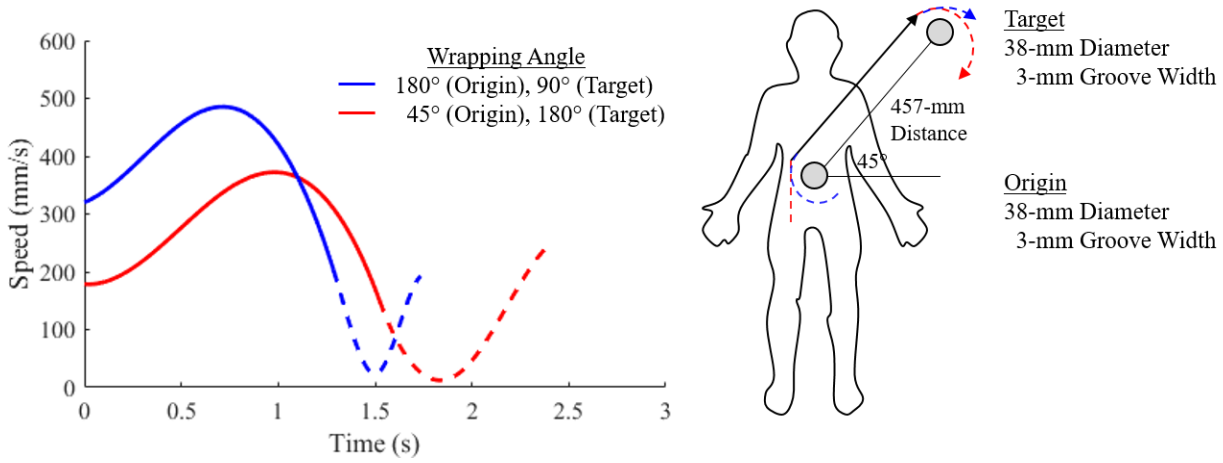

Figure 4.9. Effect of wrapping angle at the origin and target pulley on predicted speed profile shape in the transition phase (solid line) and pulley-interaction phase (dotted line) for task conditions shown on the right.

Figure 4.10 shows an average effect of target groove width (top panel; for a target pulley diameter of 38-mm) and target diameter (bottom panel; for a target pulley groove width of 3-mm) on predicted speed profile shape with all other task parameters held constant. Target groove width and diameter tended to primarily affect the predicted peak speed in the latter portion of the transition phase, with wider target groove widths and smaller diameters corresponding to increases in predicted peak speed. In the pulley-interaction phase, narrower target groove widths were associated with decreases in minimum predicted speeds and longer predicted times (Figure 4.10, top panel). Larger target pulley diameters were associated with a longer duration of pulley interaction (Figure 4.10; bottom panel). Both, narrower groove widths and larger diameters (which increases the arc-length of contact) corresponded to smaller tolerances and longer movement times providing evidence of a speed-accuracy tradeoff.

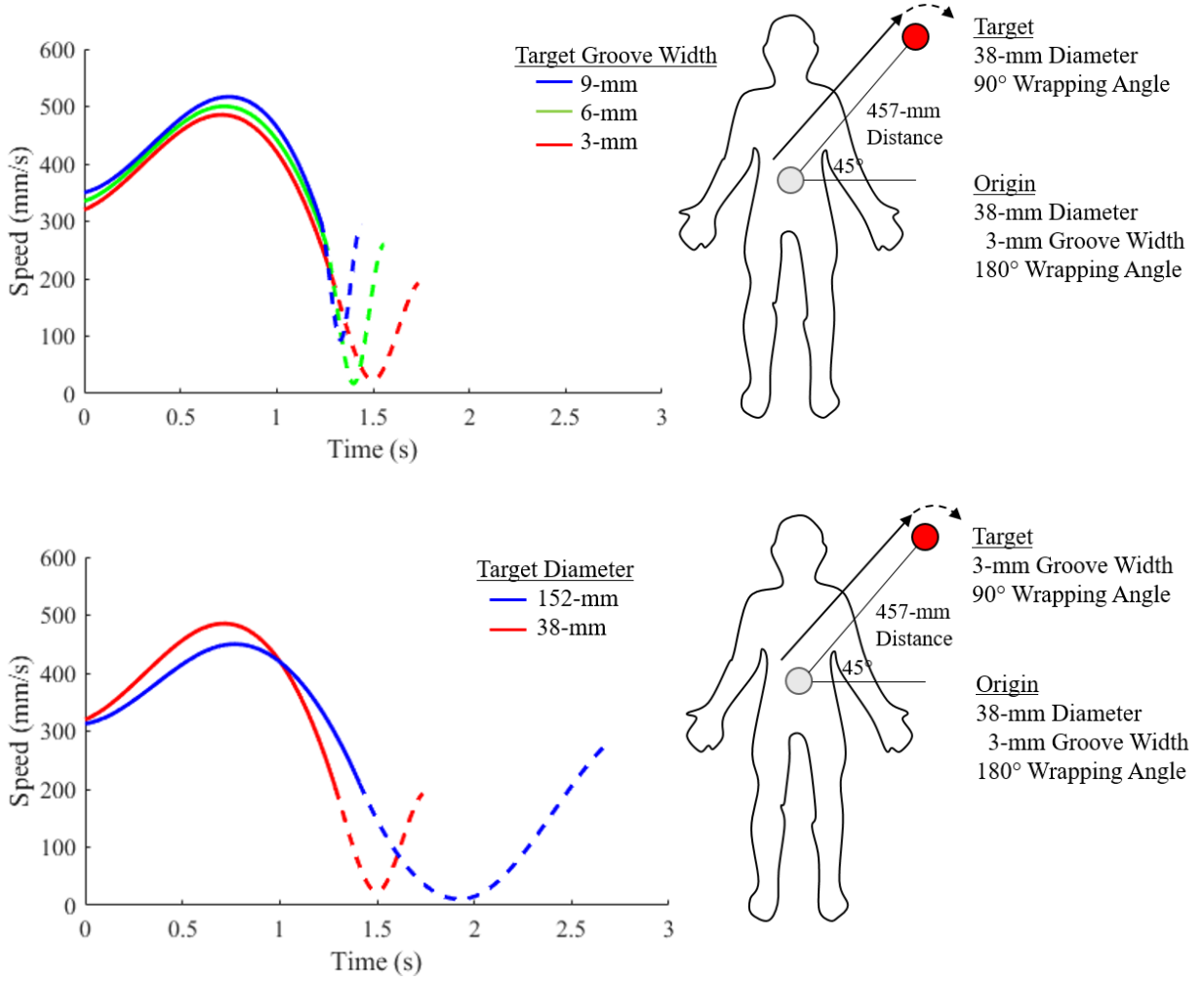

Figure 4.10. Average effects of target groove width (Top) and target diameter (Bottom) on predicted transition phase (solid line) and pulley-interaction phase (dotted line) speed profiles for task conditions depicted on the right.

Lastly, Figure 4.11 shows an example effect of inter-pulley distance on predicted speed profile shape for reaching toward a target pulley with a 38-mm diameter and 3-mm groove width and all other task parameters held constant. Predicted speed profile shape was generally scaled by inter-pulley distance in terms of the predicted speed magnitude and duration. Reach movements toward target pulleys with shorter inter-pulley distances corresponded to decreases in predicted peak and average speeds in the transition phase and shorter durations in the pulley

interaction phase. For the specific inter-pulley distances of 457-mm, 342-mm, and 229-mm compared in Figure 4.11, average predicted speeds in the transition phase were 288 mm/s, 259 mm/s, and 230 mm/s, respectively.

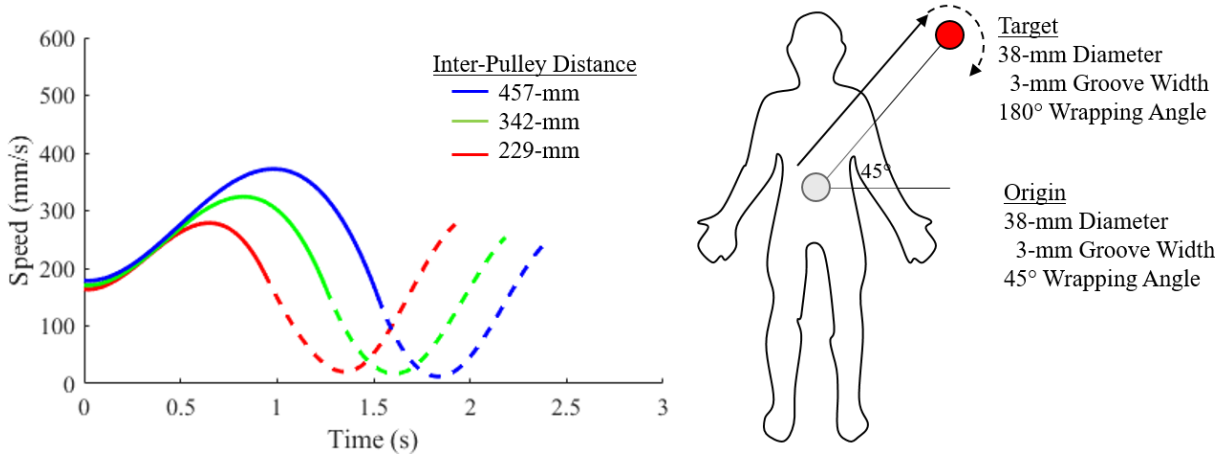

Figure 4.11. Average effect of inter-pulley distance on predicted transition phase (solid line) and pulley interaction-phase (dotted line) speed profile shape for task conditions shown on the right.

4.4.2 Transition Phase: Model Performance

The goodness of fit of the model for predicting speed profiles in the transition phase was assessed by comparing the root mean square error between time-normalized predicted and measured speed profiles, $RMSE_{P\text{-}M}$ and between measurement repetitions, $RMSE_{M\text{-}M}$. Table 4.5 provides summary statistics for the overall mean, standard deviation, and the 95% percentile value of $RMSE_{P\text{-}M}$ and $RMSE_{M\text{-}M}$. Overall, the speed profile shape predictions had large observable errors. Average RMSE values between the predicted and measured speed profiles, were lower compared to the inherent within-person variability in measured speed profiles. This indicates that the prediction model (i.e., the aggregate effect of the regression equations for 5 control points) captured a portion of the variance in speed profiles associated with different task

conditions. This was more evident when comparing the average speed magnitude across the transition phase. The average $\overline{Speed}_{\text{Error}}$ was 2.45 ± 91 mm/s across all task conditions.

Table 4.5. Summary statistics for overall speed profile model performance.

	Mean (± SD)	95th Percentile	Total # of trials
$RMSE_{P\text{-}M}$	124 ± 68 mm/s	222 mm/s	9396
$RMSE_{M\text{-}M}$	190 ± 103 mm/s	158 mm/s	3132

Table 4.6 summarizes results from the one sample t-tests comparing the difference between the average predicted speed profile and average measured speed, $\overline{Speed}_{\text{Error}}$ for different values of target groove width and inter-pulley distance. Figure 4.12 shows the corresponding boxplots of $\overline{Speed}_{\text{Error}}$. Across measured values of groove width and inter-pulley distance, the mean errors were small (-2.4 mm/s to 17.5 mm/s) however the errors were highly variable. Generally, $\overline{Speed}_{\text{Error}}$ increased for hand trajectories towards target pulleys with shorter inter-pulley distances, excluding an inter-pulley distance of 381-mm which had a significant error of -17.5 mm/s. The results showed $\overline{Speed}_{\text{Error}}$ was not significantly different from 0 mm/s for inter-pulley distances of 342- and 457-mm, whereas the model slightly overestimated average speed for inter-pulley distances of 229- and 305-mm.

Table 4.6. One sample t-tests analyzing differences in average predicted and measured speeds in the transition phase compared to 0 mm/s.

	Level	t	df	*p*	Mean error (mm/s)	[95% CI]
Target Groove Width (mm)	3	5.561	2834	***< 0.001**	8.6	[5.5, 11.6]
	6	-3.661	3062	***< 0.001**	-6.3	[-9.7, -2.9]
	9	3.449	1713	***0.001**	8.0	[3.4, 12.5]
Inter-pulley Distance (mm)	229	4.335	2583	***< 0.001**	7.9	[4.3, 11.4]
	305	3.482	708	***0.001**	11.0	[4.8, 12.1]
	342	-1.119	1797	0.263	-2.4	[-6.5, 1.8]
	381	-5.299	725	***< 0.001**	-17.5	[-24, -11.0]
	457	1.918	1794	0.055	4.2	[-0.1, 8.5]

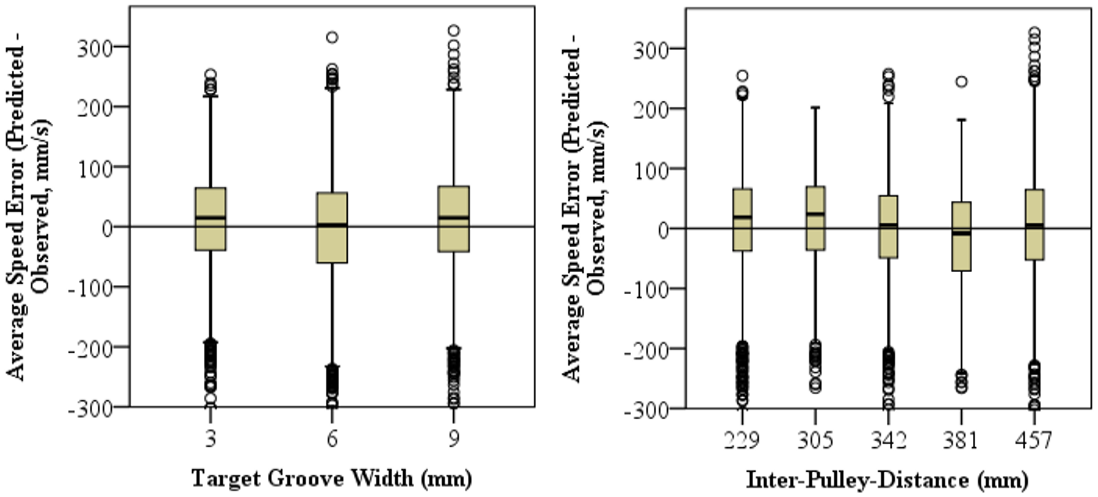

Figure 4.12. Error in average speed predictions across target pulley groove width (Left) and inter-pulley distance (Right)

4.4.3 Pulley-Interaction Phase: Regression Results Time Prediction

Table 4.7 summarizes results for the regression analysis on LN($Time_{PI}$). Aside from inter-pulley distance and the two-way interaction between the horizontal (X) and vertical (Z) location of the target pulley, all of the predictors had statistically significant effects on pulley interaction

time. Most of the explained variance in LN($Time_{PI}$) was attributable to target pulley diameter (β = 0.46), groove width (β = -0.23), wrapping angle (β = 0.32), and the horizontal (X-coordinate) location of the target pulley (β = -0.14). Pulley-interaction phase time increased significantly when threading target pulleys with a larger diameter, narrower groove width, larger wrapping angle, and when the target pulley was located on the contralateral side of the body compared to the ipsilateral side.

Table 4.7. Regression analysis results for the pulley-interaction phase duration, LN($Time_{PI}$).

Predictor	β	*p*
Intercept	-1.296	< .001
Target Diameter	0.46	< .001
Target Groove Width	-0.23	< .001
Target Location X	-0.14	< .001
Target Location Z	-0.03	0.002
Target Threading Direction	-0.16	< .001
Target Initial Contact Angle	0.12	< .001
Approach Angle	0.08	< .001
Target Wrapping Angle	0.32	< .001
Target Wrapping Angle x Diameter	-0.11	< .001
$\hat{R}^2_{adj}$	0.307	

The regression model performance for predicting $Time_{PI}$ was assessed by comparing difference in measured and predicted $Time_{PI}$ across all task conditions. Overall, the regression model underestimated pulley-interaction phase time by 0.29 seconds (95% CI: [-0.31, -0.27], $p <$ 0.001). Table 4.8 summarizes results of one-sample t-tests comparing $Time_{PI,Error}$ to 0 seconds at different values of target groove width and wrapping angle. Additionally, for datasets 2 and 3, task conditions were stratified by target pulley location region for conditions with and without line of sight with the initial contact angle. Across different values of target groove width and

wrapping angle, pulley interaction times were consistently underestimated and showed no noticeable trends. Stratifying $Time_{PI,Error}$ by target pulley region and line of sight revealed $Time_{PI,Error}$ increased in when threading pulleys that had on direct line of sight with the initial contact angle, and likely resulting in more corrective movements. $Time_{PI,Error}$ was not significantly different from 0 seconds for target pulley located at the Bottom – Right, Top – Left, and Bottom – Left in conditions with line of sight.

Table 4.8. One sample t-tests comparing differences in predicted minus observed pulley-interaction phase time across levels of target groove width, target wrapping angle, and target pulley region by whether or not there was line of sight with the initial contact angle.

	Condition	*t*	df	*p*	Mean error (s)	[95% CI]
Target Groove Width (mm)	3	-17.603	3283	***< 0.001**	-0.38	[-0.42, -0.34]
	6	-11.410	3693	***< 0.001**	-0.17	[-0.19, -0.14]
	9	-16.305	2129	***< 0.001**	-0.36	[-0.4, -0.31]
Target Wrapping Angle	45°	-14.276	2820	***< 0.001**	-0.26	[-0.3, -0.23]
	90°	-18.266	2828	***< 0.001**	-0.35	[-0.39, -0.32]
	135°	-8.226	1317	***< 0.001**	-0.23	[-0.29, -0.18]
	180°	-10.269	2139	***< 0.001**	-0.26	[-0.31, -0.21]
Target Pulley Location	**LoS**					
Top – Right	No	-6.993	278	***< 0.001**	-0.38	[-0.49, -0.28]
	Yes	-4.038	182	***< 0.001**	-0.24	[-0.36, -0.12]
Bottom – Right	No	-8.435	258	***< 0.001**	-0.50	[-0.62, -0.39]
	Yes	-0.087	171	0.931	0.00	[-0.11, 0.10]
Top – Left	No	-6.216	270	***< 0.001**	-0.48	[-0.63, -0.33]
	Yes	0.749	183	0.455	0.05	[-0.09, 0.19]
Bottom – Left	No	-3.967	274	***< 0.001**	-0.29	[-0.44, -0.15]
	Yes	-2.745	177	0.007	-0.18	[-0.30, -0.05]
Center	Yes	-7.870	900	***< 0.001**	-0.24	[-0.30, -0.18]

4.5 Discussion

This chapter presented a statistical model using b-splines and functional regression analysis for predicting hand speed profiles in a sequential reach task with continuous material. Use of functional analysis methods allowed for both compression and smoothing of the speed profiles and incorporating of this information into a statistical prediction model. This accounted for some important properties intrinsic to sequential reaches. First, use of b-splines clamped at the ends (i.e., using repeated knots) allowed for combining predicted trajectory segments associated with transition and pulley-interaction phases, while maintaining continuity in speed magnitude and gradient (i.e., acceleration) between segments. This feature was key in order to model sequential reach tasks as alternating transition and pulley-interaction phases, i.e., with the hand speed at the end of each movement phase progressing into the start of the next movement phase in the sequence. Second, the use of b-splines also helped account for differences in hand speed at the start vs end of each movement phase. In particular, interpolating the speed profile in the pulley interaction phase helps account for differences in the initial and terminal speed magnitudes. Third, the model maintained integrity in distance travelled and time duration (and hence speed) between movement trajectory shape and speed profiles. This requirement was critical to support potential implementation of these models into a DHM framework (Reed et al., 2006).

Across the different task parameters, the predicted speed profiles reveal an approximately bell-shape, characteristic of rapid aiming tasks during the transition phase (Atkeson & Hollerbach, 1985; Beggs & Howarth, 1972; Georgopoulos et al., 1981; Morasso, 1981). Additionally, the pulley-interaction phase displayed an inverted bell-shaped profile. These systematic patterns provide evidence of a common underlying speed control mechanism.

While variability in speed across task conditions and participants was expected, the measured speed profiles displayed notably high variability within each motion trial. Overall, the model was able to capture the average speed of the hand trajectory in the transition phase with an average error of 2.4 mm/s. However, the regression analysis for control points was unable to account for a substantial portion of the variance (i.e., 12% vs. 34 % when predicting trajectory shape control points), resulting in large RMSE values between time-normalized predicted and observed speed profiles (i.e., 124 ± 68 mm/s). These findings suggest that while cubic b-splines addressed the primary study objective of capturing the underlying average shape of the speed profile it did not adequately account for rapid fluctuations in measured hand trajectory speed for this task. Increasing the number of control points in the b-spline fitting process would have likely reduced the error between the fitted b-splines and measured speeds profiles, though it would not have likely improved prediction accuracy. However, it is very likely that naturally occurring variability in human movement attributes to a portion of the unexplained variance in this task, as evidenced by the large root mean square error within repeated conditions (190 ± 103 mm/s).

From a motor control perspective, the high speed variability within each motion trial are particularly insightful. Two potential sources of these variabilities are postulated. The first pertains to handling of continuous material. Participants in this task had to continually process information for maintaining tension in the material while reaching towards the target pulley, as opposed to a discrete reach task where the operator is solely focused on controlling movement of the hand towards the target location. Maintaining material tension had particular implications for the pulley-interaction phase. Excessive movement speed would result in unspooling of the material, i.e., slack. Small amount of slack in the thread could be compensated by reaching past the target pulley. Excessive slack in the flexible thread would make it nearly impossible to

position and route the material along the pulley group. Participants had to continually modulate movement generation and speed control towards reaching the target and simultaneously maintain adequate material tension. Routing the thread along the pulley groove required continuous tracking since the hand movement was directed by a specific pathway (e.g., arc-length or wrapping angle along the pulley groove). Therefore, it is possible that participants utilized online or intermittent control mechanisms in both transition and pulley interaction phases reflected in closed-loop speed corrections throughout the measured reach movements.

The second proposed source of speed variability pertains to forearm pronation and supination. This task involved considerable changes in movement direction in both the transition phase, (e.g., determined by location of the origin and target pulleys) and pulley interaction phase (i.e., wrapping the hand around the pulley circumference). While the presented models of trajectory shape and speed focused on translation, video observations also revealed substantial internal rotation of the forearm during online changes in movement direction, especially curvilinear movements. Regardless of source, the fluctuations in measured speed may not necessarily suggest a limitation in information processing but rather provide evidence of continuous modulation of the movement trajectory and the potential for compensatory adaptations as a function of the spatiotemporal task demands.

Prediction of duration in the pulley-interaction phase had an average error of -0.30 seconds. This error was largely influenced by positive skewness in the time distribution. Prior researchers have classified corrective movements as shifts in speed from deceleration to acceleration when the hand approaches the target location (Miall et al., 1993). In discrete reach movement tasks, corrective movements at the target location are common, especially under conditions with a low tolerance (Carlton, 1980). In the present task, classifying and accurately

quantifying movement corrections was difficult due to the large variability in the speed profile shapes in both phases of the task. However, as evidenced by increases in pulley-interaction phase duration, roughly half the threading trials contained multiple movement corrections in the pulley-interaction phase which can likely explain the error in time predictions. Time prediction error was not a function of target groove width, but we did find improvements when there was line of sight with the initial contact angle.

Despite these errors, predictions of pulley-interaction phase time captured average effects of target tolerance, size, movement amplitude, and line of sight availability. The trends in predicted times align with movement time predictions in the Fitts' paradigm, where increasing index of difficulty leads to increasing movement times. Additionally, these findings align with findings from Chapter 2 where an increase in target tolerance (diameter and groove width) increased movement time.

4.5.1 Study limitations

This study was limited to modeling the hand speed profiles due to translations in the 2D frontal plane. As such, the model did not account for changes in posture, such as forearm pronation/supination, which may have influenced speed variations during the transition and pulley-interaction phases. Another limitation of the speed profile model is that the movement phases were not segmented based on criteria defined by the speed profile shapes. Instead, they were segmented using the trajectory segmentation scheme presented in Chapter 3, which was based on hand location relative to the target pulley geometry. This is necessary so the predicted trajectory paths correspond to the predicted speed profiles. Segmenting the trajectories by speed transitions might have improved model performance and possibly minimized some effects of specific task parameters. For instance, smaller origin wrapping angles resulted in lower speeds

and longer acceleration times in the earlier portion of the transition phase. This could be a result of the minimum speed at the target pulley location occurring in the beginning portion of the next transition phase for conditions with smaller wrapping angles.

Lastly the study did not manipulate material properties, given its primary focus on modeling the effects of task parameters pertaining to target tolerance, reach amplitude and direction, and line of sight. The constant material used was a flexible polyester thread. It is likely that material properties such as elasticity (e.g., stretchable fiber vs. inelastic wire), cross-section (i.e., circular vs. rectangular), material size relative to pulley groove, and coefficient of friction with the pulley groove could influence the forces needed to unwind material and consequently affect speed control. Likewise, emphasizing movement accuracy alone without temporal constraints (vs. emphasis no speed and accuracy as in this study) would result in very different speed profiles however would result in very long and less generalizable movement times to address the applied problem. Nevertheless, the current study improves our understanding of positional and speed control, and provides a foundation for future research that could investigate the effects of material properties and the relative contribution of spatial vs. temporal task criteria on movement performance.

4.6 Conclusions

This chapter presented a statistical model for predicting hand speed profiles in a sequential reach task with continuous material using b-splines. The model produced a continuous speed profile between alternating transition and interaction phases in absolute time, and can be extended to any number of pulleys in a threading sequence. The model was able to accurately predict average speeds during the transition and interaction phases, but did not account for the substantial variability in speed profiles. The speed variability were considered to reflect closed-

loop speed corrections in both transition and pulley-interaction phases providing evidence of online control mechanisms to address the unique spatial and temporal demands of this task.

The model also provides a means for computing the task completion time for a complete sequential reach task as the linear sum of movement times for alternating phases of transition and pulley-interaction and for consecutive pairs of origin to target pulleys. The subsequent chapter 5 provides a systematic and detailed validation of the continuous trajectory shapes and speed profiles, and estimated tasks completion times.

CHAPTER 5

Hand Trajectory Shape and Speed Model Validation

Summary

The previous chapters presented statistical models to predict hand trajectory shape and speed, and task completion time in a sequential reach task with continuous material using task parameters as predictors. Model development used data from three experiments to account for the effects of target tolerance, size, location, and threading sequence on hand trajectory shape and speed. Model goodness of fit was assessed internally against motion trials used in model development. The purpose of this study was to empirically assess the generalizability of the model performance in predicting hand trajectory shape and speed in a novel set of task conditions (i.e., task configurations that were different from those used in model development). This study recruited 4 participants to complete a sequential threading task across 4 unique setups that varied in target pulley tolerances (diameter and groove width), location, and inter-pulley distances. Goodness of fit in predicted hand trajectory shape and speed, and task completion time was examined. Applications of the models to workstation design and digital human models are discussed.

5.1 Introduction

Computer-aided ergonomic analysis using digital human modeling (DHM) is a valuable tool for evaluating workstation design towards improving worker productivity and safety.

Simulating manufacturing tasks such as precision material handling for reachability, hand clearances, and worker postures using inverse kinematics rely on input about the reach locations. Users of DHM software typically spend a substantial amount of time posturing the human manikin to reach locations, with software then interpolating intermediate reach movements and postures. Current models for predicting reach trajectory kinematics and movement times are limited to discrete aiming and positioning movements, and do not consider the effects of handling continuous material and reaching to sequential targets. Simulating this task is particularly challenging since the hand reaches past and around the targets (and hence not known *a priori*), and is continually moving with speed undulations specific to the task properties. Algorithms to auto-generate positional and temporal inputs for the digital manikin would reduce the need for DHM users to make assumptions about reach locations and postures, thereby increasing the accuracy of task simulations.

This research was focused on developing such models to predict reach trajectory shape and speed profiles during sequential reaches with continuous material that could be implemented into a DHM framework. Task-specific trajectory shapes combined with hand speeds would also allow for estimating completion times, a key indicator of productivity. The long-term goal was to improve the capabilities of DHM software to simulate material handling tasks that involve sequential reach movements with continuous material, thereby improve the capability of DHM users and engineers to proactively evaluate the effects of the work setup and location of reach targets in alternative configurations on task performance prior to production.

The previous chapters 3 and 4 presented statistical models to predict hand trajectory shape and speed, and task completion time in a sequential reach task with continuous material using task parameters as predictors. However, the goodness of fit of the trajectory shape and

speed was assessed internally against motion trials used in model development. Thus, the objective of this laboratory study was to empirically validate the predictive model of hand trajectory shape, speed and task completion time in sequential reach tasks with continuous material in novel task conditions different from those used in model development.

5.2 Methodology

5.2.1 Participants

Four right-handed adults participated in the experiment. All participants were free of any neurological and musculoskeletal disorders, had normal or corrected vision, and had no prior experience performing the task conducted in the experiment. The study was approved by the university's institutional review board and written informed consent was obtained from all participants prior to participation.

5.2.2 Experiment Setup

The experiment apparatus consisted of an acrylic work surface (1.2 m x 2.4 m) oriented vertically so that the pulley axes were all horizontal and parallel (Figure 5.1). The threading task involved threading a pre-defined sequence of pulleys. The pulleys were custom-made to specific combinations of pulley outer diameters (i.e., 38-mm, 76-mm, and 152-mm) and groove widths (i.e., 3-mm, 6-mm, and 9-mm). The pulleys had a constant groove width of 6-mm. Participants stood at a comfortable distance away from the work surface and could self-select body postures and movements during the trials to complete the threading tasks. The thread (100% polyester, Coats & Clark, Dual Duty XP Heavy Thread) was pulled from a fishing reel (Shakespeare Alpha Baitcasting Reel) clamped onto the right edge of the board.

Four threading sequences were examined in this study (Figure 5.2). Each sequence consisted of a series of 9 pulleys on a rectangular grid resulting in 8 reach movements between consecutive pairs of pulleys where the first target pulley served as the origin for the following reach movement, and so on. The pulleys numbered 1 to 9 had different outer diameters and groove widths, however these parameters were kept consistent for all four sequences. The four threading sequences differed in vertical and horizontal grid spacing (long vs. short) and in movement direction with pulleys located primarily on the contralateral side (left) vs. the ipsilateral side (right). The lowest row of target pulleys were situated at a vertical height of 600-mm from the floor (Figure 5.1). These configurations were designed to include a diversity of target pulley locations about the workspace, inter-pulley distances (250-mm, 300-mm, 375-mm, 390-mm, 400-mm, and 550-mm), and approach angles (0-315°).

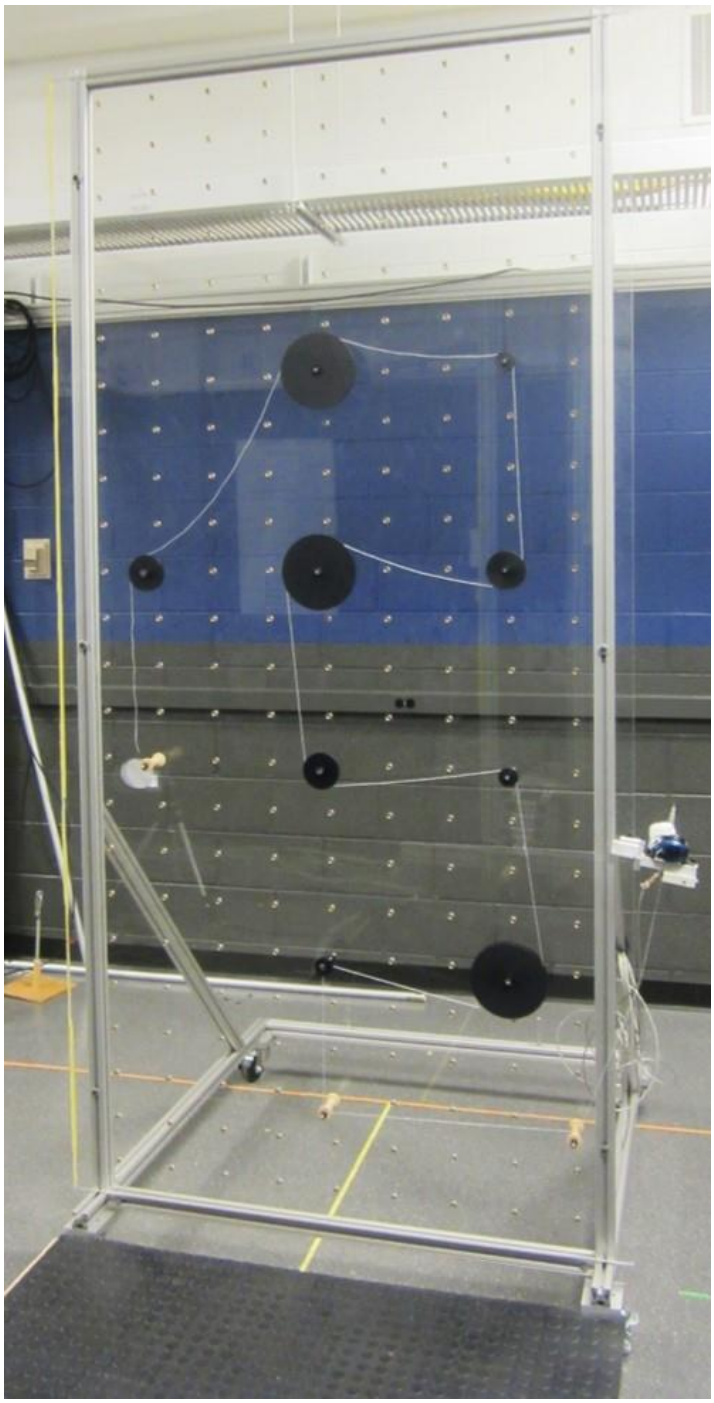

Figure 5.1. Experiment apparatus for validation experiment. The pulley arrangement shown represents the Right-Long threading sequence.

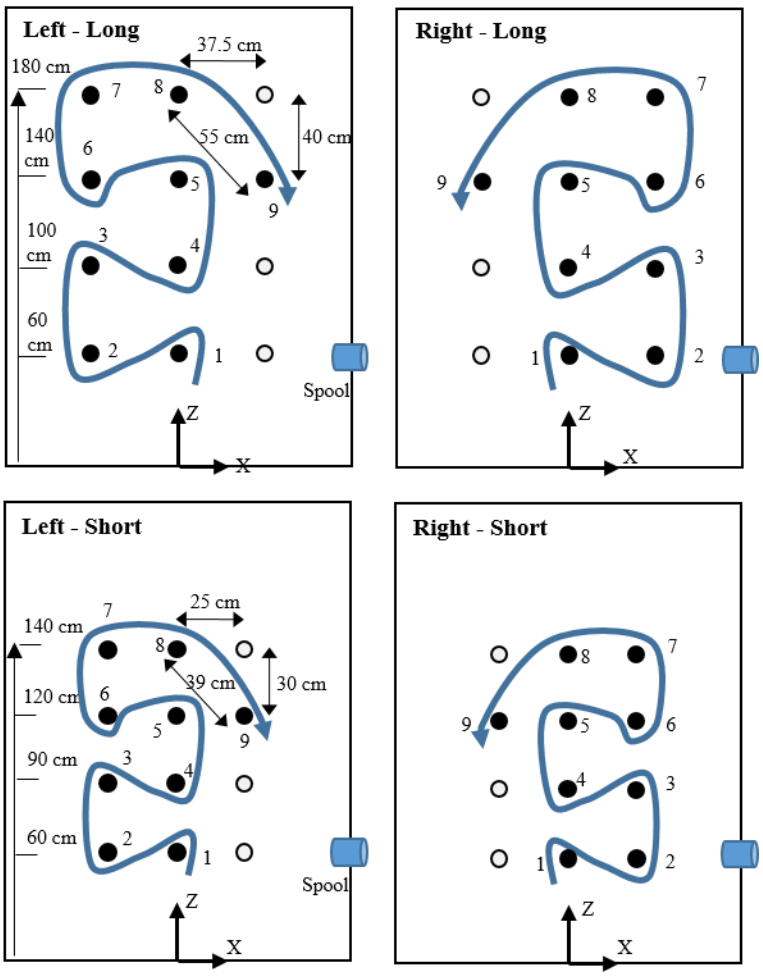

Trajectory Segment	$Traj_{1-2}$	$Traj_{2-3}$	$Traj_{3-4}$	$Traj_{4-5}$	$Traj_{5-6}$	$Traj_{6-7}$	$Traj_{7-8}$	$Traj_{8-9}$
Pulley Number	**1 → 2**	**→ 3**	**→ 4**	**→ 5**	**→ 6**	**→ 7**	**→ 8**	**→ 9**
Diameter (mm)	38	152	38	76	152	76	38	152	76
Groove Width mm)	3	9	6	3	3	6	9	6	9

Figure 5.2. The four threading sequences (in clockwise order, Left – Long, Right – Long, Right – Short, Left – Short) along with the target pulley parameters (bottom table) used for empirical validation of model for trajectory shape, speed profiles, and task completion times.

5.2.3 Experiment Procedure

Each trial began with the participant grasping the end of the polyester thread from the spool with their right hand using a thumb-forefinger pinch grip. The participant then moved their hand end effector over to a motion capture marker located on the spool for a static 3-second calibration pose after which the threading task could commence. Participants then completed 3 repetitions in each of the 4 threading sequence (Figure 5.2) that were presented in counterbalanced fashion. Participants were instructed to complete the task as quickly as possible but to primarily focus on threading all of the pulleys successfully. At the start, participants aligned the midline of their torso to the middle of the panel. Side steps and torso leaning were allowed if necessary when reaching to the pulley locations. Up to six practice trials were provided prior to the presentation of each new threading sequence to have participant memorize the pathway.

5.2.4 Instrumentation and Data Processing

An optical motion capture system (Qualisys, Göteborg, Sweden) was used to measure hand movements at a sampling frequency of 120 Hz. Three-dimensional coordinate data from the motion capture system was filtered using a 2nd-order low-pass Butterworth filter with a 6-Hz cut-off frequency. A passive-marker triad located on the back of the participants' right hand estimated the position of the thumb-forefinger pinch grip based on the pretest calibration pose. From the measured static calibration pose, two-dimensional position of the end effector trajectory data in the frontal plane (i.e., parallel to work surface) was computed for each of the motion trials. These trajectories, by task and by segment (i.e., between 8 pairs of pulleys) served as comparison data for the analysis. Of the 384 measured trajectory segments (i.e., 4 participants

x 4 sequences x 3 repetitions x 8 segments), 7 segments were excluded due to marker drop outs resulting in an effective sample size of 377 segments.

5.2.5 Predictions of Trajectory Shape, Speed Profile, and Task Time

Statistical models for trajectory shape (Chapter 3) and speed profiles (Chapter 4) were applied to predict each trajectory segment (one transition and one pulley-interaction phase) of the threading sequence using task parameters as predictors. In this study, predictors in the regression equations for control points were calculated from the geometry and location of the origin and target pulleys, origin and target wrapping angles, inter-pulley distance, target approach angle, and target initial contact angle from the 4 sequences (Figure 5.2). A separate prediction was obtained for each of the 4 participants since individual stature was used for normalizing pulley locations.

The algorithms for combining trajectory shape and speed presented in Chapters 3 and 4 were applied to generate continuous trajectory shape and speed profiles based on statistical predictions of each trajectory segment (one transition and one pulley-interaction phase) of the threading sequence. The model for predicting pulley-interaction phase time presented in Chapter 4 was applied to generate predictions of pulley-interaction phase time for each trajectory segment ($\widehat{Time}_{PI}$). Likewise, the process presented in Chapter 4 for integrating predicted trajectory shape and speed was applied to obtain predictions of transition phase time for each trajectory segment ($\widehat{Time}_{T}$). The total task completion time ($\widehat{Time}_{Total}$) was the summation of the corresponding $\widehat{Time}_{T}$ and $\widehat{Time}_{PI}$.

5.2.6 Model Assessment

Three categories of goodness of fit measures were examined:

***Trajectory Shape*:** Goodness of fit in trajectory shape predictions was assessed by computing the root mean square error between predicted and measured reach trajectory paths for each origin to target pulley trajectory ($RMSE_{Path}$). For this value, error at each time point on the predicted trajectory corresponded to the resultant distance to the closest point on the measured trajectory.

Trajectory Speed: Goodness of fit in speed profile predictions was assessed by computing the root mean square error (RMSE) between time-normalized predicted and measured speed profiles for each trajectory segment ($RMSE_{Speed}$). The $RMSE_{Speed}$ corresponded to the difference in speed at each normalized time point on the predicted speed profile for one transition and pulley-interaction phase. Additionally, to assess error in average speed predictions, difference in predicted vs. measured average speed in the transition phase ($\Delta\overline{Speed_T}$) and the pulley-interaction phase ($\Delta\overline{Speed_{PI}}$) was computed.

***Task Time**:* Error in predicted time was assessed by comparing total task completion time. In addition, the difference in predicted vs. measured time for each of the 8 trajectory segments ($\Delta\widehat{Time}_{Total}$) by sequence was analyzed. Lastly, to determine the contribution of error by movement phase, differences in predicted minus measured times in the transition phase ($\Delta\widehat{Time}_{T}$) and pulley-interaction phase ($\Delta\widehat{Time}_{PI}$) were analyzed.

5.3 Results

5.3.1 Participant Characteristics

Four right-handed adults (2 men and 2 women) participated in the experiments. Participants had a mean ± SD age of 19.3 ± 1.5 years, stature of 174.1 ± 11.0 cm, and mass of 72.2 ± 12.3 kg.

5.3.2 Measured vs. Predicted Continuous Hand Trajectories

Figure 5.3 depicts the 12 measured hand trajectories (= 4 participants x 3 repetitions; shown in gray) for the Left-Long and Right-Long threading sequences, and in Figure 5.4 for the Left-Short and Right-Short threading sequences. The predicted hand trajectory (based on one participant's stature = 1655 mm) for the four sequences are overlaid in blue and red for each transition and pulley-interaction phase, respectively. In all four sequences, the first origin pulley was located at the bottom row aligned with the participant's mid-sagittal plane.

The measured trajectory shapes displayed patterns in movement though with variability between participants and repetitions consistent with findings in Chapter 3. Figure 5.3 and Figure 5.4 also indicated the prevalence of movement corrections in some motion trials around nearly every target pulley location. Movement corrections and occasions when participants reach far past a target pulley generally caused noticeable aberrations in trajectory shape. Overall, the predicted trajectory shape tracked the middle of the measured trajectory pathway, aside from $Traj_{1\text{-}2}$ (i.e., moving between pulleys 1 to 2) in the Left-Short and Left-Long sequences. In these movements the model overestimated the distance from the pulley center in the pulley-interaction phase. A distinguishing property of these shape trajectories is the hand reaching past and around the target pulleys, thus the actual reach distances and cumulative displacement are different from the geometric distances between pulley centers.

5.3.3 Predicted Speed Trajectories

Figure 5.5 shows the predicted and measured speed profiles for the Left-Long and Right-Long threading sequences on a time-normalized scale, i.e., normalized to the predicted duration of the transition and pulley-interaction phase for each trajectory segment. Figure 5.6 shows the corresponding predicted speed profiles in absolute time. Figure 5.7 and Figure 5.8 show the

predicted speed profiles for the Left-Short and Right-Short threading sequences on a time-normalized and absolute time scale respectively. The red and blue lines represent the transition and pulley-interaction phases. The speed profiles are time normalized by. The model predictions for speed profile capture undulations and trends expected in the transition and pulley-interaction phases across task parameters aligned with findings in Chapter 4. For example, comparing predicted speed profiles in $Traj_{1\text{-}2}$ across all 4 sequences, the predicted speed was higher in movements with a longer inter-pulley distance (i.e., the Left-Long and Right-Long conditions) compared to movements with a shorter inter-pulley-distance (i.e., Left-Short and Right-Short conditions). Additionally, a longer duration for predicted pulley-interaction phase time was obtained for movements directed to the contralateral side of the body (Left-Long and Left-Short) compared to the ipsilateral side (Right-Long and Right-Short), which also align with findings from Chapter 2 and 4. A distinguishing property of these speed profiles was the different speed magnitudes at the beginning and end of each transition (blue) and pulley-interaction (red) phase.

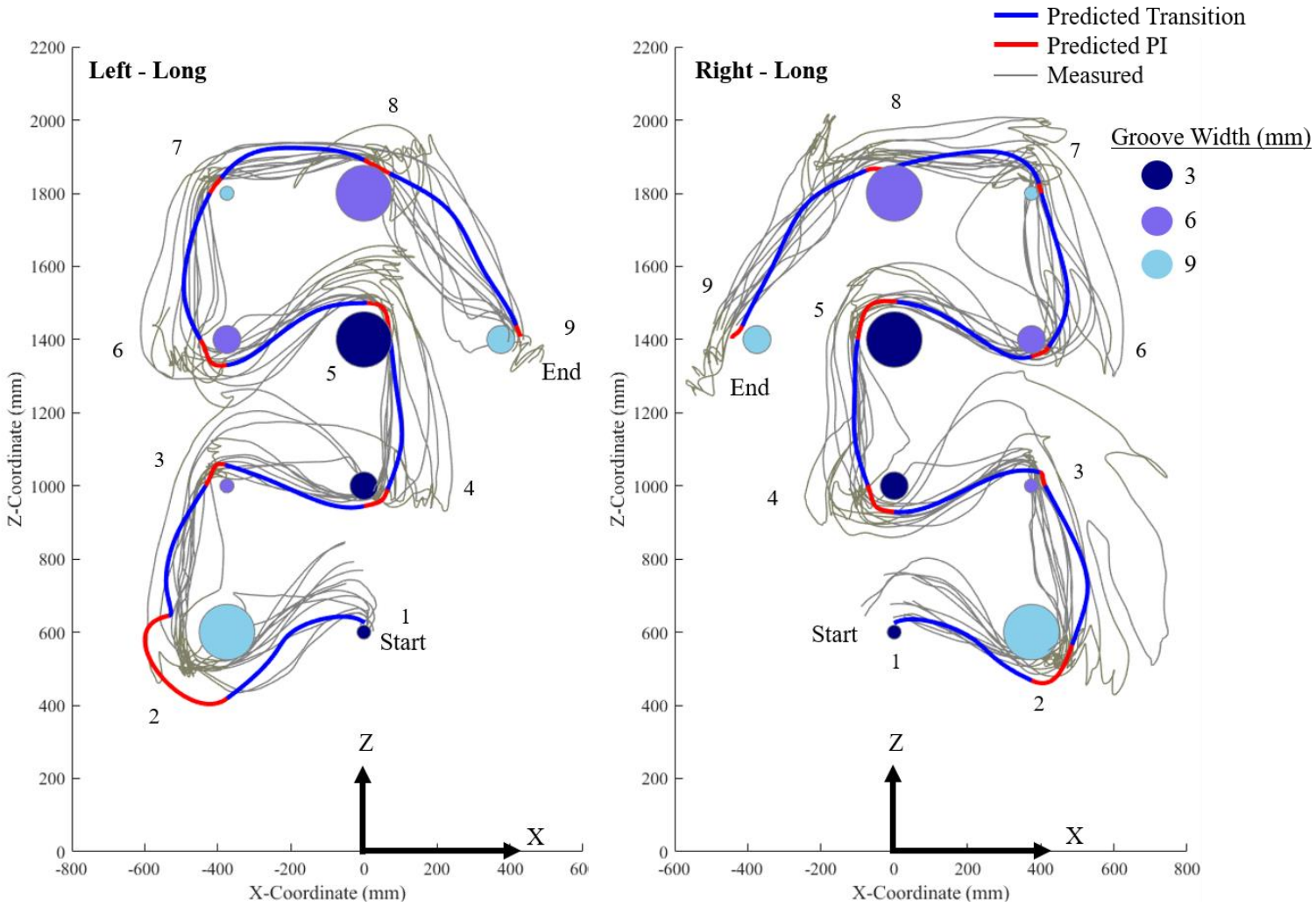

Figure 5.3. Predicted hand trajectory (blue: transition phase, red: interaction phase) for the Left-Long and Right-Long conditions based on one participant's stature of 1655 mm overlaid on measured hand trajectories (gray) from 12 motion trials (= 4 participants x 3 repetitions).

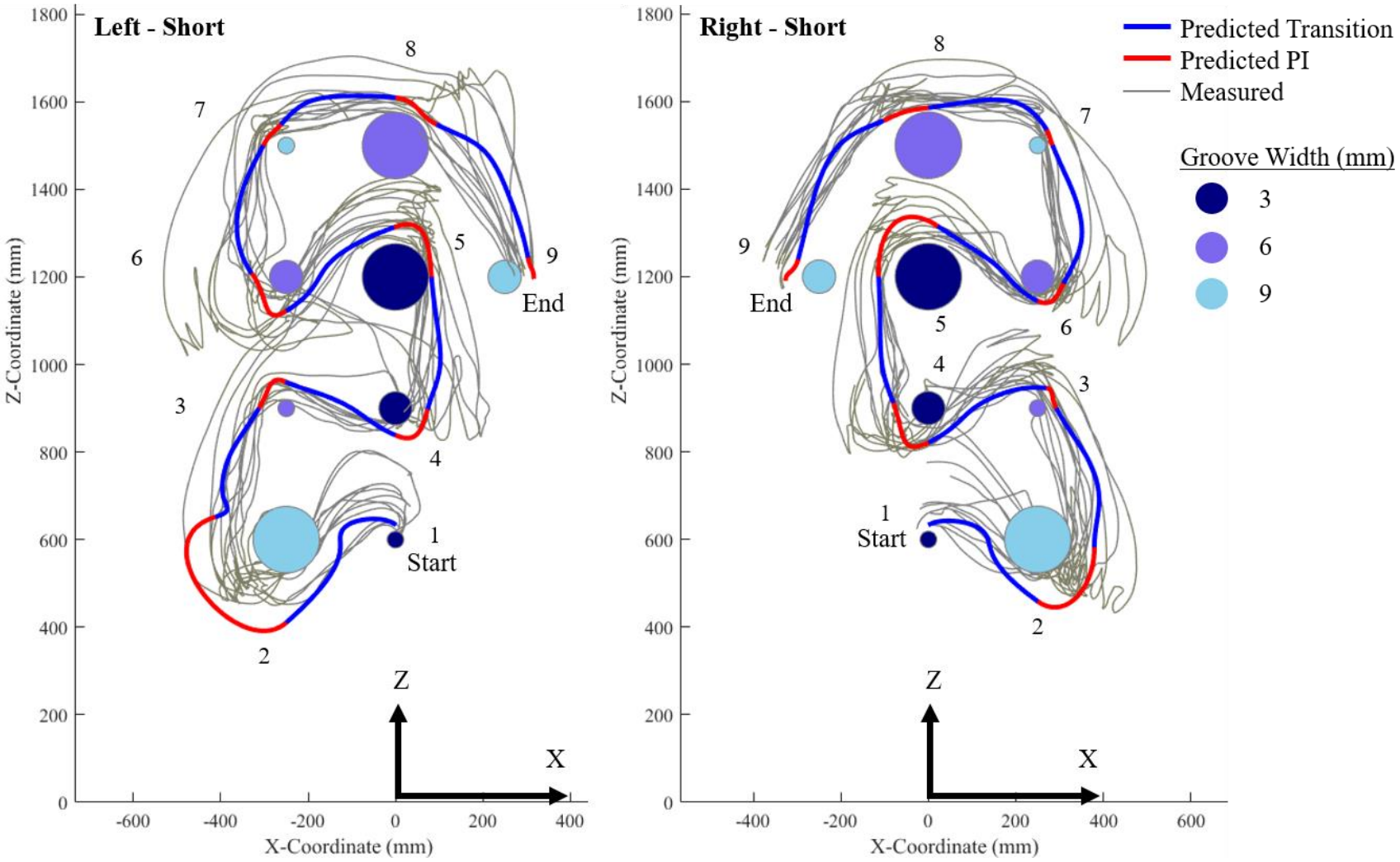

Figure 5.4. Predicted hand trajectory (blue: transition phase, red: interaction phase) for the Left – Short and Right - Short conditions based on one participant's stature of 1655 mm overlaid on measured hand trajectories (gray) from 12 motion trials (= 4 participants x 3 repetitions).

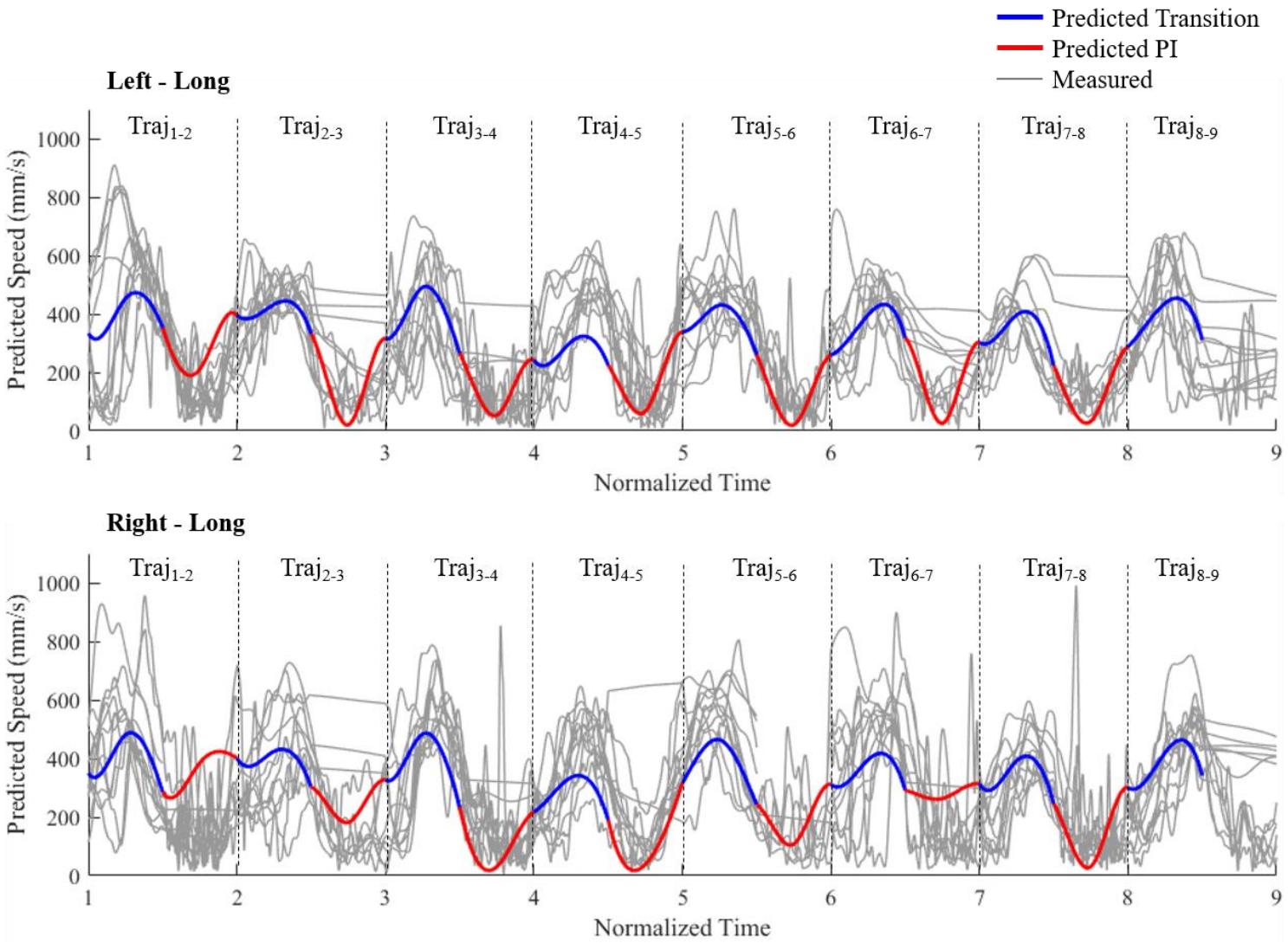

Figure 5.5. Predicted time normalized speed profiles (blue: transition phase, red: interaction phase) for the Left – Long and Right - Long conditions based on one participant's stature of 1655 mm overlaid on measured speed profiles (gray) from 12 motion trials (= 4 participants x 3 repetitions).

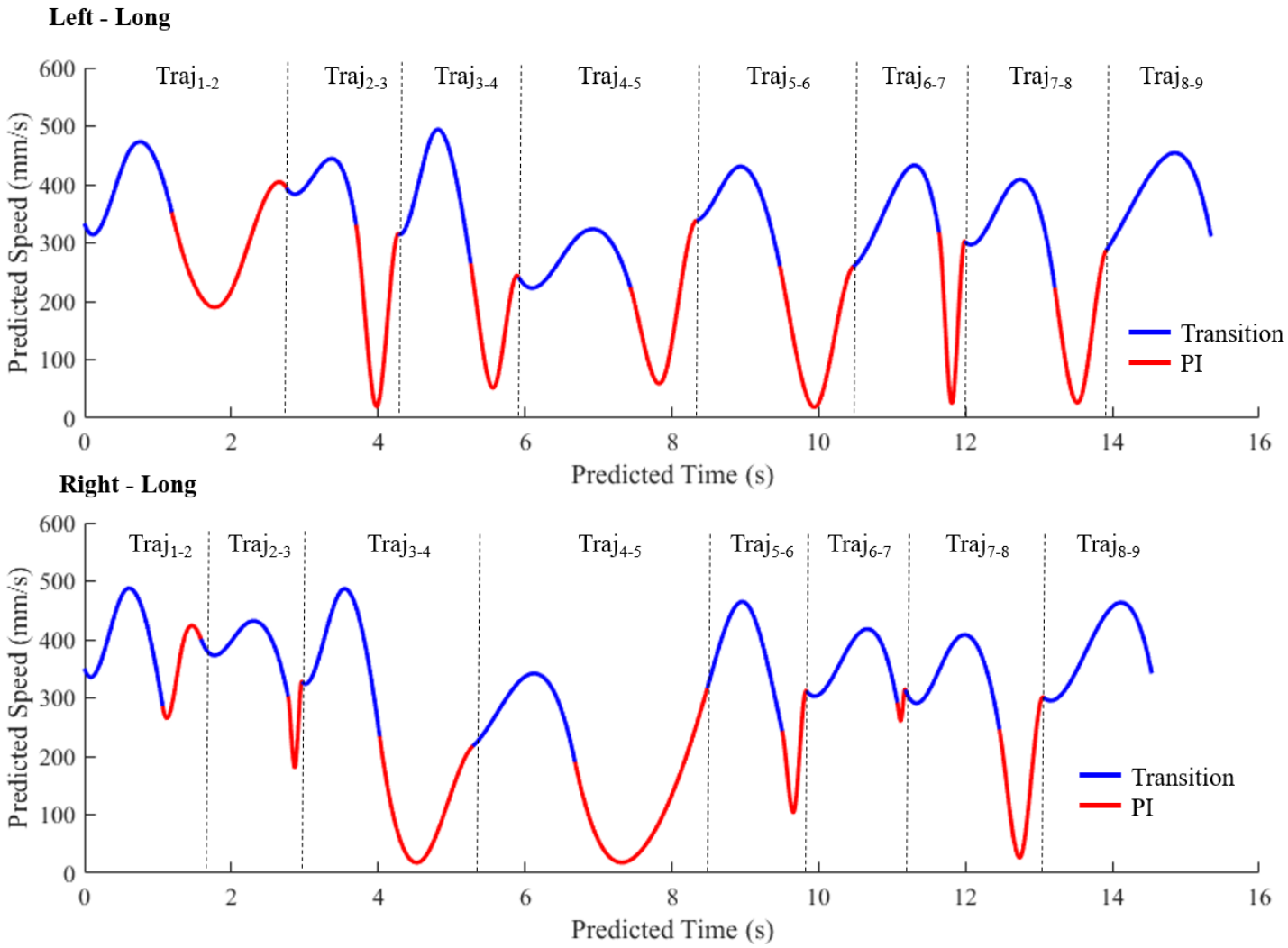

Figure 5.6. Corresponding predicted speed profile in absolute time in the Left-Long (top panel) and Right-Long threading sequences for a participant of 1655 mm stature.

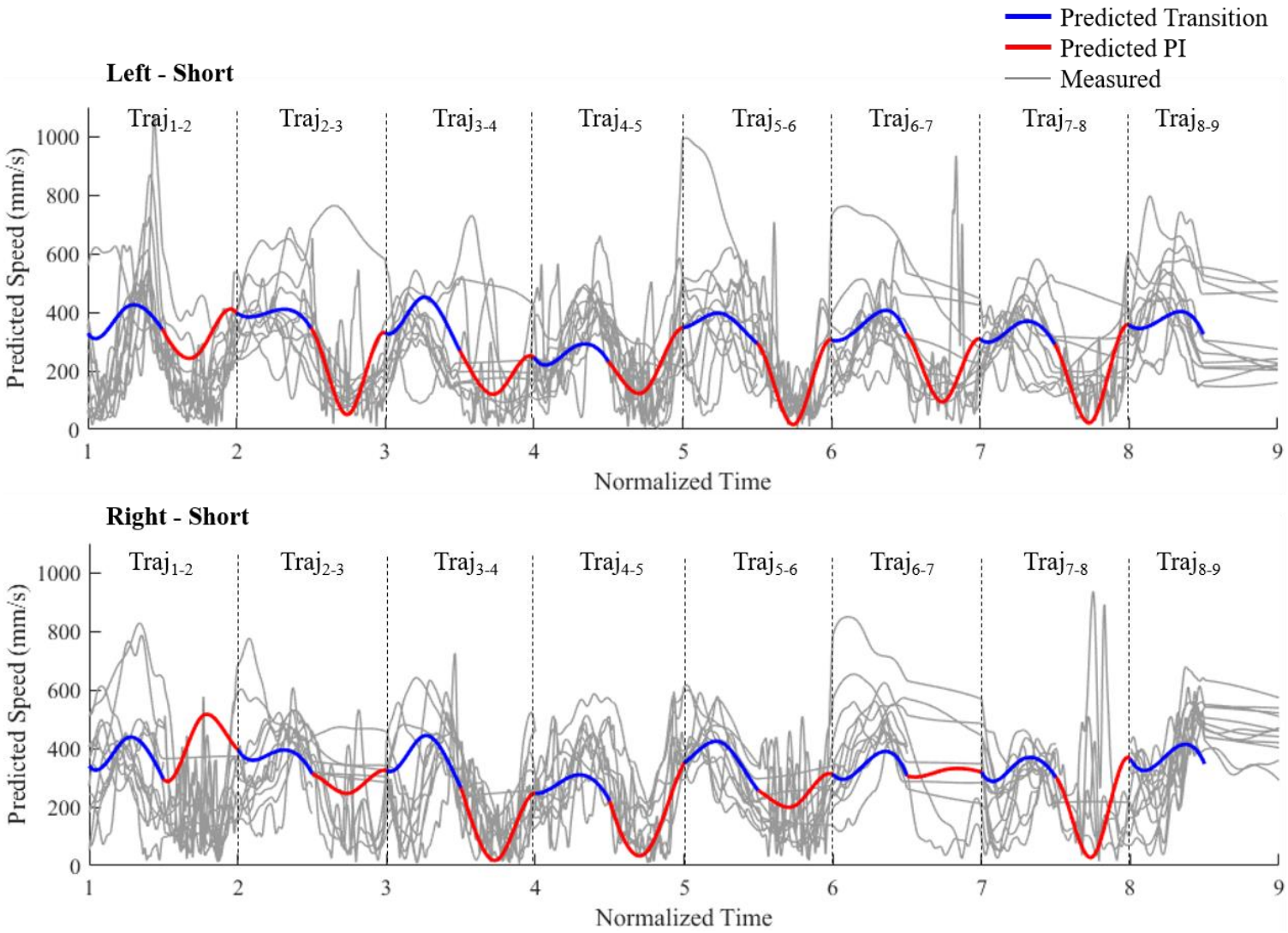

Figure 5.7. Predicted time normalized speed profiles (blue: transition phase, red: interaction phase) for the Left – Short (top panel) and Right - Short (bottom panel) threading sequences based on one participant's stature of 1655 mm overlaid on measured speed profiles (gray) from 12 motion trials (= 4 participants x 3 repetitions).

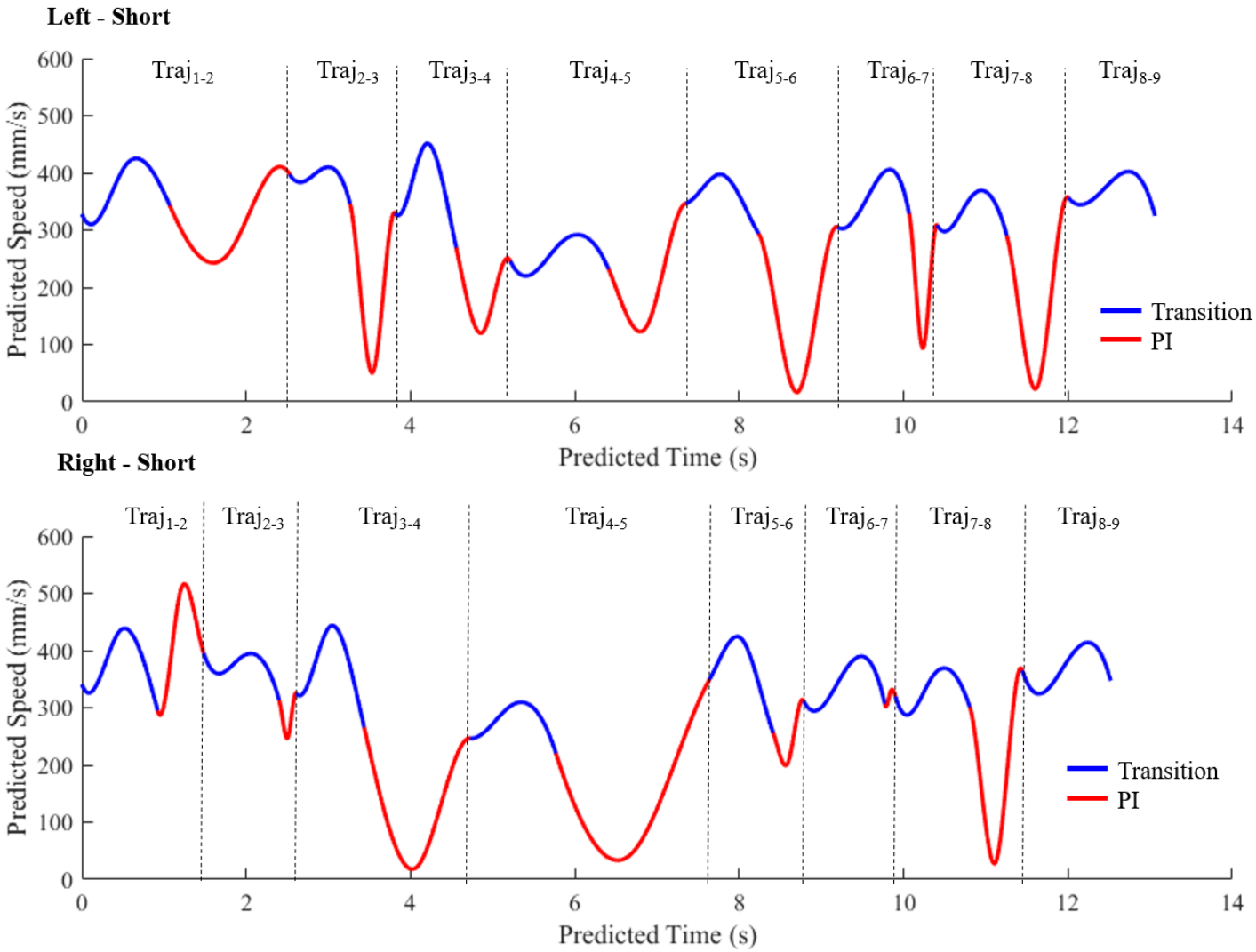

Figure 5.8. Corresponding predicted speed profiles in absolute time for the Left-Short (top panel) and Right-Short (bottom panel) threading sequences for a participant of 1655 mm stature.

5.3.4 Goodness of fit: Hand Trajectory Shape

Table 5.1 summarizes the overall mean $RMSE_{Path}$ stratified by the threading sequence condition. The mean $RMSE_{Path}$ represents the mean ± SD error in measured vs. predicted trajectory shapes for the four sequences aggregated across all 8 trajectory segments (i.e., $Traj_{1\text{-}2}$ to $Traj_{8\text{-}9}$) and 12 motion trials. Goodness of fit in shape prediction improved for the Right-Long and Right-Short sequences, compared to Left-Long and Left-Short. This is consistent with findings from Chapter 3 on trajectory shape, wherein trajectory predictions were less robust for reach movements to target pulleys located on the contralateral side of the body. In other words, the model determines that the hand reaches further past the pulley with horizontal eccentricity from the mid-sagittal plane.

Table 5.1. Summary statistics for overall error in trajectory shape predictions stratified by sequence.

Sequence	Mean (± SD) $RMSE_{Path}$	95th Percentile	Total # of trajectories
Left-Long	48 ± 27 mm	100 mm	94
Left-Short	48 ± 25 mm	91 mm	94
Right-Long	45 ± 26 mm	95 mm	96
Right-Short	38 ± 22 mm	71 mm	93

Figure 5.9 provides boxplots for the average $RMSE_{path}$ stratified by origin to target pulley trajectory segment (i.e., $Traj_{1\text{-}2}$ to $Traj_{8\text{-}9}$) and 4 threading sequences. The average $RMSE_{path}$ was below 50 mm. Generally, an increase in inter-pulley distance within the same trajectory segment was associated with an increase in error. As previously mentioned, goodness of fit in trajectory shape prediction in all 4 sequences was lowest for $Traj_{1\text{-}2}$, which involved reaching toward target pulley-2 with a 152-mm diameter and 9-mm groove width, no direct line of sight to the initial

contact point, and located on the contralateral side at a height of 600 mm (i.e., close to knee height). For this movement, the predicted trajectory overestimated the distance from the target pulley center in the pulley-interaction phase.

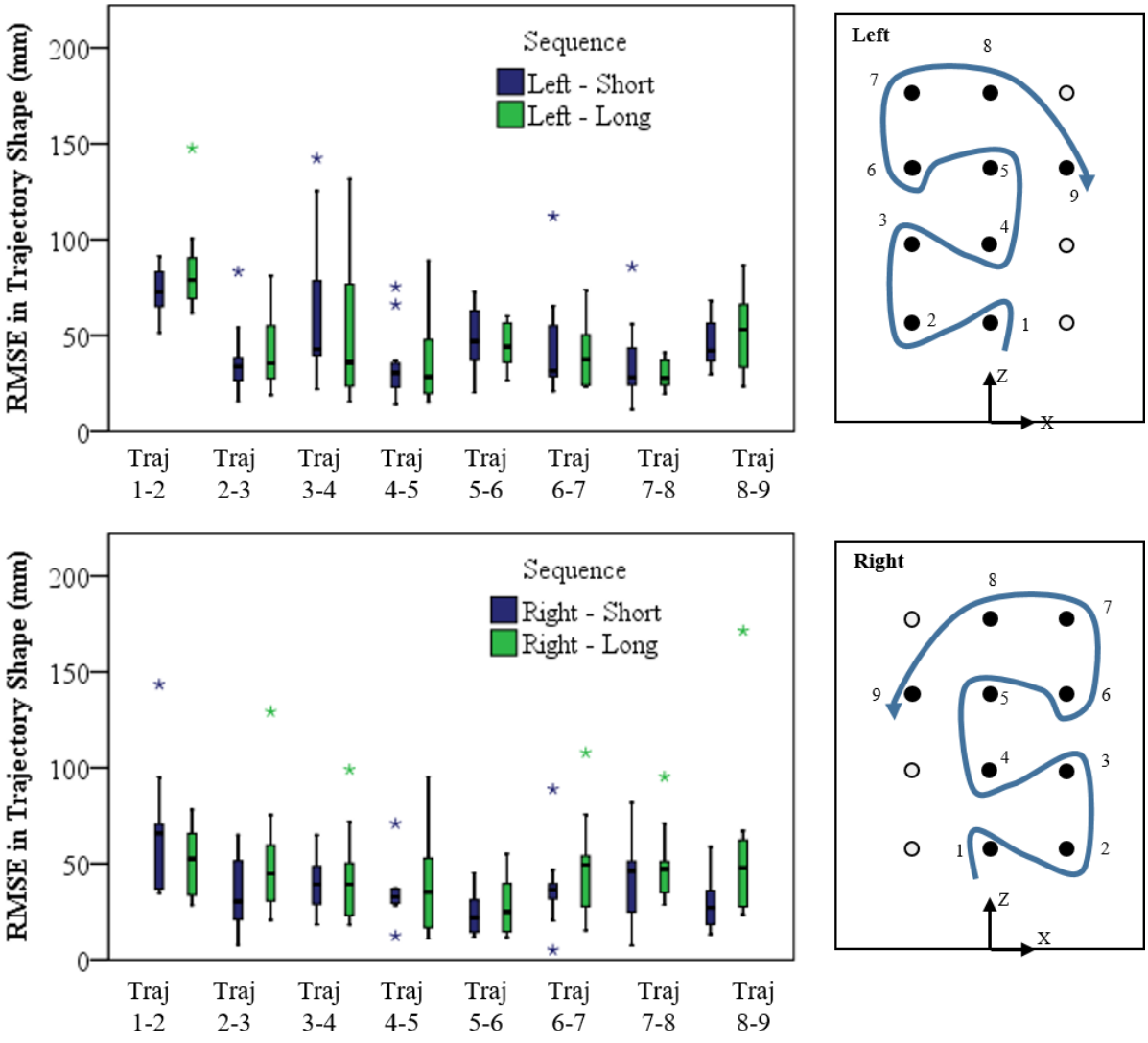

Figure 5.9. Root mean square error in predicted vs. measured trajectory shapes (N = 12 trials) stratified by trajectory segment (i.e., *Traj*$_{1\text{-}2}$ to *Traj*$_{8\text{-}9}$) and 4 threading sequences. Asterisks indicate outlier values exceeding 3 times the inter-quartile range.

Overall, variability in *RMSE*$_{path}$ was higher when reaching toward pulley-4 *Traj*$_{3\text{-}4}$ in the Left-Short and Left-Long sequences compared to corresponding segments on the right (lateral)

side (Figure 5.9). This segment involved reaching toward pulley-4 of (76-mm diameter and 3-mm groove width) with counter-rotation (CW to CCW). For this specific segment, some measured trajectories tended to not cross the centerline until the hand was at or passed the target pulley location (Figure 5.10).

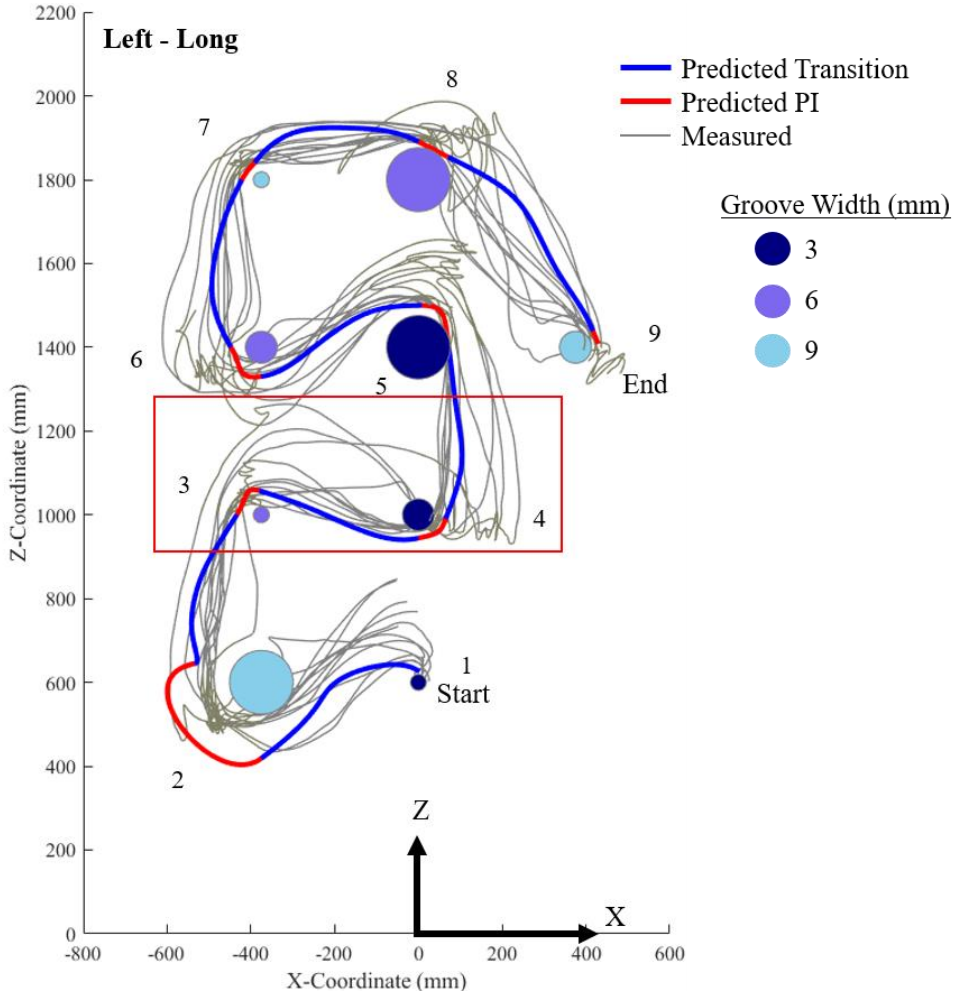

Figure 5.10. Tendency in measured trajectories to not cross the centerline until the latter portion of the transition phase when reaching toward target pulley-4 in the Left-Long threading sequence.

5.3.5 Goodness of fit: Speed

The overall error in speed ($RMSE_{Speed}$) averaged across all 8 trajectory segments and 4 threading sequences was 159 ± 65 mm/s (95th percentile: 360 mm/s). Consistent with Chapter 4, the measured speeds showed high variability, while the predicted speeds representing the average speed profiles did not account for this variability about the average. On average, the model for speed profile underestimated the measured average speed in both phases of the reach movement, though this difference was larger in the pulley-interaction phase. The underestimation of average speed in the pulley-interaction phase is expected since the speed profile shape in the pulley-interaction phase was interpolated, rather than it being directly modeled. Thus, the pulley-interaction phase speed profile were less representative of measured speed profile shapes, especially when multiple movement corrections were measured.

Table 5.2 shows the overall average difference in predicted minus measured average speeds in the transition phase ($\Delta\overline{Speed_T}$) and the pulley-interaction phase ($\Delta\overline{Speed_{PI}}$). On average, the model for speed profile underestimated the measured average speed in both phases of the reach movement, though this difference was larger in the pulley-interaction phase. The underestimation of average speed in the pulley-interaction phase is expected since the speed profile shape in the pulley-interaction phase was interpolated, rather than it being directly modeled. Thus, the pulley-interaction phase speed profile were less representative of measured speed profile shapes, especially when multiple movement corrections were measured.

Table 5.2. Summary statistics for overall error in predicting the difference in average speed in the transition and pulley-interaction phases.

	Mean (± SD)	95th Percentile	Total # of trials
$\Delta\overline{Speed_T}$	-6 ± 100 mm/s	132 mm/s	377
$\Delta\overline{Speed_{PI}}$	-45 ± 131 mm/s	162 mm/s	377

Figure 5.11 shows the difference in $\Delta\overline{Speed_T}$ and $\Delta\overline{Speed_{PI}}$ stratified by threading sequence. One sample t-tests showed that $\Delta\overline{Speed_T}$ did not statistically differ from 0 mm/s for any of the threading sequences, whereas the underestimation of average speed in the pulley-interaction phase was consistent across trajectory segments and threading sequences.

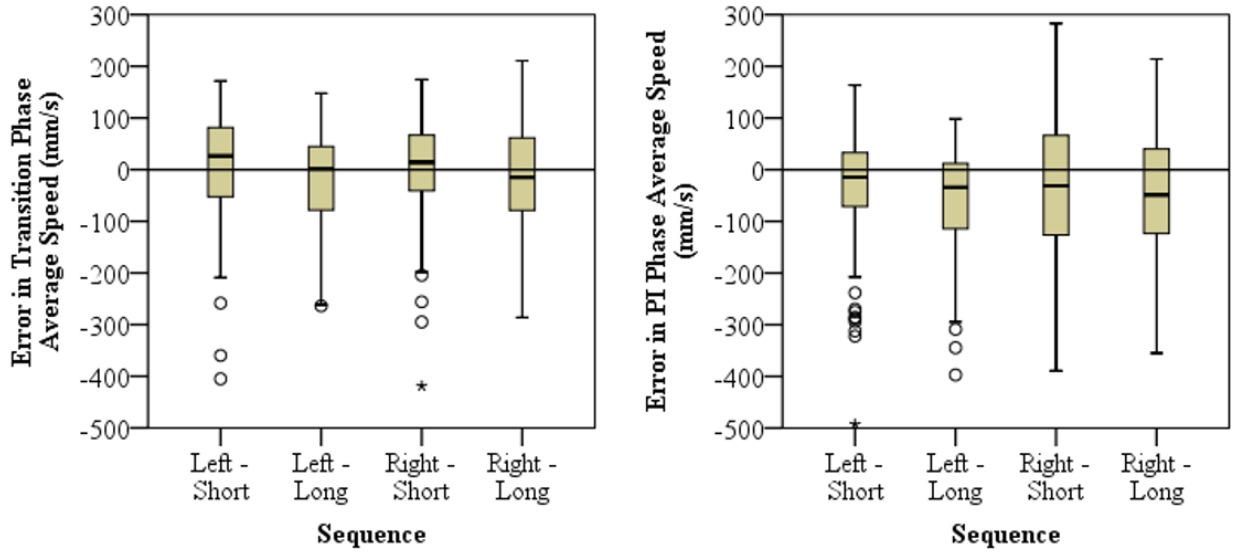

Figure 5.11. Difference in predicted minus measured average speeds in the transition and pulley-interaction phases stratified by threading sequence. Circles denote outlier values exceeding 1.5 times the inter-quartile range, while asterisks indicate outlier values exceeding 3 times the inter-quartile range.

5.3.6 Model Assessment: Task Time

Figure 5.12 shows the average measured and predicted aggregated total completion times for each of the threading sequences. On average, model predictions underestimated the total completion times compared to measured values in all four sequences (Left-Short: -3.84 ± 3.14 s, Left-Long: -3.99 ± 4.18 s, Right-Short: -3.30 ± 2.49 s, Right-Long, -5.39 ± 4.12 s). Both, measured and predicted task completion times indicated an increase in time with increasing inter-pulley distance (i.e., long vs. short).

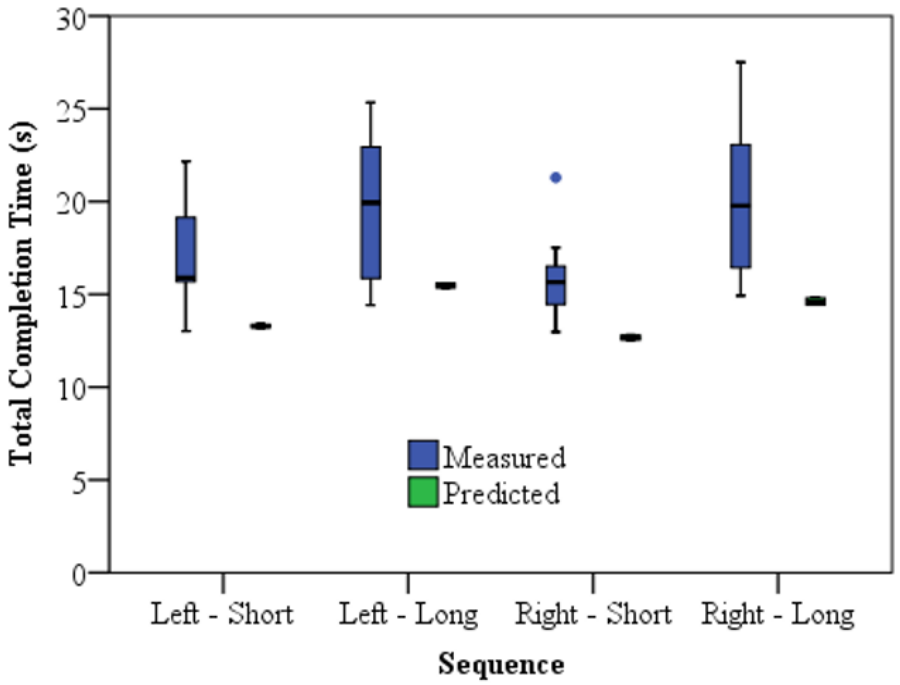

Figure 5.12. Measured (N = 12) and predicted (N = 4) aggregated total task completion times, stratified by threading sequence. Error bars indicate ± 1 SD.

Figure 5.13 compares the difference in predicted vs. measured total completion times stratified by trajectory segment and threading sequence. Generally, in the majority of the trajectory segments, the model underestimated total time, with the variability in $\Delta\widehat{Time}_{Total}$ tending to increase with an increase in inter-pulley distance within the same trajectory segment and sequence. The largest mean difference was observed for $Traj_{7\text{-}8}$ in the Right-Long threading sequence, which involved a reach movement toward target pulley-8 with a 152-mm diameter and 6-mm groove width located on the midline at a height of 1800-mm, and a 180° approach angle (Pulley-8 at the top of the Right-Long sequence in Figure 5.3). Movement corrections occurred in several measured trajectories in the pulley-interaction phase, whereas the predicted pulley-

interaction phase path and duration was short, leading to a large $\Delta\widehat{Time}_{Total}$ for this specific trajectory segment.

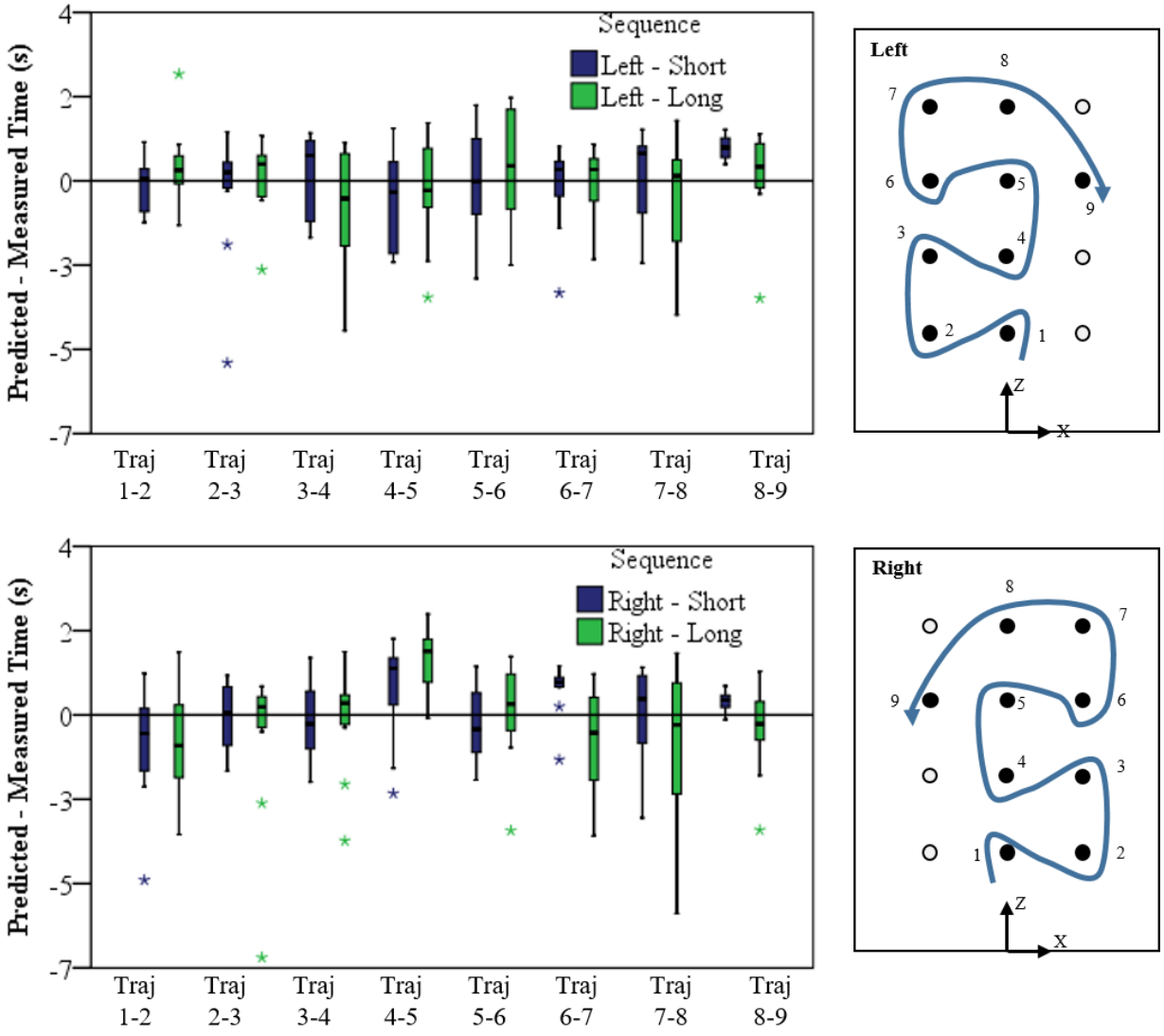

Figure 5.13. Root mean square error in predicted vs. measured movement times (N = 12 trials) stratified by trajectory segment (i.e., $Traj_{1\text{-}2}$ to $Traj_{8\text{-}9}$) and 4 threading sequences. Asterisks indicate outlier values exceeding 3 times the inter-quartile range.

Prediction errors in movement time were stratified by movement phase to get a better understanding of their error contributions towards the error in total task completion time. Table

5.3 shows the overall mean differences in predicted vs. measured total time, transition phase time, and pulley-interaction phase time aggregated by trajectory segment. Statistical analysis showed predictions of both the transition and pulley-interaction phase times contributed significantly ($p < 0.001$) to the underestimation of total completion times, with $\Delta\widehat{Time}_{PI}$ and $\Delta\widehat{Time}_{T}$ accounting for on average 79% and 21% of the difference, respectively.

Table 5.3. One sample t-tests (with a significance criteria of $p < 0.05$) comparing differences in predicted minus measured total time, transition phase time, and pulley-interaction phase time to 0 seconds.

	t	df	*p*	Mean difference (s)	[95% CI]
$\Delta\widehat{Time}_{Total}$	-8.608	376	***< 0.001**	-0.53	[-0.65, -0.41]
$\Delta\widehat{Time}_{T}$	-4.817	376	***< 0.001**	-0.15	[-0.14, -0.06]
$\Delta\widehat{Time}_{PI}$	-7.392	376	***<0.001**	-0.42	[-0.54, -0.31]

The general trend of $\Delta\widehat{Time}_{PI}$ contributing to a larger portion of $\Delta\widehat{Time}_{Total}$ was consistent across trajectory segments and threading sequences. Figure 5.14 shows the mean difference in predicted vs. measured times in the transition and pulley-interaction phases stratified by threading sequence. The high variability in $\Delta\widehat{Time}_{PI}$ shown in Figure 5.14 was attributed to movement corrections in the pulley-interaction phase in a large number of threading trials.

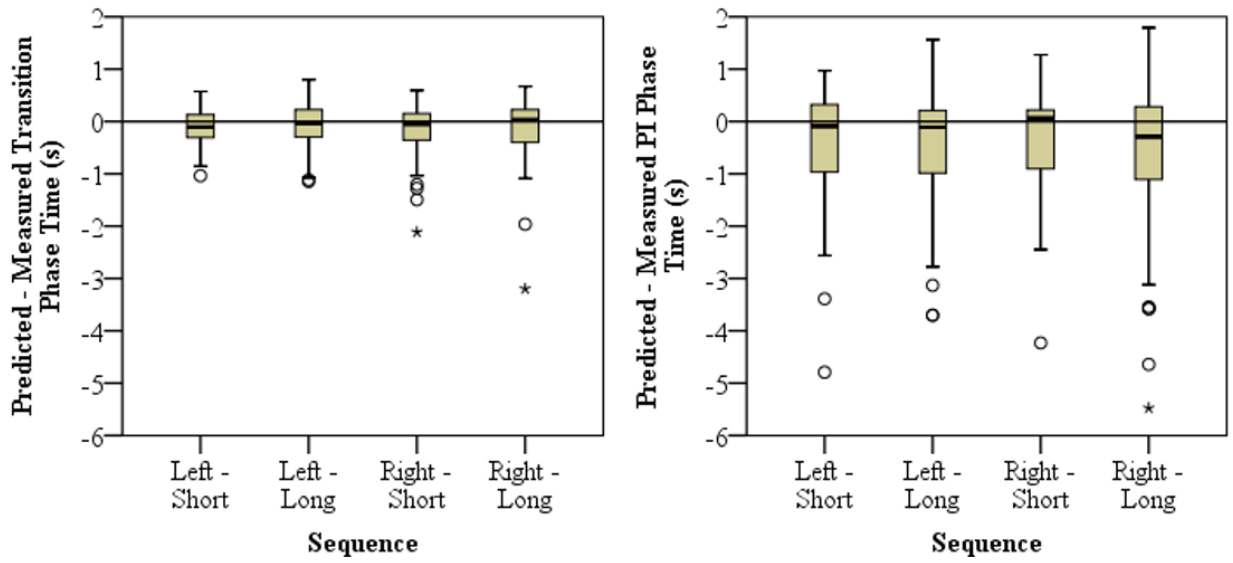

Figure 5.14. Difference in predicted minus measured time in the transition (Left) and pulley-interaction (Right) phases stratified by threading sequence. Circles denote outlier values exceeding 1.5 times the inter-quartile range, while asterisks indicate outlier values exceeding 3 times the inter-quartile range.

5.4 Discussion

The objective of this experiment was to examine the ability of the developed model to predict trajectory shape and speed and task completion times in a rather complex and realistic sequential reach movement task with continuous material. This was achieved by comparing predicted and measured values in novel tasks conditions (i.e., different from those used in model development) that involved 4 threading sequences, each containing 8 unique origin to target pulley reach movement segments. The task configurations were designed to include a variety of target pulley design parameters, locations, inter-pulley distances, and approach angles. Goodness of fit was assessed at three different levels: (1) hand trajectory shape, (2) hand speed profile, (3) and movement times obtained from the multi-segment integration of trajectory shape and speed.

5.4.1 Trajectory Shape Predictions

First, the root mean square error in trajectory shape predictions was on average less than 50 mm per reach movement trajectory. This is about 15 mm higher than the overall average error found in Chapter 3 which assessed model goodness of fit in predicting trajectories used for model development. The threading sequences in the current experiment contained a number of conditions that pushed the boundaries of some of the model's predictive parameters. For instance, the origin and target pulleys were located at a height of 600-mm (approximately knee height to mid-thigh) for the first trajectory segment in each of the threading sequences. At the model development stage, all target pulleys were located at either hip height, elbow height, or stature across all experiment conditions in datasets 1-3. However, aside from the first trajectory segment in the Left-Short and Left-Long sequences, a qualitative analysis showed the predicted trajectory shape pathway generally aligned with the average measured trajectory pathway.

Consistent with findings from Chapter 3, performance in shape prediction improved within similar trajectory segments for conditions that had shorter inter-pulley distances and when target pulleys were primarily located on the ipsilateral side of the body. Inferences about the effect of target tolerance (e.g., diameter, groove width) could not be made since target pulley diameter and groove width were not manipulated within each trajectory segment condition for any of the threading sequences.

5.4.2 Speed Profile Predictions

The predicted speed profiles captured undulations in speed magnitude associated with task parameters. The overall error in speed, averaged across all trajectory segments and threading sequences, for reach movements in the validation dataset was 159 mm/s, compared to 124 mm/s for datasets 1-3, as discussed in Chapter 4. As previously discussed, an error of this magnitude is

expected considering the variability in speed profiles throughout all phases of the reach movement. In the novel set of conditions, the model was capable of predicting average speed in the transition phase within an average of -6 mm/s, though underestimated average speed in the pulley-interaction phase by -45 mm/s on average. Error in the pulley-interaction phase speed profile predictions attributed to the majority of the speed profile error, where speed profiles were interpolated using b-splines. Thus, the pulley-interaction phase speed profile was not completely representative of measured speed profile shapes, especially when multiple movement corrections were performed, which is common in this task. Measured speeds cycled through several acceleration and deceleration phases as multiple attempts are made at positioning the thread within the tolerance of the pulley groove, whereas the predicted speed profile attempted to capture the duration and average speed of these corrections with only one deceleration and acceleration component in the pulley-interaction phase.

5.4.3 Time Predictions

Lastly, the model for total completion time was assessed by comparing measured and predicted times for each trajectory segment within each of the threading sequences. On average the model underestimated segmental movement times by 0.53 seconds. After stratifying time predictions by movement phase, 79% of the error could be attributed to error in pulley-interaction phase predicted times. This result is consistent with Chapter 4 which reported a 0.29 second underestimation in predicted pulley-interaction phase time, due to the large number and duration of measured trials that contained multiple movement corrections.

This model estimates total completion times by integrating predicted trajectory path and speed profile shape by segment. Therefore, the segmental error in both path length and speed predictions additively contribute to the error in time. In particular, the substantial

underestimations in individual pulley-interaction phases (influence by multiple movement corrections to position the thread within the target pulley groove in measured data) contributed to an overall underestimation of task completion time. It is worth noting that the trajectory shape prediction model did not predict movement corrections in terms of path length. However, an operational definition of movement corrections is not trivial considering the multiple positional and speed fluctuations around the target, and could be investigated in future research. This may contribute to improvements in model predictions by stratifying data with vs. without movement corrections.

5.4.4 Limitations

A small sample size of 4 participants is a primary limiting factor of this experiment. A larger sample would have reduced the relative contribution of outliers in measured trajectory shapes and speed profiles on the performance outcomes. In addition, this model is limited to predicting the average shape and speed for the measured sample. Other than stature used for normalizing the pulley locations, the model does not account for factors that influence between-person variability (e.g., manual dexterity, hand-eye coordination), which is a topic for future investigation. It is possible that incorporating person-specific characteristics may further explain some of the variance in hand trajectory and speed profile shapes, beyond the variance attributed to task parameters.

Evaluating the direct influence of one specific parameter on model error while controlling for the other parameter was challenging due to the sequential characteristics of the task and the larger number of task parameters accounted in the model. This study focused largely on reach direction and target location. Although multiple target pulley diameters and groove widths were used in each threading sequence, they were not directly manipulated within each trajectory

segment. In other words, the design characteristics of each target pulley remained the same throughout the experiment. Thus, differences in model performance across the trajectory segments in each of the threading sequences could not be solely attributed to the effects of target diameter and groove width.

5.4.5 Implications for Practice

This research has direct practical implications for equipment design and improved simulation capabilities in DHM software. Importantly, this research provides quantitative estimates of the actual reach distances and cumulative displacement of the hand reaching past and around the target pulleys, which was very different from the geometric distances between pulley centers. This understanding has direct implications for hand clearances near reach targets to allow for efficient and accurate hand movements in sequential reach task with continuous material. The local effects of individual reach targets can be compared to determine the preferred location and design characteristics of targets, relative to other operational considerations (e.g., extent of wrapping angle).

Ergonomics analysis of reach tasks with DHM software requires accurate representation of end-effector locations as input for posturing the digital manikin. Current DHM software require manual manipulation of the digital manikin at key frames (or time-points) along a prolonged task as input to the dynamic simulation. The models assessed in this study would provide DHM users to automatically generate more accurate end-effector locations and speeds, eliminating the need for users to make assumptions about reach locations and postures. The continuous trajectory shapes and speed profiles, are task specific and empirically based, which increases the visual realism or “naturalness” of the simulation. To our knowledge, this is the first such model to predict reach trajectories to sequential targets and associated speed profiles

wherein the hand does not come to rest at individual targets (i.e., the hand is continually in motion).

A long-term goal was to improve the capabilities of DHM software to simulate material handling tasks that involve sequential reach movements with continuous material, thereby improving the capability of DHM users and engineers to virtually and proactively analyze such tasks before production. The Human Motion Simulation Laboratory (HUMOSIM) at the University of Michigan previously developed a general framework for simulating complex tasks involving multiple movements and object manipulations with only high-level inputs (Reed et al., 2006). The HUMOSIM framework implementation (HFRI) (Reed et al., 2006; Zhou, Armstrong, Reed, Hoffman, & Wegner, 2009) contains a set of posture and motion modules that control aspects of human behavior, such as gaze (Kim, Reed, & Martin, 2010), grasping (Reed, Zhou, & Wegner, 2011), upper-extremity motion (Faraway, 2000).

To demonstrate proof-of-concept, a preliminary implementation of the model developed in the current research was conducted in the HFRI. Figure 5.15 shows a screenshot of the implementation in a sample sequential threading task. Similar implementation in commercial DHM software improve simulation capabilities of hand trajectories and speed profiles in sequential tasks with continuous material for unique task configurations. Figure 5.15 provides an example overview of the process of integrating the presented model into the ergonomics analysis workflow using DHM software.

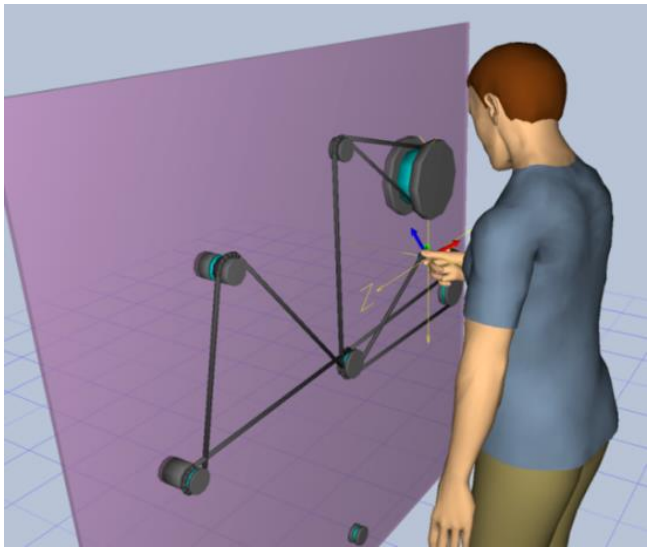

Figure 5.15. Screenshot of the output from the HUMOSIM Reference Implementation (Reed et al., 2006) of the presented model.

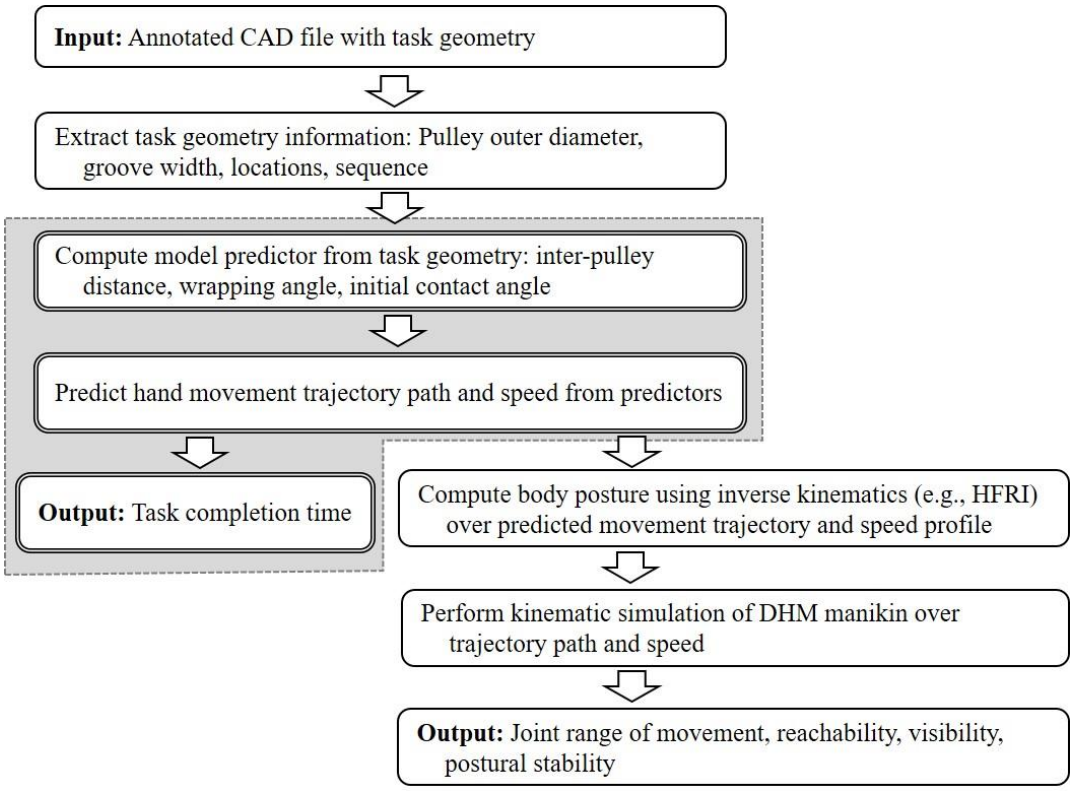

Figure 5.16. Example ergonomics analysis workflow with the role of the current research highlighted in gray.

5.5 Conclusions

This study provided empirical validation of the predictive model for hand trajectory shape, speed and task completion time in sequential reach tasks with continuous material in novel task configurations. The model used task parameters as predictors accounting for unique properties in movement trajectory and speed properties intrinsic to sequential tasks, specifically, continuous shape trajectories as the hand reached past and around the target pulleys, and speed profiles that differed in speed magnitudes at the beginning and end of each transition (blue) and pulley-interaction (red) phase.

The model was designed to be compatible with DHM software. Commercial DHM software currently lack the ability to simulate sequential reach task with continuous material. Implementation of this model in DHM software will allow workstation designers to simulate and analyze sequential reach tasks with continuous material across a diverse set of task parameters. These new capabilities will improve the ergonomic analyses of jobs requiring sequential reach movements while transferring continuous material by allowing workstation designers to make informed decisions about equipment design and placement for improving operator access and task efficiency.

CHAPTER 6

Conclusion

6.1 Summary of Findings

Chapter 1 presented a simplified conceptual model of factors that had the potential to influence performance outcomes, namely hand trajectory shape and speed, in a sequential reach task with continuous material. A detailed investigation over three studies revealed the sub-set of task parameters that had a larger effect on hand trajectory shape vs. hand speed and movement time. Figure 6.1 and Figure 6.2 show a revised conceptual model that qualitatively summarize the relative contributions of task parameters on hand trajectory shape and speed, respectively, where the line-weight of the arrows is proportion to the relative contribution.

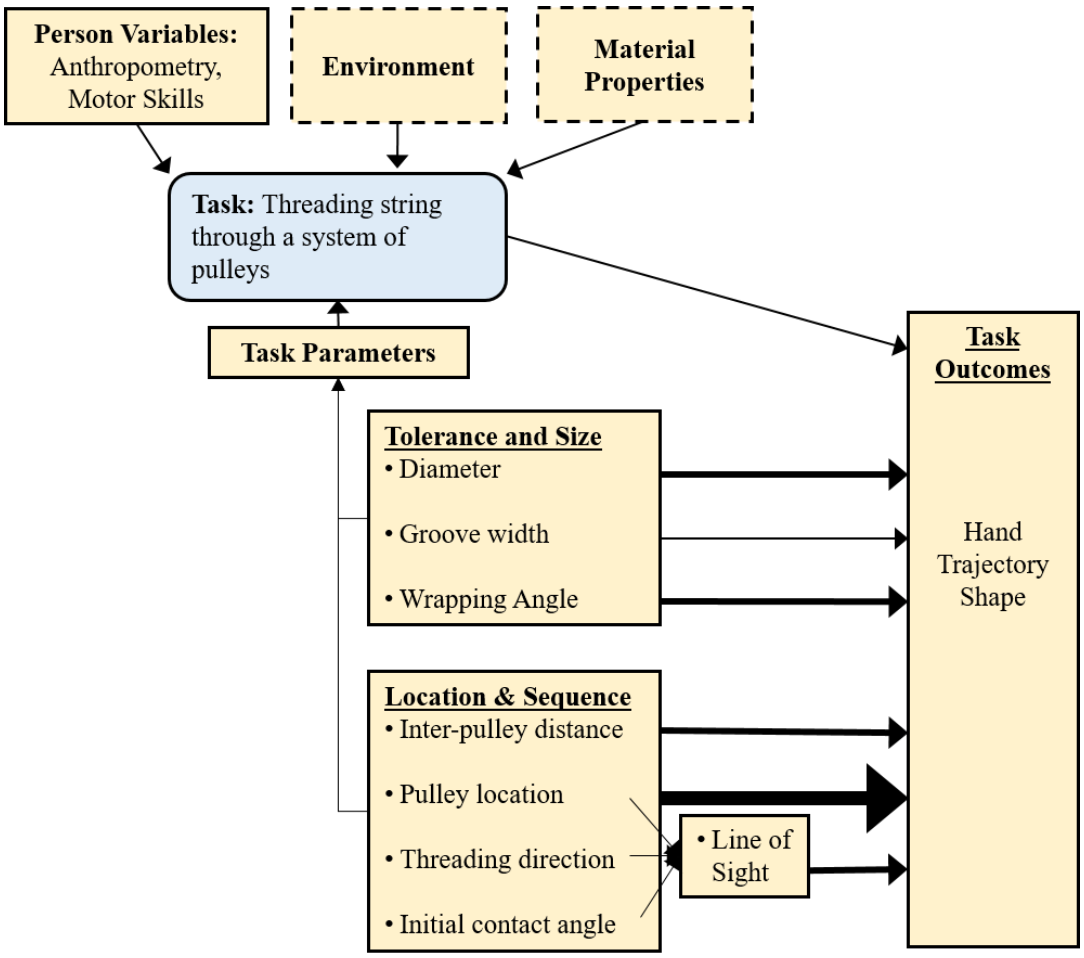

Figure 6.1. Revised conceptual model depicting the relative contributions (denoted by line-weight of the arrow) of task parameters on predicted hand trajectory shape.

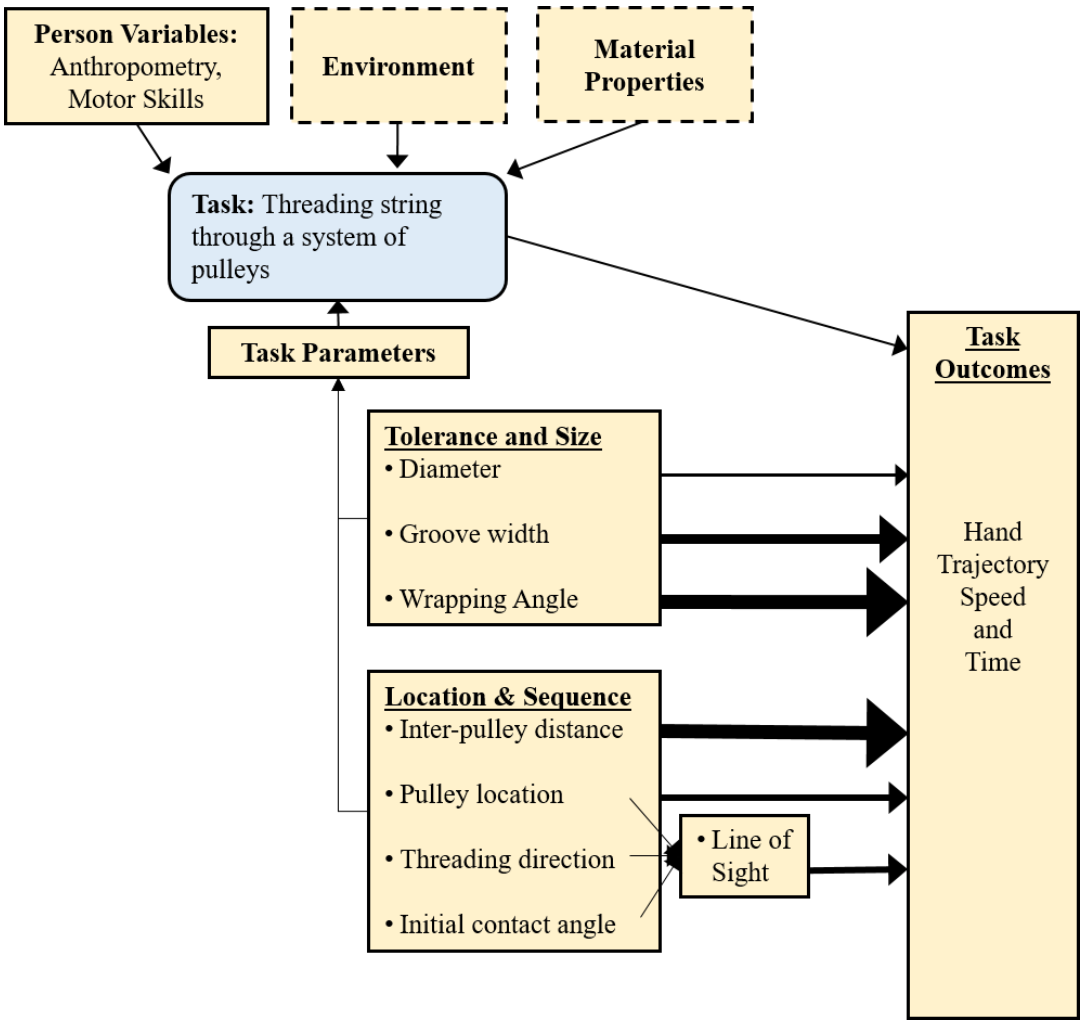

Figure 6.2. Revised conceptual model reflecting the relative contributions (denoted by line-weight of the arrow) of task parameters on predicted hand speed profiles.

The principal findings of this research are summarized and discussed in the context of the three specific aims outlined in Chapter 1.

Specific Aim 1: Quantify the effects of pulley design parameters and reach movement direction on movement time.

Chapter 2 had 22 participants complete an experiment which investigated the effects of pulley groove width and diameter, reach movement direction, and threading direction at the target pulley location on task performance in a one-handed standing sequential reach task with

continuous material. These factors were found to have systematic effects on the time to reach to and thread a target pulley. Findings showed that target pulleys with narrower groove widths, larger diameters, and target pulley locations on the contralateral side of the body were associated with longer movement times. Additionally, movement time increased when there was no line of sight with the initial contact point on the pulley groove, specifically for target pulleys located on the contralateral side. Importantly, these findings provided evidence of a speed-accuracy trade-off in a multi-segment continuous movement (i.e., when the hand was continually in motion). The findings aligned with prior research on discrete reach movement tasks in the Fitts law paradigm wherein average movement times increase with lower target tolerance and larger movement amplitude, with their combined effect represented in the dimensionless Index of Difficulty (Fitts, 1954; Langolf et al., 1976).

Specific Aim 2: Develop a model to predict (a) hand trajectory shape and (b) speed profiles in a sequential reach task with continuous material using task parameters as predictors.

Chapter 3 presented the development of a model to predict average hand trajectory shape during sequential reach movements using b-splines. The model successfully predicted trajectory shape based on a diverse set of task parameters, accounting for an average of 32% of the variance in the control point locations for the transition phase and 36% for the pulley-interaction phase, and an average RMSE of 31 mm when compared to measured trajectory data.

Parameters that tended to have the greatest impact on hand trajectory shape were movement amplitude and the lateral eccentricity of target pulley location relative to the mid-sagittal plane. Trajectories tended to be more flat with an increase in the movement amplitude, defined by the inter-pulley distance, and for reach movements that were directed towards target

pulleys located at standing height on both the contralateral and ipsilateral side of the body. Availability of visual feedback at the target pulley location also influenced trajectory shape. The hand and arm occluded vision with the target pulley groove when reaching toward target pulleys located on the contralateral side of the body. Under these conditions, the hand extends further past the pulley edge, compared to target pulleys located on the ipsilateral side, resulting in longer net movement of the hand. Although, target tolerance had a large impact on speed and movement time, reach movements toward target pulleys of different groove width sizes varied only a small amount in the transition phase of the movement.

Chapter 4 presented the development of a model to predict hand speed profiles during sequential reach movements using b-splines. The model was only able to explain on average 12% of the variance in control point locations and there was an average RMSE of 124 mm/s between time-normalized predicted and measured speed profiles. Measured speed profiles, in both phases of the movements, were highly variable, in terms of overall magnitude and fluctuations between periods of hand acceleration and deceleration, which partially explains the large error between predicted and measured speeds. However, despite the observed variability in the speed profile shape, overall, the model was able to capture the average speed of the hand trajectory in the transition phase with an average error of 2.4 mm/s.

Collectively, the findings on hand trajectory shape and speed indicate that task parameters had systematic local effects on movement kinematics even as the hand was continually moving. Consistent with discrete reach movement tasks in the Fitts' paradigm, the study found hand speeds to increase in the transition phase associated with increases in movement amplitude (i.e. inter-pulley distance) and target tolerance (i.e. target pulley groove width) indicative of a speed-accuracy tradeoff.

Movement corrections, in the pulley-interaction phase, which were observed in a large proportion of the measured trials, contributed to errors in hand trajectory shape, speed, and estimations of task time. Manual transfer of continuous material in sequential reach movements increased the task complexity in terms of information processing compared to discrete reaches. In the case of discrete object transfer or pointing tasks, corrective submovements directed toward the target location largely occur in the latter closed-loop phase of the movement when the hand undershoots or overshoots the target (Crossman & Goodeve, 1983; Meyer et al., 1988). For threading trials in this research where participants failed to position the thread within the target pulley groove, in an attempt to maintain thread tension, corrective movements are directed away from the target pulley. Due to the sequential characteristics of the task, movement corrections affected the speed and location of the hand in the current pulley-interaction phase and the next transition phase, indicating a spillover effect.

Specific Aim 3: Empirically validate the predictive model of hand trajectory shape, speed and task completion time in sequential reach tasks with continuous material.

Chapter 5 investigated the goodness of fit of the integrated trajectory shape and speed model in predicting task outcomes in a novel dataset of experiment conditions. Prediction errors in 4 threading sequences in terms of trajectory shape (average RMSE of 45 mm) and speed (average RMSE of 159 mm/s) were marginally higher compared to the errors assessed at the model development stage. However, the diverse locations of target pulleys selected represented more extreme cases compared to the model development. The model underestimated the measured completion times at each segment (i.e., one origin to target pulley reach movement) by an average of 0.53. Despite these limitations, the model accounted for systematic trends in

trajectory shape, speed and movement time associated with the selected task parameters, specifically inter-pulley distance and target pulley location.

6.2 Methodological Contributions

This research presented the first model to predict hand trajectory shape and speed in target-directed sequential movement tasks while transferring continuous material. The model provides a means to quantify the relationship between hand trajectories and a variety of key task setup parameters including, target tolerance, target size, target location, movement amplitude, and line of sight availability. Related to this primary research contribution, certain methodological contributions are also worth emphasizing.

1. This research provides a nomenclature for describing the relevant parameters affecting operator performance in terms of task geometry, including operationalizing target tolerances (in terms of pulley diameter and groove width), line of sight (based on target location and initial contact angle), and movement amplitude (e.g. inter-pulley distance). These operational definitions are unique to the ergonomics literature, and were developed through multiple, iterative experimentation. Importantly, this nomenclature provides a method for converting task geometry (e.g., obtained from CAD data) into complex variables that relate to human performance, i.e., predictors to the trajectory shape and speed model.
2. This research developed a methodology for segmenting hand trajectories in a sequential reach task with continuous material (i.e., when the hand is continually moving throughout) into a series of discrete reach movements. For the sequential reach task operationalized in this research, a hand trajectory segmentation scheme was developed that segmented hand trajectories into a series of two phases based on task geometry,

namely, (i) a *transition* phase where the hand is reaching between two consecutive pulley locations and (ii) a *pulley-interaction* phase where the hand is engaged in threading the target pulley.

3. The process of modeling hand trajectories and speed profiles with b-splines provided a means for combining multiple predicted trajectory segments associated with transition and pulley-interaction phases into a continuous trajectory while maintaining certain properties that were intrinsic to sequential reaches. Specifically, a method for developed for ensuring continuity in (i) position and gradient for trajectory shape, and (ii) speed magnitude and gradient for the corresponding speed profile between consecutive movement phases. This methodology could benefit the modeling of shape profiles in human movement that display similar kinematic properties.

6.3 Theoretical Contributions

This research contributes in our understanding about coordination and control of movement generation in sequential reach tasks. First, a few key findings are worth summarizing for context.

1. The human factors literature is replete with studies investigating speed and accuracy during discrete reach movements. Studies quantifying human performance in sequential precision reaches (i.e., the hand remains in motion) while manipulating continuous material are absent. Consistent with discrete reach movement tasks in the Fitts' paradigm, this research found hand speeds to increase in the transition phase associated with increases in movement amplitude (i.e. inter-pulley distance) and target tolerance (i.e. target pulley groove width) indicative of a speed-accuracy tradeoff.

2. Hand trajectory shapes and speed profiles were highly variable between repeated movements from the same participant for a task that has the same set of conditions. The combination of the sequential properties of the task and the added difficulty of transferring continuous material plays a major role in this variability.
3. Hand trajectory shapes for a typical reach movement with continuous material were generally smooth when transitioning between target locations, while measured hand speed was highly variable. This suggests the prioritization of accuracy in terms of the hand location or during the reach movement at the cost of increased fluctuations or entropy in speed.
4. Target tolerance (pulley diameter and groove width) had a large effect on speed profile shape and the duration of the reach movement, yet on average there was little variation in hand trajectory shape across reach movements to targets of varying tolerance levels. The movement amplitude (inter-pulley distance), target size (diameter) and the target location with respect to the person, generally had the greatest impact on trajectory shape.
5. This research initially expected that the reach movements would consist of an open-loop phase (transition) and a closed-loop phase with visual feedback (pulley-interaction) akin to discrete reaches, even though the hand was continually in motion. Measured speed profiles were roughly bell-shaped and reached peak speed during the open-loop phase. Identification of the start and end of the closed-loop phase was difficult due to the high variability in the speed profiles near the target location. However, the large fluctuations in speed observed in both phases of the movement suggested that participants continuously used feedback of the thread tension/location to control the movement in both phases.

Woodworth (1899) was the first to study discrete rapid-aiming movement tasks, and hypothesized that aiming movements are controlled by an initial impulse phase followed by a second current control phase (i.e., a "homing" phase that is under feedback-based control). Many others researchers have since investigated factors that influence motor planning, coordination, and performance in tasks that involve aiming movements (Crossman & Goodeve, 1983; Meyer et al., 1988; Schmidt et al., 1979) and continuous tracking (Craik, 1947; Miall et al., 1993).

Findings from this research suggest that quantitative modeling of motor control in sequential reach tasks with continuous material is not as straightforward as a sequence of open-loop and closed-loop phases with feedback as initially hypothesized. The general bell-shape of hand speed profiles were emblematic of rapid aiming tasks (Atkeson & Hollerbach, 1985; Beggs & Howarth, 1972; Georgopoulos et al., 1981; Morasso, 1981) suggesting an underlying initial open-loop phase when transitioning between target locations, followed by a closed-loop phase with visual feedback. However, hand speed cycled through multiple intermittent periods of acceleration and deceleration in alternating transition and pulley-interaction phases of the sequential reach movement, represented a notable departure from speed profiles in rapid aiming tasks. This finding provided evidence that online control mechanisms may be applied in the transition phase of the movement, suggesting control mechanisms are similar to those in continuous tracking (Craik, 1947). Two potential sources of variability in hand speed were discussed in Chapter 4. First, participants had to continually process information for maintaining tension in the material while reaching towards the target pulley, which is critical to being able to successfully position the thread within the target pulley groove. Small amount of slack in the thread could be compensated by reaching past the target pulley. Secondly, hand speed variability may be a result of modifications in lower arm and wrist posture, as evidenced during data

collection and a qualitative video analysis. Collectively, the evidence of closed-loop speed corrections throughout the measured reach movements indicated continual modulations in movement generation and speed control to meet the multiple objectives of quick and accurate reach movements to the target while simultaneously maintaining adequate material tension. Further, the prioritization of positional control over speed control indicates that online execution mechanisms might be capable of selectively enforcing certain task-relevant dimensions while allowing variability in other redundant dimensions, aligned with the theory of optimal feedback control (Todorov & Jordan, 2002). In other words, for the task studied in this research, speed control may serve as a "buffer" in an attempt to reduce positional variance.

6.4 Implications for Ergonomics Practice

This research has direct practical implications for equipment design and improved simulation capabilities in DHM software. Quite broadly, this research generated new knowledge and models for quantifying both local and aggregate effects of the design characteristics and location of individual targets in a sequential reach task on movement performance. Workplace design and locating of targets in sequential reach tasks can take advantage of this finding that certain reach movements can be performed more efficiently than others. Specific practical implications are described below.

1. Digital human modeling is a critical part of the process in designing efficient and ergonomic workstations. It allows designers to visualize how humans interact with the workstation prior to production or even physical prototyping. The Human Motion Simulation Laboratory at the University of Michigan previously developed empirically-based statistical models to improve the realism of movements in DHM software in order to aid ergonomic analysis of workstation design (Reed et al., 2006). This research

provides a model to simulate hand trajectory movement pathways and speed profiles for characterizing sequential reach movements with continuous material that is compatible with the Human Motion Simulation framework. Implementation of this model in digital human modeling software will allow for the capability to simulate these types of tasks for ergonomic analysis. For example, workstation designers will have the capability to simulate and analyze sequential reach tasks with continuous material for access, in terms of hand clearance and reachability) across a diverse set of task parameters and operator anthropometry. These new capabilities would allow engineers to make informed decisions about equipment design (e.g., target characteristics and locations) for improving operator access and task efficiency.

2. Predetermined motion time systems, such as Methods-Time Measurement (MTM), are used primarily in industrial settings to analyze methods used to perform manual tasks and to set a standard time in which a worker can complete that task. MTM is currently limited in its ability to predict movement time for tasks that involving transferring continuous material. This model could be used to predict movement times in tasks that involve handling continuous material while reaching to multiple target locations in a specific sequence, given the target locations and design parameters.
3. This research was motivated by an industrial task in textile manufacturing wherein workers have to perform sequential reach movements with continuous material, such as thread, when preparing equipment for operation. Though the research used thread as an example of continuous material, this model could be applied to handling other types of types of material including ribbons and paper towels, or wire harnesses in auto manufacturing. Workplace design and locating of targets in sequential reach tasks can

take advantage of the fact that certain reach movements can be performed more efficiently than others.

4. Tasks that are potentially harmful to operators, highly repetitive, or require high force exertions are increasingly selected for automation, whereas human operators are relegated to complex precision tasks that require intricate hand movements and fine motor control skills, i.e., dexterous tasks that are difficult to automate. Currently, for the example of transferring thread through a system of pulleys, the transferring and positioning of continuous material within the target tolerances presents significant challenges for automation. The methods and models developed in this research could contribute to control algorithms for robotics applications aimed at automating dexterous and precision handling of light-weight continuous material.

6.5 Limitations and Next Steps

This dissertation addressed many unanswered questions about how humans conduct sequential reach movements while transferring continuous material, and about the key task setup parameters that influence task performance. Certain limitations of this research are worth acknowledging and provide avenues for future work to improve model performance and our theoretical understanding of movement planning and control.

1. The sample population for model development consisted only of young healthy right-handed participants, with the model predictions relegated to predicting average performance based on resulting measurements in the three data collection experiments. Aside from stature, no person-specific information was included as predictors for hand trajectory shape or speed. Studies that account for between-subject differences in

anthropometry attributes and measures of motor performance capabilities (e.g., manual dexterity, hand-eye coordination) would likely improve model performance.

2. To simplify the research problem, environmental factors and the material properties were not manipulated in any of the experiments. Standard polyester thread represented the continuous material in each of the experiments. Further research is necessary to determine if human and model performance varies for different types of material (e.g., elastic fiber, fine wire).
3. The hand trajectory movement phases were not segmented based on speed profile shape criteria. Thus, this research presents a limited analysis on the coordination of hand movements in a sequential reach task with continuous material, including how task parameters affect the peak and minimum speeds during the reach movement and the transition timing of the acceleration and deceleration phases.
4. This analysis was limited to one handed reach movements with continuous material. Transferring continuous material often requires the use of two-hands, especially for reach movements to extreme locations. Though participants were able to successfully and accurately complete all of the presented task conditions using only their dominant hand, it is unknown if they would have performed differently provided they weren't constrained to using one hand.
5. The analysis was limited to 2-dimensional sequential reach movements to targets in the frontal plane. A preliminary analysis showed little evidence of deviation in hand trajectory path along the anterior-posterior axis. Future research is necessary to determine if model predictions hold for target directed movements in the transverse plane.

6. Error in predicted trajectory shape and in predicted speed profiles combined to compound error in predicted movement time. Typical movement time prediction models in target-directed discrete movement tasks directly predict movement time as a function of the task index of difficulty. Further analysis is required to develop an index of difficulty for sequential reach movement tasks with continuous material. Though, this research identified key task effects that should be included in such a parameter.
7. Lastly, this research was limited to model predictions for hand trajectory movement paths and speed profiles. Current DHM software has the capability to predict postural adjustments using inverse kinematics, if provided the hand movement path. However, certain interesting postural movements (e.g., forearm internal rotation during curvilinear movements, torso lateral bending and twisting during contralateral reaches; head movements and gaze direction) were observed in the experiments which inverse kinematics in existing DHM software might not capture when analyzing such task. Future studies that model these upper extremity postural adjustments and head location will likely improve the realism of predicted postural adjustments and ergonomics analysis capabilities in DHM software. Nonetheless, the current research provides a foundation to support these future studies and research extensions.

6.6 Concluding Remarks

The overall goal of this research was to model the spatial and temporal properties of a reach movement in a sequential reach task that involves handling continuous material. To that end, this research presented a novel empirically-based model to predict reach trajectories to sequential coplanar targets and associated speed profiles wherein the hand does not come to rest at individual targets (i.e., the hand is continually in motion) with specific task parameters as

predictors. The research makes important contributions in our theoretical understanding of how the CNS plans and coordinates movements in sequential reach tasks. A proof of concept implementation within the Human Motion Simulation Framework was conducted to demonstrate the practical significance of this research, namely, extending the simulation capabilities of DHM software to analyze similar precision handlings of light-weight flexible material in industrial applications.

APPENDICES

APPENDIX A

Post Prediction Adjustment of Trajectory Shape Control Points

To assure the continuity in location and gradient in the trajectory shape at the transition between the transition and pulley-interaction phases, a post prediction algorithm was implemented to force collinearity of the control points (Figure A.1) at the end of the transition phase ($P_{T1,4)}$, the start of the of the pulley-interaction phase ($P_{PI,0}$), and the second control point in the pulley-interaction phase ($P_{PI,1}$). First, the angle (Θ) between vectors $\overrightarrow{P_{PI,0}P_{T1,4}}$ and $\overrightarrow{P_{PI,0}P_{PI,1}}$ was computed using equation A.1. Control points $P_{T1,4}$ and $P_{PI,1}$ were then rotated by Φ (= (180°-Θ)/2).

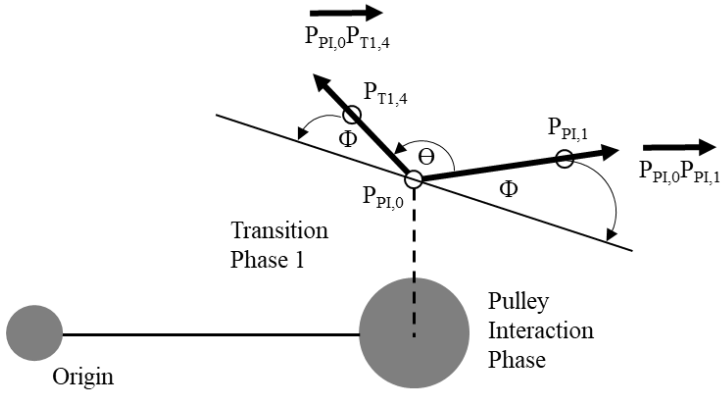

Figure A.1 Schematic of post prediction adjustment of control points.

$$\cos\theta = \frac{\overrightarrow{P_{PI,0}P_{T1,4}} \cdot \overrightarrow{P_{PI,0}P_{PI,1}}}{\left\|\overrightarrow{P_{PI,0}P_{T1,4}}\right\|\left\|\overrightarrow{P_{PI,0}P_{PI,1}}\right\|}. \qquad [A.1]$$

APPENDIX B

Regression Equations for Trajectory Shape Control Point Locations

Table B.1. Unstandardized beta coefficients for significant predictors ($p < 0.05$) of control point coordinates (X, Z) in the transition phase. A blank cell indicates a non-significant effect. The total row provides a measure of explained variance using the $\hat{R}^2_{adj}$ values for each regression model. Note: $P_{T5,X}$ is not predicted.

Predictors	**Transition Phase Control Points**											
	P_{T0}		***P_{T1}***		***P_{T2}***		***P_{T3}***		***P_{T4}***		***P_{T5}***	
	X	***Z***	***X***	***Z***	***X***	***Z***	***X***	***Z***	***X***	***Z***	***X***	***Z***
Intercept (mm)	0.00075	0.00182	0.00085	0.00159	0.00071	0.00133	0.00044	0.00083	0.00012	0.00045		0.00033
Origin Diameter (mm)	-0.00857		-0.00950		-0.00781	0.00790	-0.00378	0.00799	-0.00118	0.00703		0.00628
Origin Groove Width (mm)	-0.00008	-0.00007	-0.00025		-0.00029	0.00030	-0.00014	0.00062	-0.00011	0.00089		0.00106
Target Diameter (mm)	-0.00279	-0.00161	-0.00566		-0.00733	0.00663	-0.00263	0.00828	-0.00106	0.00666		0.00445
Target Groove Width (mm)							0.01408	-0.08639		-0.08925		-0.09611
Target Location X (% Stature)	0.02231	-0.02235		-0.01791	0.04001	-0.06784		-0.07707		-0.07459		-0.06955
Target Location Z (% Stature)	0.04142	-0.04277	0.07853	-0.07353	0.07152	-0.20348	0.02016	-0.37470	-0.00365	-0.44538		-0.41562
Origin Threading Direction (CW: 0 or CCW: 1)	0.03358	-0.06545	0.06536	-0.09159	0.07217	-0.22479	0.02022	-0.38776		-0.45484		-0.42881
Target Threading Direction (CW: 0 or CCW: 1)	-0.00004	-0.00017	-0.00011	-0.00015	-0.00016		-0.00003	0.00012	-0.00002	0.00011		0.00012
Target Initial Contact Angle (°)		-0.86802		-0.84715	0.19379	-1.18030	0.07225	-1.50387	0.04105	-1.18767		-1.13492
Inter-pulley Distance (% Stature)	-0.00089	-0.00061	-0.00147	-0.00022	-0.00134	0.00090	-0.00053	0.00080	-0.00019	0.00042		0.00024
Origin Wrapping Angle (°)	0.00037		0.00065	-0.00014	0.00056	-0.00067	0.00020	-0.00049	0.00009	-0.00035		-0.00031
Target Wrapping Angle (°)	-0.00007	-0.00011	-0.00009	-0.00005		-0.00004		-0.00009	-0.00002	-0.00010		-0.00007
Approach Angle (°)	-0.08382	0.08072	-0.15784	0.14823	-0.16103	0.42978	-0.05162	0.73686		0.86367		0.81139
Origin x Target Threading Direction				-0.04346	0.02665	-0.08872			0.00622			
Target Location X x Z	0.00075	0.00182	0.00085	0.00159	0.00071	0.00133	0.00044	0.00083	0.00012	0.00045		0.00033
$\hat{R}^2_{adj}$	.18	.34	.28	.31	.26	.34	.12	.46	.12	.58		.59
Mean (± SD) $\hat{R}^2_{adj}$	0.32 ± 0.16											

Table B.2. Unstandardized beta coefficients for significant predictors ($p < 0.05$) of control point locations (θ, R) in the pulley-interaction phase. Blank cells indicate statistically non-significant effects. Note: $P_{I0,\,\theta}$ is not predicted

Predictors	**Pulley-Interaction Phase Control Points**							
	P_{PI0}		P_{PI1}		P_{PI2}		P_{PI3}	
	θ	R	θ	R	θ	R	θ	R
Intercept		4.26622	61.53682	4.25446	44.94279	4.29975	30.10451	4.20093
Target Diameter (mm)		0.00701	-0.03862	0.00711	0.11067	0.00842		0.00742
Target Groove Width (mm)		0.02585	2.00400	0.00585	1.26763	-0.01171	1.81693	
Target Location X (% Stature)			11.48488	-0.63861	47.97043	-0.73023	66.33236	-0.55920
Target Location Z (% Stature)		-0.74763		-0.70673		-0.68099	12.92159	-0.54476
Target Threading Direction (CW: 0 or CCW: 1)		-0.24611	-1.43243	-0.15310		-0.07338	6.15762	
Target Initial Contact Angle (°)		0.00042	-0.01718	0.00032		0.00029	-0.01548	0.00018
Inter-pulley Distance (% Stature)		-0.71865		-1.31212	52.76072	-1.24480	75.97632	-0.97673
Approach Angle (°)			-0.01896	0.00057		0.00067	-0.02379	0.00054
Target Wrapping Angle (°)		-0.00158	-0.17785	0.00152	-0.24719	0.00215	-0.49056	-0.00081
Target Wrapping Angle x Diameter		0.00000	0.00046	0.00001	-0.00172		-0.00147	
Target Location X x Z		-0.43846			-32.33807		-45.90277	
$\hat{R}^2_{adj}$		0.44	0.07	0.45	0.33	0.40	0.47	0.37
Mean (± SD) $\hat{R}^2_{adj}$	0.36 ± 14							

APPENDIX C

Post Prediction Adjustment of Speed Profile Control Points

In some situations, the interpolated pulley-interaction speed profile may contain negative speed values (Figure C.1). This typically occurs in situations when there is a long predicted pulley-interaction phase time and a short predicted pulley-interaction phase path length, which leads to a relatively low average speed prediction. Figure C.1 shows the original predicted hand speed profile for a reach movement that involved reaching to a target pulley with a 76-mm diameter, 3-mm groove width, and a wrapping angle of 90° ($Traj_{3\text{-}4}$ in the Right-Long threading sequence from the validation experiment in Chapter 5).

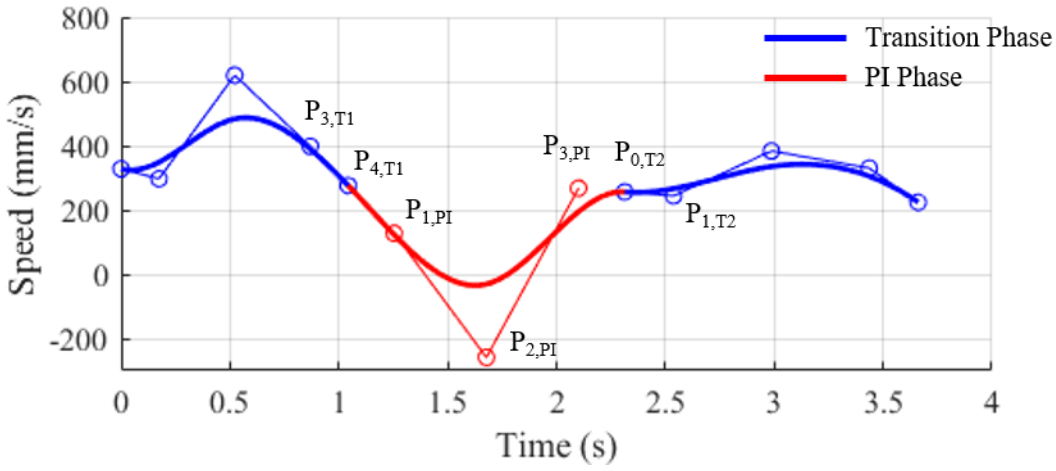

Figure C.1. Example of predictive speed profile for a sample condition where the interpolated pulley-interaction phase speed reaches a negative minimum speed.

In order to resolve this issue, a post-prediction adjustment algorithm is run. An overview of the algorithm is shown in Figure C.2. First, the algorithm checks if the minimum speed in the pulley-interaction phase is below a threshold of 10 mm/s. The algorithm exits the loop if it is greater than 10/mm/s. If the minimum speed is below the threshold then the algorithm proceeds to step 2, where the final control point of the first transition phase ($P_{4,T1}$) and the first control point of the next transition phase ($P_{0,T2}$) are decreased in magnitude to lower speed at the start and end of the pulley-interaction phase. In step 3, the transition phase speed profiles are reconstructed with the adjusted control points. In step 4, the pulley-interaction phase speed profile is re-interpolated and then the process repeats. Figure C.3 shows the adjusted predicted speed profile for the example shown in Figure C.1.

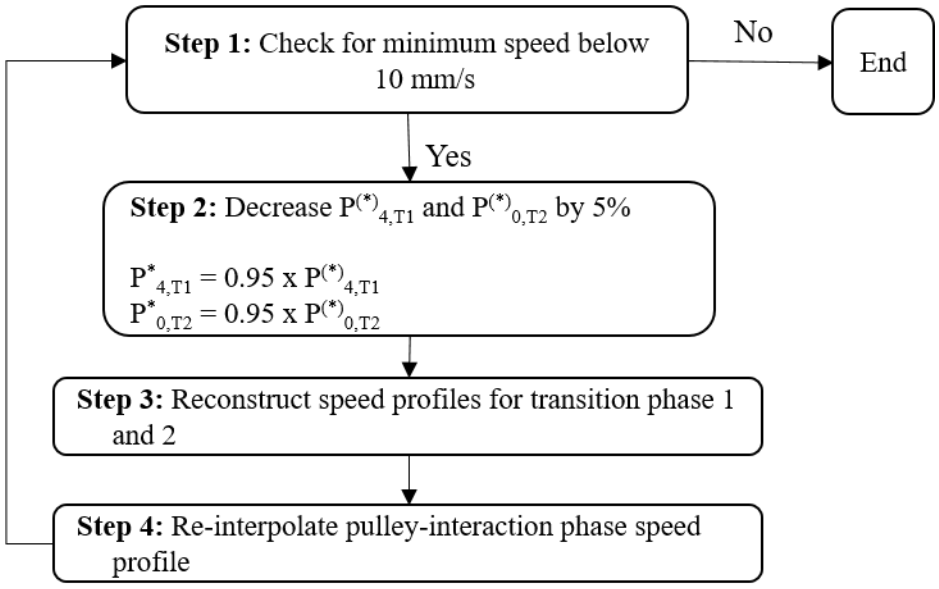

Figure C.2. Overview of algorithm for adjusting transition phase speed profile control points.

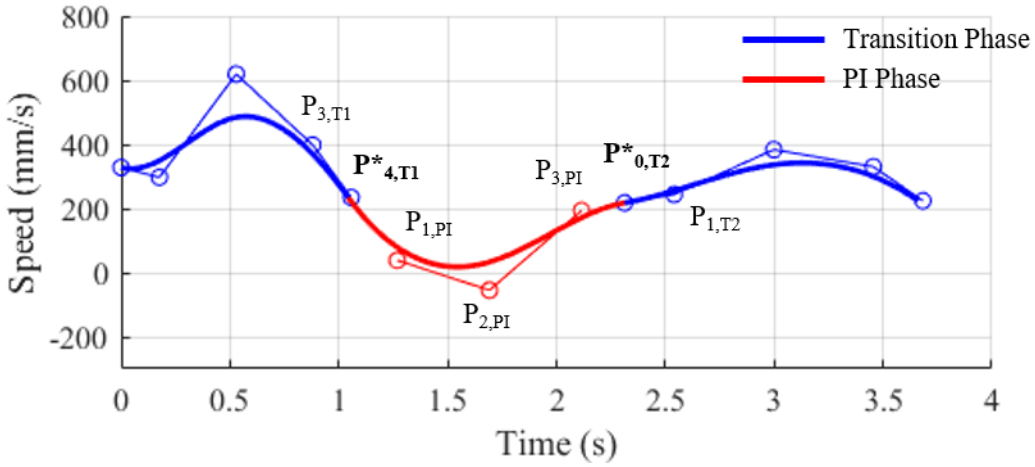

Figure C.3. Example of an adjusted predicted speed profile and corresponding adjusted control points in the transition phase ($P^*_{4,T1}$ and $P^*_{0,T2}$).

APPENDIX D

Regression Equations for Transition Phase Speed Profile Control Point Locations

Table D.1. Unstandardized beta coefficients for significant predictors ($p < 0.05$) of the 1-dimensional control point coordinates (mm/s) of b-splines fit to the transition phase speed profile. A blank cell indicates a statistically non-significant effect.

Predictors	**Transition Phase Speed Profile Control Points from datasets 1-3**				
	$\boldsymbol{P_{T0}}$	$\boldsymbol{P_{T1}}$	$\boldsymbol{P_{T2}}$	$\boldsymbol{P_{T3}}$	$\boldsymbol{P_{T4}}$
Intercept (mm)	168.55495	108.68394	202.74132	254.88802	248.81804
Origin Diameter (mm)	0.54514	0.73256	-0.38389	-0.35054	
Origin Groove Width (mm)	10.99384	7.64141	12.96999	6.50538	6.10826
Target Diameter (mm)	-0.06153	-0.21838	-0.30252	-0.37467	-0.15232
Target Groove Width (mm)	5.05248	2.51338		12.42111	10.34166
Target Location X (% Stature)			110.00013	-80.00862	-170.66756
Target Location Z (% Stature)	-87.06547		-58.01388	-72.59901	-75.49510
Origin Threading Direction (CW: 0 or CCW: 1)	24.53682	27.18380	140.08273		
Target Threading Direction (CW: 0 or CCW: 1)	28.95474	31.52487	153.64016		
Target Initial Contact Angle (°)	0.13967	0.16076	0.20739		
Inter-pulley Distance (% Stature)	107.35339		903.30565	710.32028	
Origin Wrapping Angle (°)	0.74098	1.02943	0.79957	0.22901	0.23163
Target Wrapping Angle (°)	-0.45656	-0.43861	-0.51843	-0.21234	-0.21147
Approach Angle (°)					0.05904
Origin x Target Threading Direction	-42.45341	-88.41182	-287.82521		
Target Location X x Z	92.20608	139.20312			108.85776
$\boldsymbol{\hat{R}^2_{adj}}$	0.16	0.12	0.13	0.09	0.08
Mean (± SD) $\boldsymbol{\hat{R}^2_{adj}}$	0.12 ± 0.03				

BIBLIOGRAPHY

Annett, J., Golby, C., & Kay, H. (1958). The measurement of elements in an assembly task-the information output of the human motor system. *Quarterly Journal of Experimental Psychology, 10*(1), 1-11.

Atkeson, C., & Hollerbach, J. (1985). Kinematic features of unrestrained vertical arm movements. *The Journal of Neuroscience, 5*(9), 2318-2330.

Beggs, W. D. A., & Howarth, C. I. (1972). The Movement of the Hand towards a Target. *Quarterly Journal of Experimental Psychology, 24*(4), 448-453.

Bertucco, M., Cesari, P., & Latash, M. L. (2013). Fitts' Law in early postural adjustments. *Neuroscience, 231*(Supplement C), 61-69.

Bootsma, R. J., & Van Wieringen, P. C. (1992). Spatio-temporal organisation of natural prehension. *Human Movement Science, 11*(1), 205-215.

Carlton, L. G. (1980). Movement control characteristics of aiming responses. *Ergonomics, 23*(11), 1019-1032.

Chaffin, D. B., Thompson, D., Nelson, C., Ianni, J. D., Punte, P. A., & Bowman, D. (2001). *Digital Human Modeling for Vehicle and WorkPlace Design*: Society of Automotive Engineer.

Craik, K. J. (1947). Theory of the Human Operator in Control Systems: I. The Operator as an Engineering System. *British Journal of Psychology. General Section, 38*(2), 56-61.

Crossman, E., & Goodeve, P. (1983). Feedback control of hand-movement and Fitts' law. *The Quarterly Journal of Experimental Psychology, 35*(2), 251-278.

Faraway, J. J. (2000). Modeling reach motions using functional regression analysis. *SAE Technical Paper*.

Faraway, J. J., & Reed, M. P. (2007). Statistics for digital human motion modeling in ergonomics. *Technometrics, 49*(3), 277-290.

Faraway, J. J., Reed, M. P., & Wang, J. (2007). Modelling three-dimensional trajectories by using Bezier curves with application to hand motion. *Journal of the Royal Statistical Society: Series C (Applied Statistics), 56*(5), 571-585.

Fitts, P. M. (1954). The information capacity of the human motor system in controlling the amplitude of movement. *Journal of Experimental Psychology, 47*(6), 381.

Fitts, P. M., & Peterson, J. R. (1964). Information capacity of discrete motor responses. *Journal of Experimental Psychology, 67*(2), 103.

Flash, T., & Hogan, N. (1985). The coordination of arm movements: an experimentally confirmed mathematical model. *Journal of Neuroscience, 5*(7), 1688-1703.

Georgopoulos, A. P., Kalaska, J. F., & Massey, J. T. (1981). Spatial trajectories and reaction times of aimed movements: effects of practice, uncertainty, and change in target location. *Journal of Neurophysiology, 46*(4), 725-743.

Hoff, B., & Arbib, M. A. (1993). Models of trajectory formation and temporal interaction of reach and grasp. *Journal of motor behavior, 25*(3), 175-192.

Hoffman, S. G. (2008). *Whole-Body Postures during Standing Hand-Force Exertions: Development of a 3D Biomechanical Posture Prediction Model.* (Dissertation), University of Michigan.

Hogan, N., & Sternad, D. (2007). On rhythmic and discrete movements: reflections, definitions and implications for motor control. *Experimental brain research, 181*(1), 13-30.

Jeannerod, M. (1984). The timing of natural prehension movements. *Journal of motor behavior, 16*(3), 235-254.

Jung, E. S., Kee, D., & Chung, M. K. (1995). Upper body reach posture prediction for ergonomic evaluation models. *International Journal of Industrial Ergonomics, 16*(2), 95-107.

Keele, S. W. (1968). Movement control in skilled motor performance. *Psychological bulletin, 70*(6p1), 387.

Kim, K. H., Reed, M. P., & Martin, B. J. (2010). A model of head movement contribution for gaze transitions. *Ergonomics, 53*(4), 447-457.

Klapp, S. T. (1975). Feedback versus motor programming in the control of aimed movements. *Journal of Experimental Psychology: Human Perception and Performance, 1*(2), 147.

Langolf, G. D., Chaffin, D. B., & Foulke, J. A. (1976). An Investigation of Fitts' Law Using a Wide Range of Movement Amplitudes. *Journal of motor behavior, 8*(2), 113-128.

Liu, X., Tubbesing, S. A., Aziz, T. Z., Miall, R. C., & Stein, J. F. (1999). Effects of visual feedback on manual tracking and action tremor in Parkinson's disease. *Experimental brain research, 129*(3), 477-481.

MacKenzie, C. L., Marteniuk, R., Dugas, C., Liske, D., & Eickmeier, B. (1987). Three-dimensional movement trajectories in Fitts' task: Implications for control. *The Quarterly Journal of Experimental Psychology, 39*(4), 629-647.

MacKenzie, I. S., & Buxton, W. (1992). *Extending Fitts' law to two-dimensional tasks.* Paper presented at the Proceedings of the SIGCHI conference on Human factors in computing systems.

Marteniuk, R. G., Leavitt, J. L., MacKenzie, C. L., & Athenes, S. (1990). Functional relationships between grasp and transport components in a prehension task. *Human Movement Science, 9*(2), 149-176.

Meyer, D. E., Abrams, R. A., Kornblum, S., Wright, C. E., & Keith Smith, J. (1988). Optimality in human motor performance: Ideal control of rapid aimed movements. *Psychological review, 95*(3), 340.

Miall, R. C., Weir, D. J., & Stein, J. F. (1993). Intermittency in human manual tracking tasks. *Journal of motor behavior, 25*(1), 53-63.

Morasso, P. (1981). Spatial control of arm movements. *Experimental brain research, 42*(2), 223-227.

Murata, A., & Iwase, H. (2001). Extending Fitts' law to a three-dimensional pointing task. *Human Movement Science, 20*(6), 791-805.

Plamondon, R. (1993). Looking at handwriting generation from a velocity control perspective. *Acta Psychologica, 82*(1-3), 89-101.

Plamondon, R., Alimi, A. M., Yergeau, P., & Leclerc, F. (1993). Modelling velocity profiles of rapid movements: a comparative study. *Biological Cybernetics, 69*(2), 119-128.

Plamondon, R., Yu, L.-d., Stelmach, G. E., & Clément, B. (1991). On the automatic extraction of biomechanical information from handwriting signals. *IEEE transactions on systems, man, and cybernetics, 21*(1), 90-101.

Reed, M. P., Faraway, J. J., Chaffin, D. B., & Martin, B. J. (2006). The HUMOSIM Ergonomics Framework: A new approach to digital human simulation for ergonomic analysis. *SAE Technical Paper*.

Reed, M. P., Zhou, W., & Wegner, D. M. (2011). *Automated Grasp Modeling in the Human Motion Simulation Framework.* Paper presented at the Proceedings of the SAE Digital Human Modeling for Design and Engineering Conference.

Ricker, K. L., Elliott, D., Lyons, J., Gauldie, D., Chua, R., & Byblow, W. (1999). The utilization of visual information in the control of rapid sequential aiming movements. *Acta Psychologica*, *103*(1), 103-123.

Samuels, M. A., Reed, M. P., Arbogast, K. B., & Seacrist, T. (2016). Modeling spatial trajectories in dynamics testing using basis splines: application to tracking human volunteers in low-speed frontal impacts. *Computer methods in biomechanics and biomedical engineering, 19*(10), 1046-1052.

Schmidt, R. A., & Wrisberg, C. A. (2000). *Motor learning and performance: A problem-based learning approach* (2nd ed.): Human Kinetics.

Schmidt, R. A., Zelaznik, H., Hawkins, B., Frank, J. S., & Quinn Jr, J. T. (1979). Motor-output variability: A theory for the accuracy of rapid motor acts. *Psychological review, 86*(5), 415.

Sheikh, I. H., & Hoffmann, E. R. (1994). Effect of target shape on movement time in a Fitts task. *Ergonomics, 37*(9), 1533-1547.

Smiley-Oyen, A. L. (1996). Distribution of Programming in a Rapid Aimed Sequential Movement. *The Quarterly Journal of Experimental Psychology Section A, 49*(2), 379-397.

Todorov, E. (2004). Optimality principles in sensorimotor control. *Nature Neuroscience, 7*(9), 907.

Todorov, E., & Jordan, M. I. (2002). Optimal feedback control as a theory of motor coordination. *Nature Neuroscience, 5*, 1226.

Uno, Y., Kawato, M., & Suzuki, R. (1989). Formation and control of optimal trajectory in human multijoint arm movement. *Biological Cybernetics, 61*(2), 89-101.

Wang, X. (1999). Three-dimensional kinematic analysis of influence of hand orientation and joint limits on the control of arm postures and movements. *Biological Cybernetics, 80*(6), 449-463.

Wang, X., & Verriest, J. P. (1998). A geometric algorithm to predict the arm reach posture for computer-aided ergonomic evaluation. *The Journal of Visualization and Computer Animation, 9*(1), 33-47.

Woodworth, R. S. (1899). Accuracy of voluntary movement. *The Psychological Review: Monograph Supplements, 3*(3), i-114.

Wu, J., Yang, J., & Honda, T. (2010). Fitts' law holds for pointing movements under conditions of restricted visual feedback. *Human Movement Science, 29*(6), 882-892.

Zhang, X., & Chaffin, D. (2000). A three-dimensional dynamic posture prediction model for in-vehicle seated reaching movements: development and validation. *Ergonomics, 43*(9), 1314-1330.

Zhou, W., Armstrong, T. J., Reed, M. P., Hoffman, S. G., & Wegner, D. M. (2009). *Simulating complex automotive assembly tasks using the HUMOSIM framework* (0148-7191).